MODIFICATION OF A MATTAUCH-HERZOG GEOMETRY MASS SPECTROMETER FOR IMPROVED RESOLUTION ION KINETIC ENERGY SPECTROMETRY

By

ROBERT JOSEPH RYBA

Bachelor of Science in Chemistry

Wayne State University

Detroit, Michigan

1967

Submitted to the Faculty of the Graduate College
of the Oklahoma State University
in partial fulfillment of the requirements
for the Degree of
DOCTOR OF PHILOSOPHY
May, 1976

MODIFICATION OF A MATTAUCH-HERZOG GEOMETRY MASS

SPECTROMETER FOR IMPROVED RESOLUTION

ION KINETIC ENERGY

SPECTROMETRY

Thesis Approved:

Thesis Adviser

Dean of the Graduate College

ACKNOWLEDGEMENTS

I owe my gratitude to my major advisor, Dr. Gilbert J. Mains for his guidance and encouragement throughout the course of this study. I have found his breadth and depth of knowledge in science an inspiration and his friendship constant and supportive. I appreciate his many efforts to secure revenue to insure financial support for summer research.

For their guidance and incisive critiques on the initial drafts of this thesis I thank my advisory committee: Drs. L. M. Raff, S. E. Scheppele, and G. R. Waller. I am grateful to E. Chait and DuPont Instruments for supplying the bellows assembly and to H. Hall and F. Vulgamore for their construction of and their suggestions on the design of the apparatus to insert the electron multiplier into the mass spectrometer.

I am indebted to Continental Oil Company, Phillips Petroleum Company, and Oklahoma State University Department of Chemistry for financial assistance during the course of my graduate study.

I would like to acknowledge my fellow graduate students for their hours of stimulating discussions and friendship over the past years.

Finally, I extend my special appreciation to my wife, Mary, for her encouragement and many sacrifices.

TABLE OF CONTENTS

LIST OF TABLES

LIST OF FIGURES

LIST OF FIGURES (Continued)

LIST OF FIGURES (Continued)

CHAPTER I

INTRODUCTION

According to the theory of mass spectra developed by Rosenstock, *et al.*, (1) the ionization process via electron impact is assumed to be a vertical process, following the Franck-Condon principle. The molecular ions formed have finite amounts of excitational energy distributed in their electronic, vibrational and/or rotational degrees of freedom. It is assumed that the excited molecular ion does not decompose immediately but undergoes several crossings to intersecting hypersurfaces. During these vibrations there is a high probability of nonradiative randomization of the excess energy over the available states. At ion source pressures usually encountered, the mean free path of the molecular ion is sufficient to rule out intermolecular energy randomization. Decomposition of the molecular ion occurs whenever sufficient energy is localized in a vibrational mode. The observed mass spectrum is thus composed of molecular ions and fragment ions produced by consecutive and competive unimolecular fragmentations of vibrationally excited ions.

For the unimolecular decomposition

$$m_1^+ \rightarrow m_2^+ + (m_1 - m_2) \qquad \text{(I-1)}$$

The phenomenological rate constant k(t) is given by Equation (I-2)(2)

$$k(t) = \frac{\int_0^\infty P(E)k(E)e^{-k(E)t}dE}{\int_0^\infty P(E)e^{-k(E)t}dE} \tag{I-2}$$

where k(E) is the microscopic unimolecular rate constant for ions of energy E and P(E) is the probability of m_1^+ having internal energy between E and E + dE.

In most mass spectrometers, ions spend approximately 1 microsecond in the ion source and 10 microseconds traversing the instrument prior to collection (3). Therefore, ions with unimolecular rate constants exceeding 10^6/second decompose in the ion source while ions with rate constants of less than 10^5/second are collected without further decomposition. Ions with unimolecular rate constants within the range 10^5-10^6/second decompose during or after acceleration but prior to collection. These decompositions are termed *metastable* and the parent ions of such decompositions are *metastable ions*. The recorded signal of the daughter ions formed from the fragmentation of metastable ions have become known as *metastable peaks*.

Metastable ions have received much attention in single focusing mass spectrometers since their original description by Hipple (4,5) who correctly interpreted them as resulting from dissociations occurring in the field-free drift region following acceleration. More recently, interest has reintensified in metastable ions as a result of studies using double focusing instruments. Metastable decompositions can occur along the entire ion flight path of a double focusing instrument. As depicted in Figure 1, such a mass spectrometer has six discrete regions. In three of the regions there are no electrostatic or magnetic forces acting on the ions; these are the *field-free* regions. During accelera-

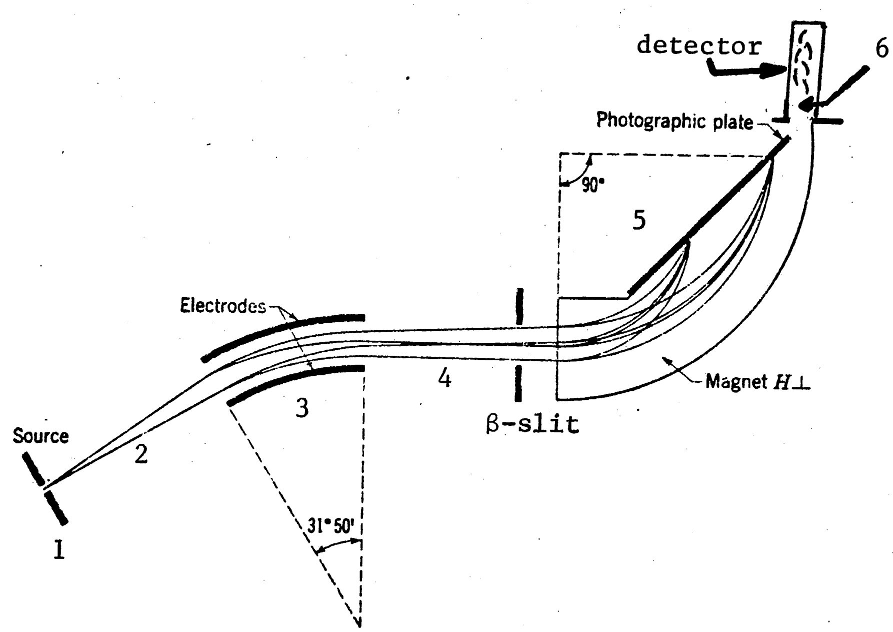

Distinct regions

1 acceleration
2 first field-free
3 electrostatic field
4 second field-free
5 magnetic field
6 final field-free

Figure 1. Double-focusing Mass Spectrometer of the Mattauch-Herzog Geometry (From *Mass Spectrometry,* Ed., Charles A. McDowell, McGraw-Hill, 1963, pp. 19)

tion, electrostatic and magnetic deflection, fields are present; therefore, these regions are referred to as *fielded*. Extensive mathematical treatment has been given to the motion of ions resulting from decompositions in the fielded (6) and field-free (7) regions of double focusing mass spectrometers. In this discussion singly charged ions are considered; however, multiply charged metastable decompositions have received considerable attention (8). When m_1^+ decomposes to m_2^+ as in Equation (I-1), the daughter ion retains a fraction, m_2/m_1, of the kinetic energy and momentum. This assumes no vibrational energy from the bond rupture appears as translation energy. When this decomposition occurs in the accelerating region before falling through a large potential difference, discriminations will be small and if the daughter ions pass through the electrostatic analyzer, they will appear in the mass spectrum as a tail on the low mass side of m_2^+. The actual apparent mass is given by (5)

$$m^* = \frac{m_2^2}{m_1}\left[1 + \frac{(m_1 - m_2)(V - V_1)}{m_2 V}\right] \qquad \text{(I-3)}$$

where V is the accelerating voltage and V_1 is the potential difference through which the ion of mass m_1 falls before decomposing. Metastable decomposition occurring after falling through nearly the entire acceleration (V_1 slightly smaller than V) will appear in the mass spectrum in the tail on the high mass side of m* if allowed to pass the electrostatic analyzer.

Daughter ions from metastable decompositions formed within the acceleration region, electrostatic sector, or magnetic field will not be collected at discrete masses but will become part of the background.

The daughter ions from metastable decompositions which are formed after passing through the collector slit are likewise of little interest since they are collected with the parent ions unless a specialized detector is used (9). The ions formed in the field-free region(s) preceding the magnetic sector of single or double focusing instruments can be observed at discrete masses. The ions formed just prior to magnetic deflection appear in the mass spectrum at m* given by Equation (I-4)

$$m^* = \frac{m_2^2}{m_1} \tag{I-4}$$

as would any ions formed in the first field-free region if permitted to pass through the electrostatic sector at the normal accelerating potential. Equation (I-4) follows from Equation (I-3) when V_1 equals V.

Decoupling the electrostatic sector voltage from the acceleration potential in order to pass ions formed in the first field-free region is termed *defocusing*. Techniques for defocusing the Nier-Johnson (10) or Mattauch-Herzog (11) double focusing instruments are well established. With the mass spectrometer set to focus stable ions at the collector (as is the case for conventional mass analysis) the electrostatic field between the electric sector plates is such that ions which received the full acceleration energy will follow a central path through the sector. Daughter ions from metastable decompositions, m_2^+, will have a smaller radius of curvature in the field and will not be transmitted because they possess only a fraction, m_2/m_1, of the necessary energy. The daughter ions from metastable decompositions can be made to follow the central path by either increasing the accelerating voltage by a factor m_1/m_2 (holding the electric sector voltage constant), or by reducing the electric sector voltage by a factor m_2/m_1 (holding the ion accelerating voltage constant). In either case, the main ion beam is not transmitted through the electrostatic sector.

The first method of defocusing has two disadvantages: as the ion accelerating voltage is changed, the tuning conditions within the ion source are altered due to changes in field penetration; and second, the voltage cannot be changed without bound, which consequently limits the ratios of m_1/m_2 that can be studied. This method has the advantage that the mass scale of the instrument is unchanged because the daughter ion of any first field-free decomposition now possesses what would be the normal acceleration energy. The magnet current can be set to observe ions at $m/e = m_2$ in the conventional mass spectrum, and as the accelerating voltage is scanned, a series of peaks are observed, each corresponding to a different metastable ion which decomposes into the m_2^+ ion.

The second defocusing method has the disadvantage that the mass scale changes during the scan of electric sector voltage, and any ions being collected will appear at m* (Equation I-4). The advantage is that all the daughter ions, without limit, can be made to pass the electric sector. In either defocusing technique described, the ion current may be monitored at the β-slit, Figure 1. The ion current plotted as a function of kinetic energy of the daughter ion constitutes the Ion Kinetic Energy Spectra, IKES (12). The observed metastable peaks in the IKES may be unambiguously assigned by setting the electric sector voltage (second defocusing method) to maximize the individual ion current at the beam monitor (β-slit) and scanning the magnetic field until m* is determined. The daughter ions will pass the electric sector when

$$\frac{E'}{E} = \frac{m_2^+}{m_1^+} \qquad \text{(I-5)}$$

where E is the electric sector voltage needed to pass the main ion beam, m_1^+, and E' the voltage necessary to pass the daughter ion, m_2^+. By knowing E, E', and m* equations (I-4) and (I-5) may be used to calculate unique values for m_1^+ and m_2^+.

The uses of metastable ions and IKES for elucidation of fragmentation pathways in mass spectrometry have been summarized in an excellent review (13). The literature has increased vastly within the last few years as the application of IKES to ion fragmentation studies has become more common. Among the recent applications are the following: consecutive metastable decompositions in the two field-free regions (14); analysis of mixtures (15); isotope measurements and effects (16); release of kinetic energy in unimolecular decompositions (17); collision-induced dissociations and charge transfer reactions (18); reverse geometry instruments (19); appearance potential measurements of metastable peaks (20); thermochemistry and energy partitioning (21); non-zero scattering angle reactions (22); and analysis of geometric isomers (23-27). In all of these IKES applications, the energy resolving power of the mass spectrometer is important.

A large percent of the double focusing instruments presently used for IKES are of either a Nier (28) or a Mattauch-Herzog (29) geometry. The Nier-Johnson mass spectrometer has a 90 degree electrostatic analyzer followed by a 90 degree magnetic sector (e.g. M.S.9 manufactured by GEC/AEl) (30). A modified Nier-Johnson geometry instrument, the RMH-2 (31) (manufactured by Hitachi-Perkin Elmer) has a 70 degree

degree electrostatic sector and a 70 degree magnetic field. The important aspect of the Nier-Johnson geometry instrument for IKES is the formation of an ion source energy image in the second field-free region at the β-slit. In Figure 2, ions of two slightly different energies but equal masses are energy focused in the plane containing the β-slit. By closing the β-slit and scanning the voltage on the electric sector plates at fixed accelerating potential, the IKES can be monitored with a detector behind the β-slit. The ability of the electrostatic sector to focus ions of the same energy to a point allows routine IKES of better than 0.5% energy resolution while recording peaks which make up only 10^{-7} to 10^{-8} of the total ion current (32). The maximum energy resolution with commercial Nier-Johnson geometry instruments for IKES is better than 0.025% (32).

In the Mattauch-Herzog geometry the ion source is located at the focal point of the $\Pi/4\sqrt{2}$ electrostatic sector forming an image at infinity. In Figure 1 ions of two slightly different energies and significantly different masses traverse the second field-free region with trajectories parallel to each other. By closing down the β-slit and scanning the voltage on the electric sector plates at fixed accelerating potential, the IKES can be monitored; however, the peaks observed will be broader than in the case of Nier-Johnson geometry with a significant loss in resolution due to the width of the intermediate image. One of the primary objectives of this research was to increase the applicability of Mattauch-Herzog mass spectrometers for IKES by increasing the energy resolution without affecting the performance of the instrument for routine mass analysis.

Once an improvement in energy resolution was realized it was a

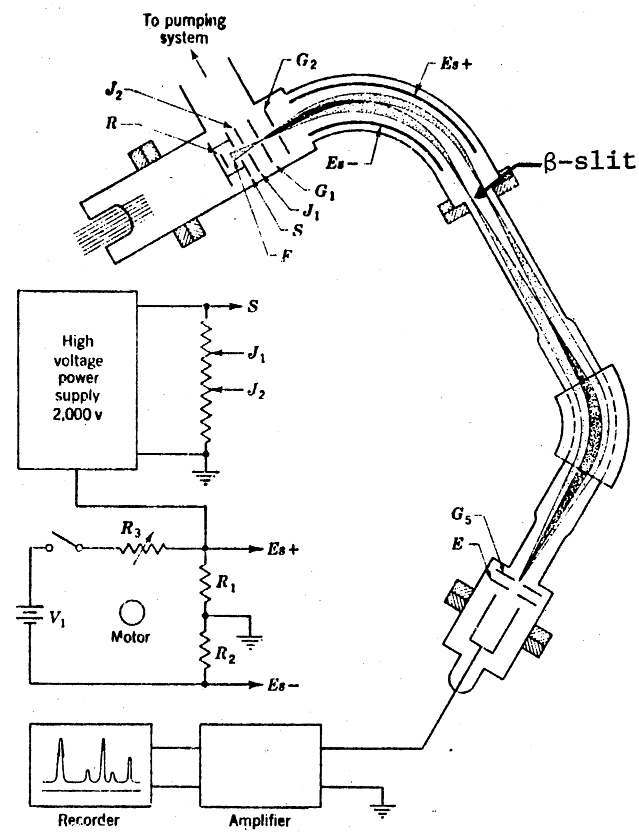

Figure 2. Double-focusing Mass Spectrometer of the Nier Geometry (From A. O. Nier, *Rev. Sci. Instr.*, 31, 1127 (1960))

further aim of this research to investigate the applicability of IKES as a structural probe. It was intended to investigate similarities or differences between normal ion abundances and those produced by decompositions in the first field-free region for a group of substituted thiophenes. Because the metastable decompositions are processes with half-lives of approximately 10^{-5} seconds these are molecular ions that have received a relatively small amount of excess energy on ionization. Ions that have received a large excess of excitation energy will decompose in the ionization chamber while those receiving less excitational energy than necessary for decomposition will reach the detector intact. The mass spectrometer is thus acting as an energy filter since the first field-free region metastable decompositions are studied by rejecting all ions that undergo rapid reaction and allow only those undergoing slow reaction to be analyzed. Because the metastable ions possess less excitational energy than their counterparts which fragment in the ion source it is becoming evident that these ions are of more importance in obtaining correlations between fragmentation patterns and ion structure. The applications of IKES to analysis of structural isomers has included the following: N. R. Daly *et al.* (23) with the *cis*- and *trans*-butenes, R. M. Caprioli, *et al.* (24) with *ortho*-, *meta*-, and *para*-phenylenediamines, E. M. Chait and W. B. Askew (25) with camphor and *trans*-8-methylhydrindan-2-one, H. W. Majors (26) with *cis*-, and *trans*-dimethyl maleate, and more recently S. Safe *et al.* (27) with isomeric chlorobenzenes and polychlorinated biphenyls. Some compounds have identical fragmentation patterns; no differences in IKES has been observed for *meta*-, and *para*-isomers of fluorophenylacetylene or for 1-butene and *cis*-2-butene (25). The lack of differences in the spectra in many cases is probably due to common structure for the molecular ion prior to meta-stable decomposition.

CHAPTER II

LOW RESOLUTION ION KINETIC ENERGY SPECTRA

Part I - Experimental Modifications

All spectra were obtained with a Mattauch-Herzog double focusing mass spectrometer (model DuPont/CEC 21-110B). For conventional mass analysis the accelerating potential of the instrument is slaved to the positive half of the electrostatic sector dual-purpose power supply. An approximate 20:1 voltage relationship exists between the acceleration and positive electrostatic sector plate (i.e. $V_{sector} = \pm \frac{V_{accel.}}{20}$). The electric sector plate potentials are not continuously variable but rather six discrete voltages can be supplied from the mass measurement chassis. It was required for metastable observation that the power supplies be separated and that the electrostatic plate potentials be continuously variable and independent of the accelerating potential. This decoupling of the power supplies was done by the addition of the circuit in Figure 3. Switch #1 (S1) is a three position multilayer rotary switch. Position #1 of S1 bypasses most of the circuit and applies the ± voltage from the mass measurement chassis to the sector plates. Switch #1 should be in position #1 for mass spectral analysis. Position #2 is an off position and applies no voltage to the electric sector plates. Position #3 applies ± 750 volts through wafers C and D to S2-A and S2-B respectively. The voltage is dropped along the fixed resistor string and

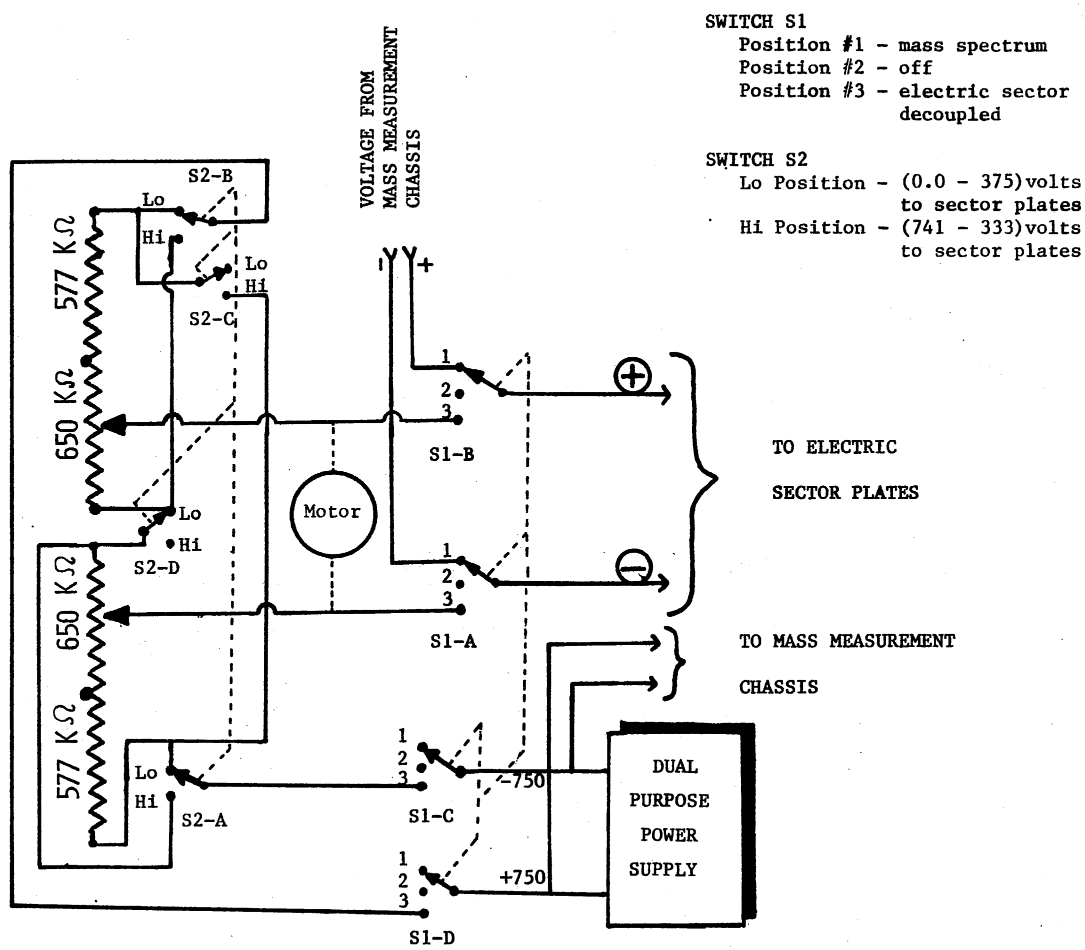

Figure 3. Circuit Diagram for Decoupling and Scanning the Electric Sector Voltage of a DuPont/CEC 21-110B Mass Spectrometer

the tandem potentiometer (Beckmann instruments precision Helipot, model #7603, R650K) where it is picked off and applied to the electric sector plates via S1-A and S1-B position #3. The electric sector voltage was monitored with Hewlett-Packard 4½ digit multimeter (model #34702A). Switch #2 electronically inverts the position of the potentiometer and the fixed resistor string and allows a low (± .8 to 375 volts) or a high (± 741 to 333 volts) range of voltages to be applied to the electric sector plates. A multiratio gearmotor (Apcor, model #2201-010) was used to drive the 10-turn tandem potentiometer at speeds of 10, 5, 2, 1, 1/2, and 1/5 RPM. The ion signal was taken off the beam monitor vacuum feed-through by a Keithley high speed picoammeter (model #417) and displayed on a Keithley recorder (model #370). The spectra were usually scanned with a potentiometer speed of 1/2 RPM (sector plates changed at ± 18 volts/min.) and a chart speed of .75 in/min. The majority of the spectra were measured from 0% through 100% electrostatic sector voltage; however, peaks were generally observed in the 50% - 100% region. Precise measurement of the energy of peaks in the IKE spectra was obtained by manually scanning the electric sector voltage to maximize the peak intensity while monitoring the digital multimeter.

The ion source temperature and pressure were noted on the spectra. Other ion source conditions were as follows except where otherwise noted: electron energy, 70 eV; trap current, 80μ amps; bilateral source slits, open maximum; and focus electrode, maximum signal at beam monitor for the main beam.

Part II - Results and Discussion

The Ion Kinetic Energy Spectra of n-decane recorded with a Nier geometry mass spectrometer (RMH-2) by Beynon, *et. al.* (33) is given in Figure 4. The metastable peak assignments are indicated in Table I. The energy resolution in Figure 4 is between .6 - .9% depending upon the metastable peaks selected (peaks F and G, C and D respectively). Chait, *et. al.* (25) has recorded the IKES of n-decane on a Mattauch-Herzog instrument (DuPont 21-110B), Figure 5. The metastable peak assignments refer to Table I. The lower energy resolution is indicated in the latter spectra by the complete loss of the C-D doublet as well as peaks E, F, G, the shoulder on the low energy side of I, and M. The calculated energy resolution is approximately 3% based on the B, C-D doublet. Both spectra were obtained by scanning the voltage on the electrostatic sector plates at fixed acceleration potential and recording the ion intensity at the β-slit. In the Nier geometry instrument with the presence of an energy image in the second field-free region, a narrow β-slit was used to yield the high energy resolution. The instrument's sensitivity and detectibility were increased for IKES by incorporation of an electron multiplier behind the energy resolving slit (12). In the Mattauch-Herzog instrument there is no intermediate image and the signal was recorded with an electrometer behind the wide (0.250 inch) β-slit.

The n-decane IKE spectra recorded with the O.S.U. mass spectrometer is given in Figure 6. Figures 5 and 6 are essentially identical except for intensity variations (e.g. peaks H, I, and J) which could be due to ion source pressure or temperature discrepancies. The authors do not indicate the ion source conditions under which Figure 5 was obtained.

To check further the performance of the O.S.U. instrument, the IKES of benzene was recorded, Figure 7. The daughter ions were mass analyzed and the metastable transitions were identified using Equations I-4 and

TABLE I

METASTABLE PEAKS AND TRANSITIONS IN THE IKES OF n-DECANE
(TAKEN FROM A. H. STRUCK & H. W. MAJOR JR.,
ASTM E-14, 1969)

Metastable Peak	Assigned Transition	Calculated m_2/m_1
a	43 → 41	.953
	41 → 39	.951
b	84 → 69	.821
c	142 → 113	.796
d	142 → 112	.789
	70 → 55	.786
e	113 → 85	.752
f	113 → 83	.735
	57 → 42	.737
g	112 → 83	.741
	56 → 41	.732
h	98 → 70	.714
	57 → 41	.719
i	142 → 99	.697
j	127 → 85	.669
	85 → 57	.671
	85 → 56	.659
k	113 → 71	.628
l	71 → 43	.606
m	142 → 85	.599
n	99 → 57	.576
o	55 → 29	.527
p	142 → 71	.500
	113 → 57	.504
	85 → 43	.506
	57 → 29	.509
	55 → 27	.491

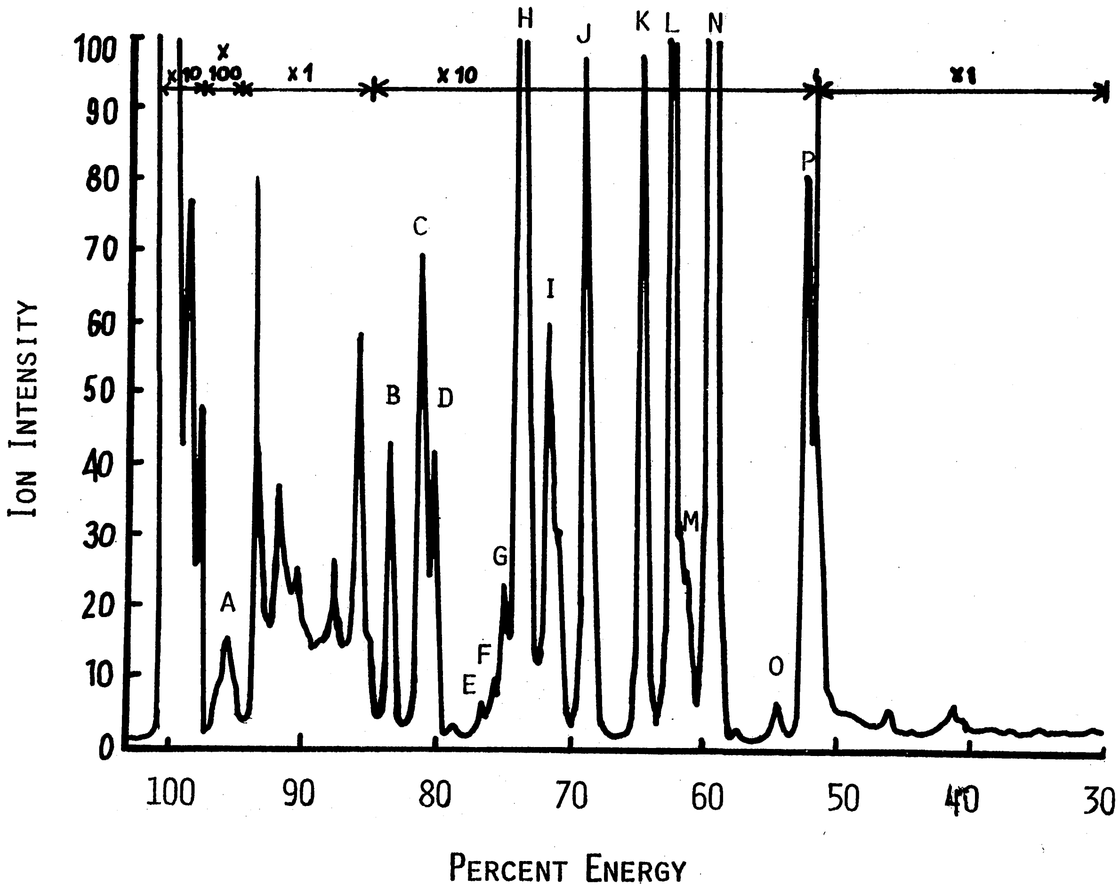

Figure 4. Ion Kinetic Energy Spectrum of n-decane With a Nier Geometry Mass Spectrometer (From Beynon, *et al.*, *Chem. Commun.*, 723 (1969))

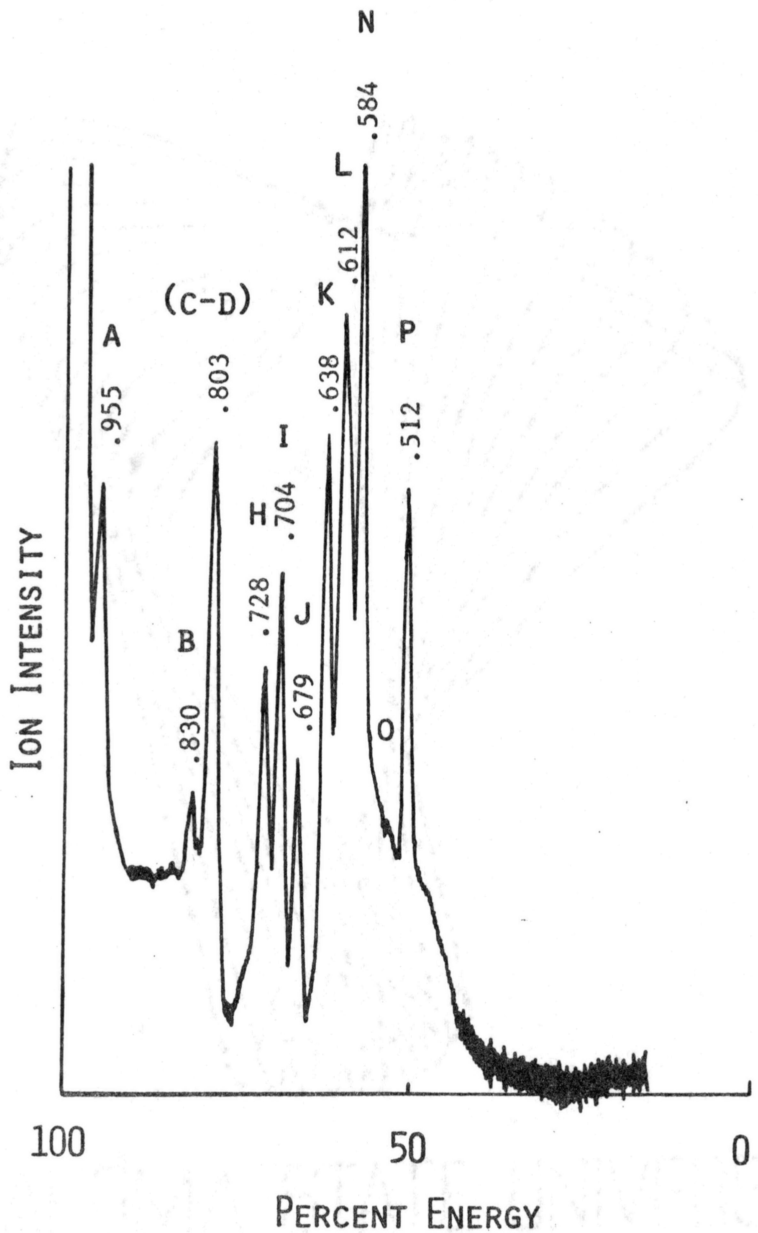

Figure 5. Ion Kinetic Energy Spectrum of n-decane With a Mattauch-Herzog Mass Spectrometer (From Chait, *et al.*, *Org. Mass Spectrom.*, 5, 147 (1971))

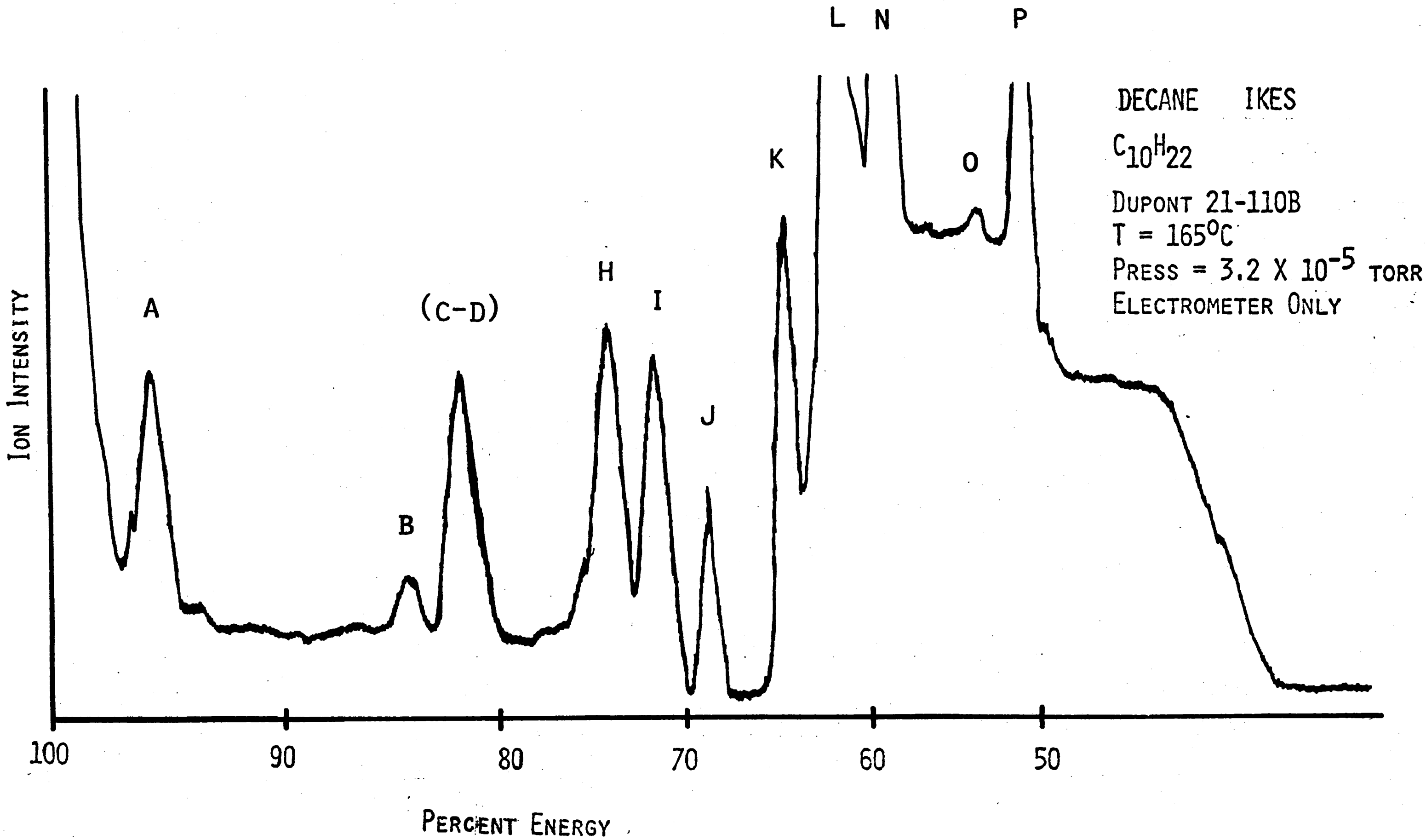

Figure 6. Low Energy Resolution Ion Kinetic Energy Spectrum of n-decane

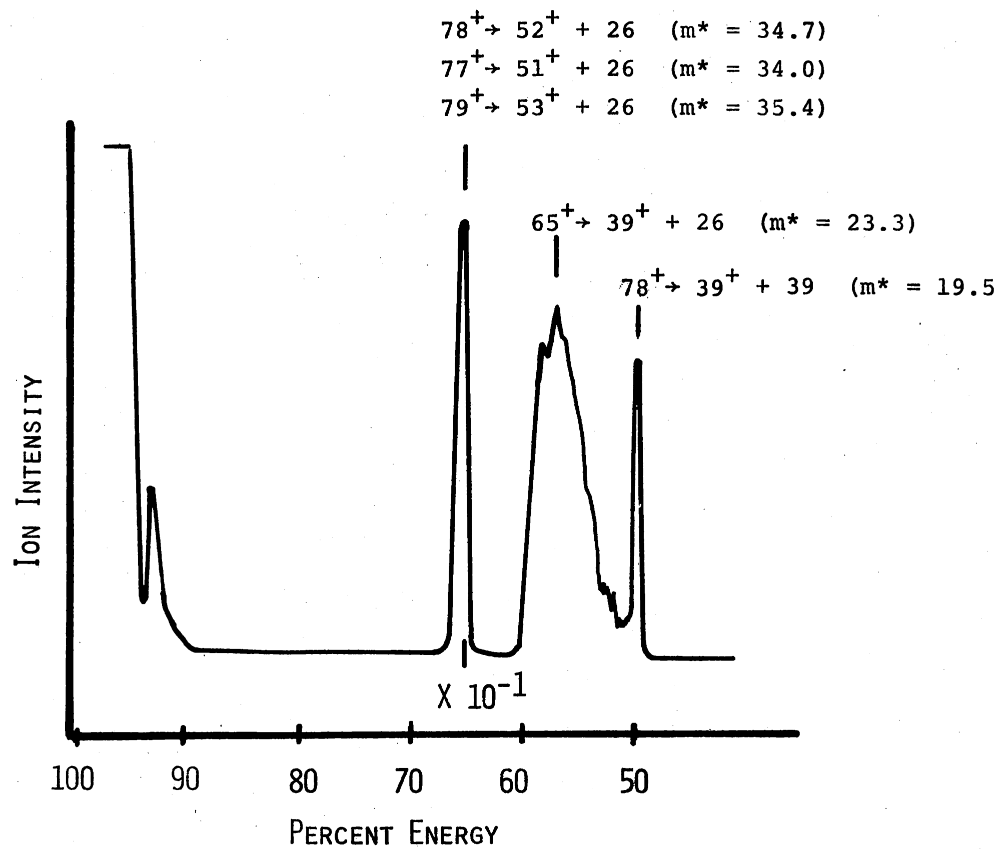

Peak # (low ESA → Hi ESA)	ESA (obs.)	m * from Plate	Transition	ESA (calc.)	m * (calc.)
1	.503	19.58	$78^+ \rightarrow 39^+ + 39$	.500	19.50
2	.599	23.27	$65^+ \rightarrow 39^+ + 26$	.600	23.4
3	.670	34.72	$78^+ \rightarrow 52^+ + 26$	.667	34.67
	.670	35.39	$79^+ \rightarrow 53^+ + 26$	.670	35.56
	.671	33.98	$76^+ \rightarrow 51^+ + 25$	.671	34.22
	.671	33.98	$77^+ \rightarrow 51^+ + 26$	.662	33.78
4	.968	72.98	$77^+ \rightarrow 75^+ + 2$	.974	73.05
	.970	73.19		.974	73.05
4	.970	74.14	$78^+ \rightarrow 76^+ + 2$	.974	74.05

Figure 7. Ion Kinetic Energy Spectrum of Benzene Below the Main Ion Beam

I-5. The IKE spectra agreed well with that of Chait, *et. al*. (25); however, the assignment of the metastable peak at 67% of the electrostatic analyzer voltage was incorrectly reported in the literature. The transition was reported as $78^+ \rightarrow 63^+ + 15$. If this decomposition does occur in the first field-free region, the daughter ion would be detected when the electric sector plates are lowered to 81%, not 67%, of the voltage necessary to pass the main ion beam. Our identification was obtained by measuring the apparent mass, m*, of the daughter ions passed at an electrostatic sector energy of 67%. An apparent mass of 34.7 uniquely determined the transition as $78^+ \rightarrow 52^+ + 26$.

The energy resolving limitations of the Mattauch-Herzog mass spectrometer were investigated computationally on an IBM 360/65 computer (Appendix B, Program #1). For computational purposes the ions were treated as point particles at ion fluxes low enough to neglect space charging effects. All metal surfaces were considered as ideal in that no charge build-up or screening was considered although this can be of considerable importance (34). The results of these computations presented in Figure 8 are for ions exiting the infinitely narrow ion source slit with divergent angles from the central axis of the instrument as indicated by α. The maximum acceptance angles of the entrance slit to the electric sector in the O.S.U. instrument is $\pm$ 0.00045 radians. The ions treated computationally in the first field-free region were those moving in the plane orthogonal to the electric sector entrance slit. In Figure 8 the final position of the ions in the plane of the exit slit of the electrostatic sector (measured from the vertex of the sector) is given as a function of the accelerating voltage and the angle of entrance (in radians) to the sector. The arrows at 63.84

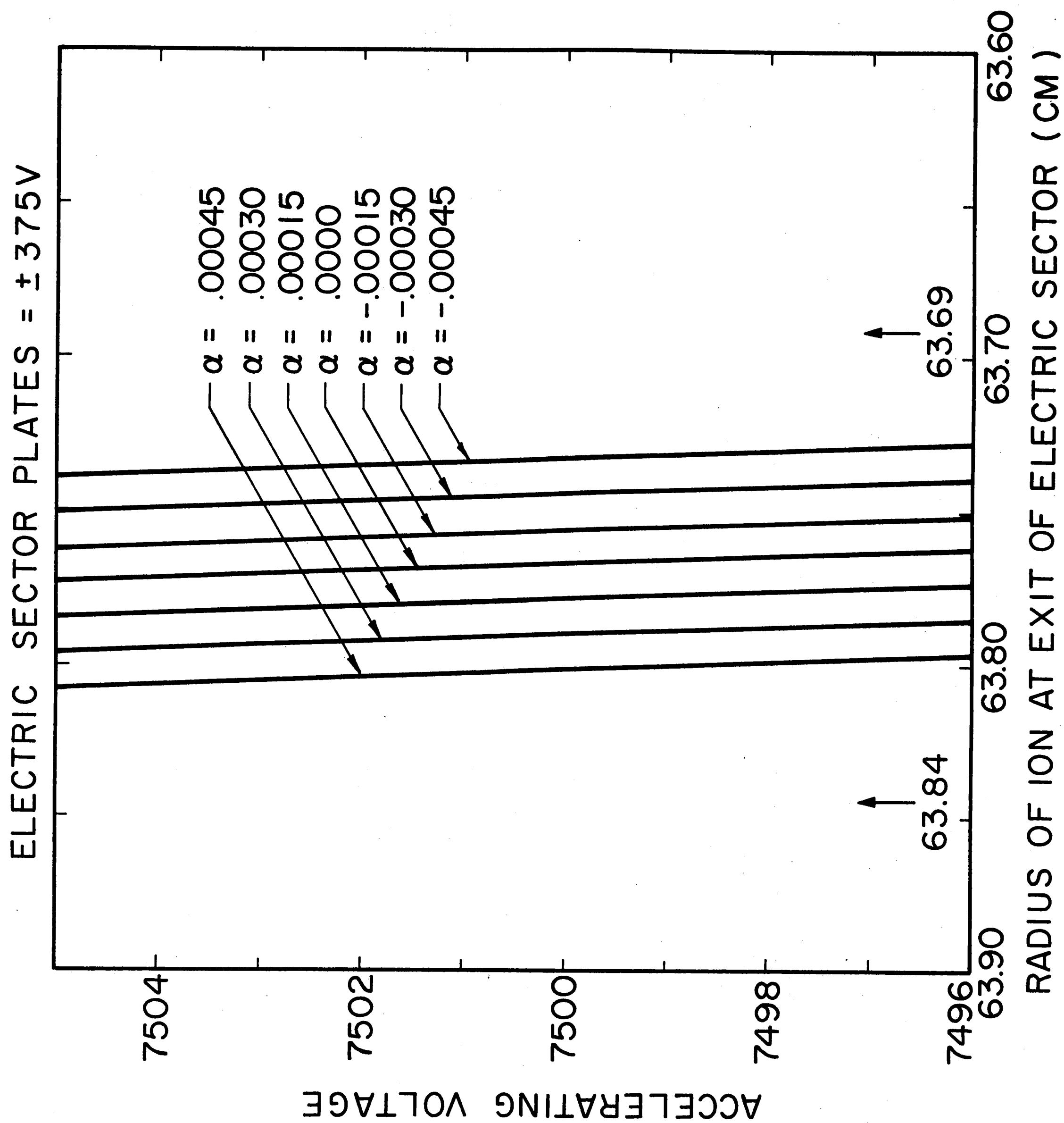

Figure 8. Profile of the Ion Beam at the Exit Slit of the Electrostatic Sector on a Mattauch-Herzog Mass Spectrometer

and 63.69 cm mark the extremes of the 0.060 inch exit slit. Opening the adjustable ion source slit by 0.001 inch has the effect of broadening each of the lines in Figure 8 by approximately that amount.

From Figure 8 it is clear that ions resulting from metastable decompositions in the first field-free region entering the electrostatic sector with differences in their translational energies greater than about 5 percent can be completely separated and detected at the β-slit using different electric sector voltages. Each group of daughter ions, although translationally monoenergetic, exit the electric sector at a fixed sector voltage at radial distances determined entirely by the angle of entrance to the sector. If the daughter ions differ in translational energy by less than about 5%, the groups of ions are not completely resolved. This accounts for the wide metastable peaks and low energy resolution observed in the IKES with the Mattauch-Herzog mass spectrometer. With an ion source slit of .002 inches, entrance and exit slit widths of the electric sector of .016 and .060 inches respectively, and an accelerating potential of 7500 eV, the computed overlap of IKE peaks on the DuPont/CEC 21-110B mass spectrometer are as follows: 80% overlap at energy differences of 1.3%; and a 10% overlap at an energy difference of 2.3%.

The energy resolution of the Mattauch-Herzog mass spectrometer can be improved by decreasing the width of the entrance slit to the electric sector. This decreases the acceptance angle α, Figure 8, narrowing the width of the ion beam at the exit slit of the sector. The energy resolution of the IKE spectra can also be improved by narrowing the exit slit to the electrostatic sector. Both methods unfortunately also decrease the sensitivity of the instrument and correspondingly limit its utility as a general purpose mass spectrometer. Hence, it was decided to attempt further improvement of the energy resolution by designing a variable β-slit which could be completely removed from the ion path during normal mass spectrometric operation of the instrument.

CHAPTER III

MEDIUM ENERGY RESOLUTION ION KINETIC ENERGY SPECTRA

Part I - Experimental Modifications

The second field-free region of a Mattauch-Herzog mass spectrometer (DuPont/CEC 21-110B) was fitted with a bellows assembly to insert a variable β-slit and an electron multiplier (Bendix Continuous-Dynode, Model 4700) into the ion beam traversing the region, Figure 9. The bellows assembly had a travel of greater than 3½ cm allowing the slit and electron multiplier to be completely removed from the ion beam when not in use. One end of the continuous-dynode resistor was grounded to the mass spectrometer. The front of the resistor string (also the entrance to the electron multiplier) was connected to a vacuum feed-through placed in the auxiliary pump-out flange behind the photoplate holder. The negative high voltage (1000 - 2800v) for the continuous-dynode electron multiplier was supplied by the power supply for the instrument's discrete dynode electron multiplier.

The slit was positioned in front of the continuous-dynode electron multiplier and was continuously variable in width from closed to approximately 0.5 cm open. With the electron multiplier-slit assembly positioned in the ion beam the variable slit acts as an adjustable β-slit. However, because the adjustable β-slit was physically connected to the

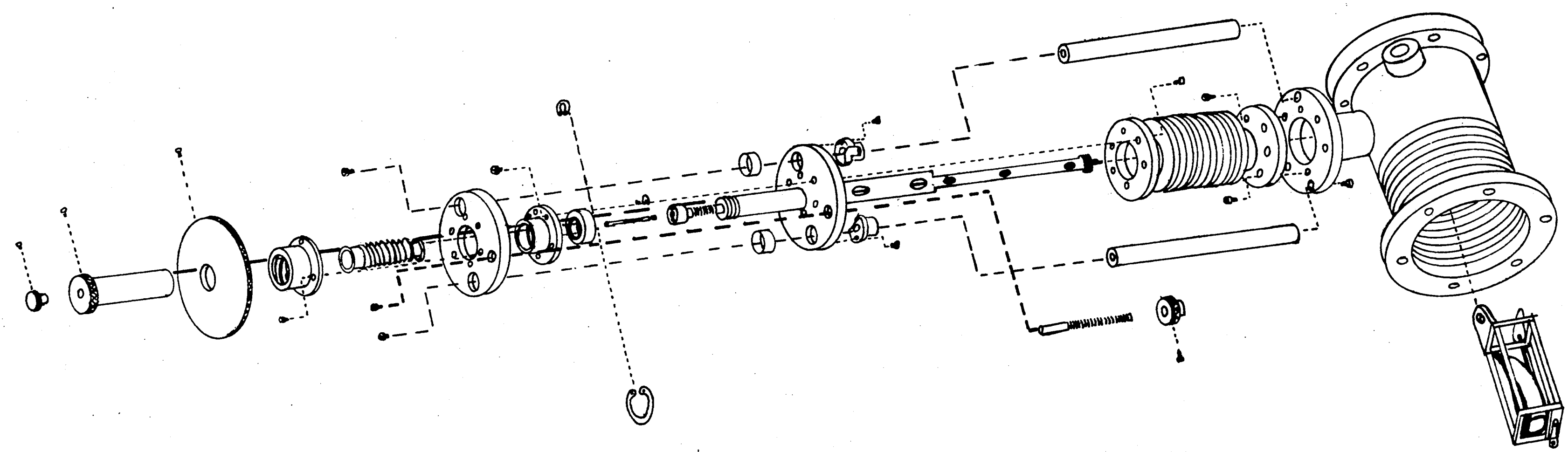

Figure 9. Diagram of the Adjustable β-slit and the Electron Multiplier Assembly

electron multiplier it cannot be inserted into the ion beam independently.

The signal from the anode of the electron multiplier was connected to the conventional beam monitor vacuum feed-through via a wiper arm. The wiper arm contact introduces a larger than normal dark current into the detection system. At 2500v a dark current of 1×10^{-12} amps was detected. The signal from the vacuum feed-through was fed into a high speed picoammeter (Keithley Model 417) and recorded on a strip chart recorder (Keithley Model 370). In order to avoid perturbations of the secondary electron trajectories within the multiplier by fringing magnetic fields the magnetic sector current was set to the minimum.

Part II - Results and Discussion

The increase in energy resolution of the mass spectrometer using the adjustable β-slit-electron multiplier is illustrated with n-decane, Figure 10. The metastable transitions and peak assignments correspond to those in Table I. The IKES of n-decane using only the electrometer detector behind the wide (~ 0.250 inch) β-slit is given in Figure 6. The increased energy resolution for IKES in Figure 10 is apparent with the splitting of additional metastable peaks from the main ion beam with daughter ions retaining 98.5% and 97.7% of the kinetic energy. Further indications of the increased energy resolution and sensitivity are the resolution of the C-D doublet; the appearance of peaks e, f, and g; the splitting of peak i; and the appearance of the m doublet. The energy resolution of n-decane in Figure 10 is comparable to that reported with a Nier geometry instrument, Figure 4; however, in the former case the adjustable β-slit was set for maximum energy resolution

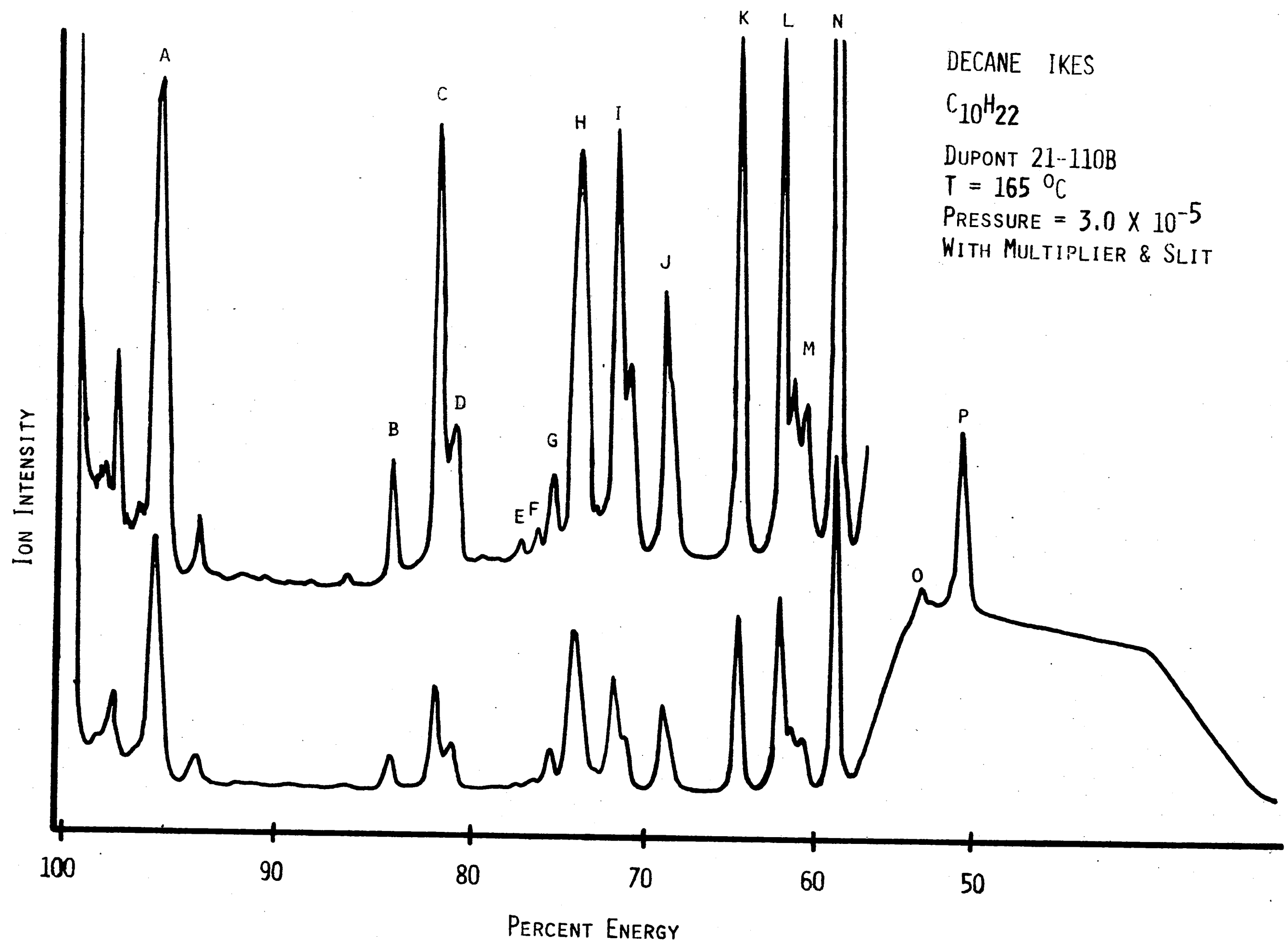

Figure 10. Ion Kinetic Energy Spectrum of n-decane With the Adjustable β-slit and Electron Multiplier

whereas in the latter this was not the case.

The minimum detectability of our Mattauch-Herzog mass spectrometer for IKES peaks was not as low as the Nier geometry. Beynon *et. al.* (12) have investigated electron transfers to multiply charged argon ions in the first field-free region. For the transition $Ar^{+4} \rightarrow Ar^{+}$ (1), $Ar^{+3} \rightarrow Ar^{+}$ (39), $Ar^{+2} \rightarrow Ar^{+}$ (820), $Ar^{+3} \rightarrow Ar^{+2}$ (123), $Ar_3^{+2} \rightarrow Ar_2^{+2}$ or $2Ar^{+}$ (9), and $Ar_2^{+2} \rightarrow Ar^{+2}$ (28) the relative intensities are given in parentheses. At maximum sensitivity we have been able to observe only $Ar^{+2} \rightarrow Ar^{+}$, and $Ar^{+3} \rightarrow Ar^{+2}$ on our instrument. Electric sector potentials required for $Ar^{+3} \rightarrow Ar^{+}$ have not been attempted due to limitations in our dual-purpose power supply; however, $Ar_2^{+2} \rightarrow Ar^{+2}$ and $Ar_3^{+2} \rightarrow Ar_2^{+}$ or Ar^{+} have not been observed. The difference in the minimum detectability is attributed to the presence in the Nier and lack in the Mattauch-Herzog geometry of a focal point for metastable daughter ions in the second field-free region. An additional factor is the increased dark current introduced by using the wiper arm in our installation of the electron multiplier in the second field-free region.

The occurrence of multiply charged metastable decompositions are well documented in double focusing mass spectrometers. Beynon, *et. al.* (8) have reported dish shaped peaks resulting from the large amounts of translational energy imparted to the ionic fragments upon bond rupture. In the IKES of benzene a dish shaped peak at electrostatic sector voltage above the main ion beam can be found at 162% of the energy. This peak corresponds to the singly charged daughter ion at m/e 63 resulting from the doubly charged molecular ion decomposing in the first field-free region. The Mattauch-Herzog instrument with an adjustable β-slit and electron multiplier has the necessary energy resolution and sensitivity to resolve the dish shaped metastable in benzene, Figure 11.

The interest in substituted thiophene compounds has been intensified recently by their presence in fossil fuels. An analysis using the 70 eV mass spectra of a liquification product mixture from coal is complicated by the predominance of common fragment ions. Due to the mass defect of sulfur, thiophene compounds with molecular weights of 200 or greater require very high mass resolution to separate their molecular ions from those of many hydrocarbons at the same nominal mass. An incomplete series of alkyl- and benzo- thiophene compounds were obtained from the ERDA laboratory in Bartlesville, Oklahoma. Two additional compounds, 2-heptylthiophene and 2-butylthiophene, were prepared by previously reported synthetic routes (35). All of the thiophene compounds were vacuum distilled and found to be 99+% pure by gas chromatography and field ionization mass spectrometry (36). The mass spectra of all of the thiophene compounds obtained have been reported (37). The IKES of the thiophene compounds were undertaken to investigate the types and number of transitions present and determine whether it would be possible to distinguish the presence of thiophene compounds generally (or specific thiophene compounds) in a mixture on the basis of their IKES. An additional aim of the analysis of the thiophenes was to determine whether structural isomers, which give similar mass spectra, could be characterized better on the basis of their IKES.

The sensitivity and energy resolution of the Mattauch-Herzog mass spectrometer using the adjustable β-slit and electron multiplier was further illustrated with 2-heptylthiophene. In Figure 12, the IKES was recorded using only the electrometer, whereas in Figure 13 the electron multiplier and adjustable β-slit was used. The spectra in Figure 12 was

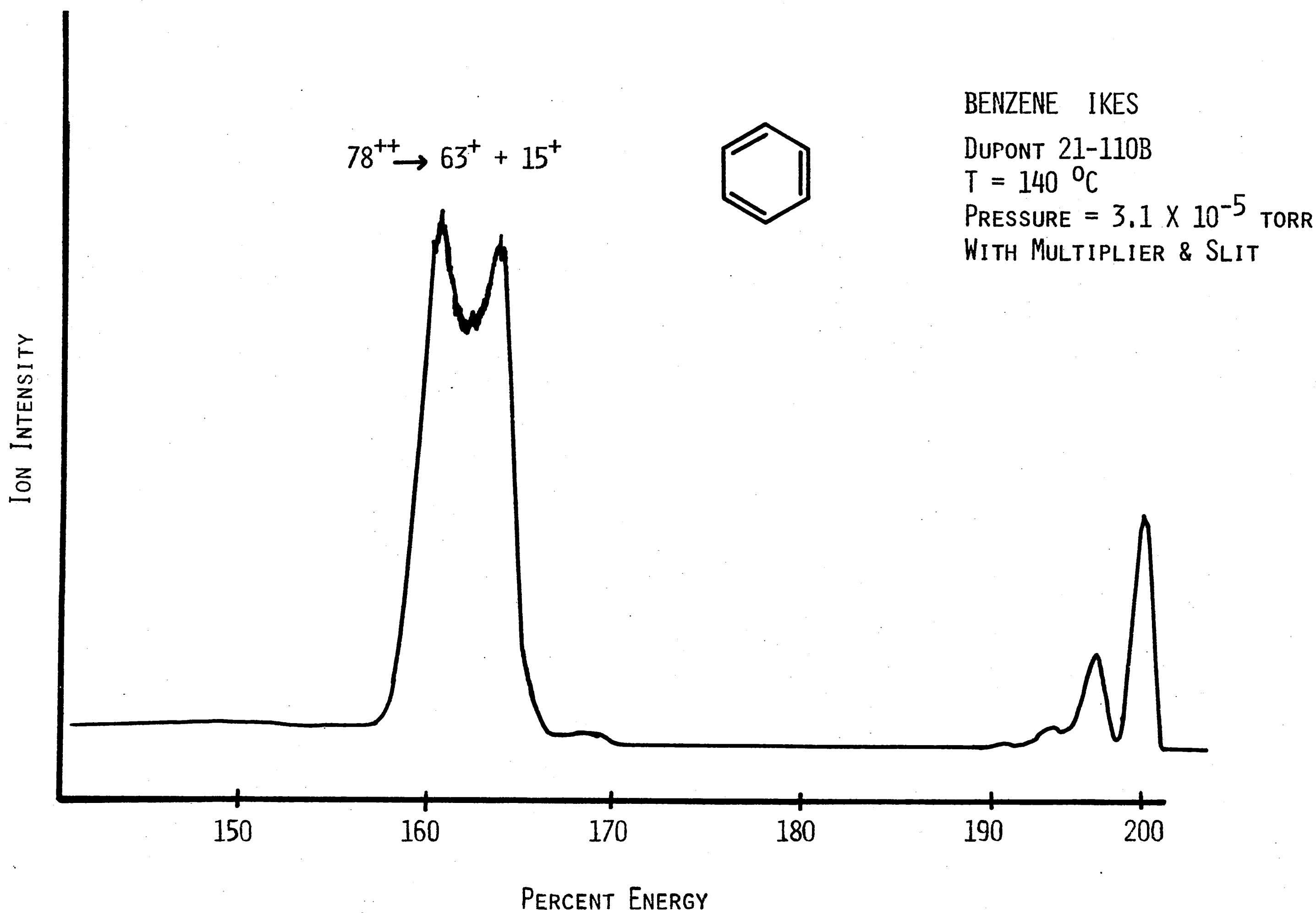

Figure 11. Ion Kinetic Energy Spectrum of Benzene Above the Main Ion Beam Energy

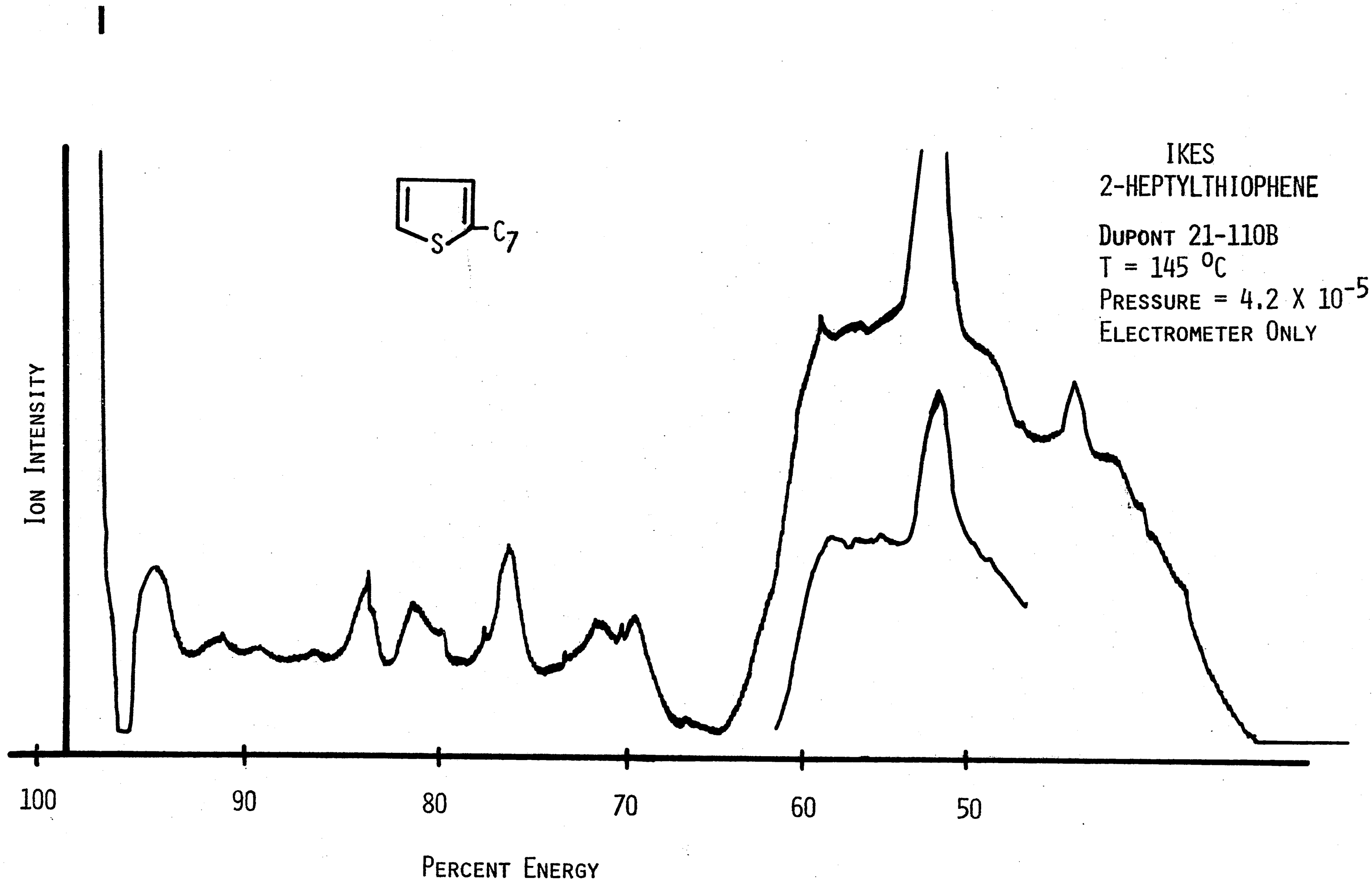

Figure 12. Ion Kinetic Energy Spectrum of 2-heptylthiophene Using Only the Electrometer Detector

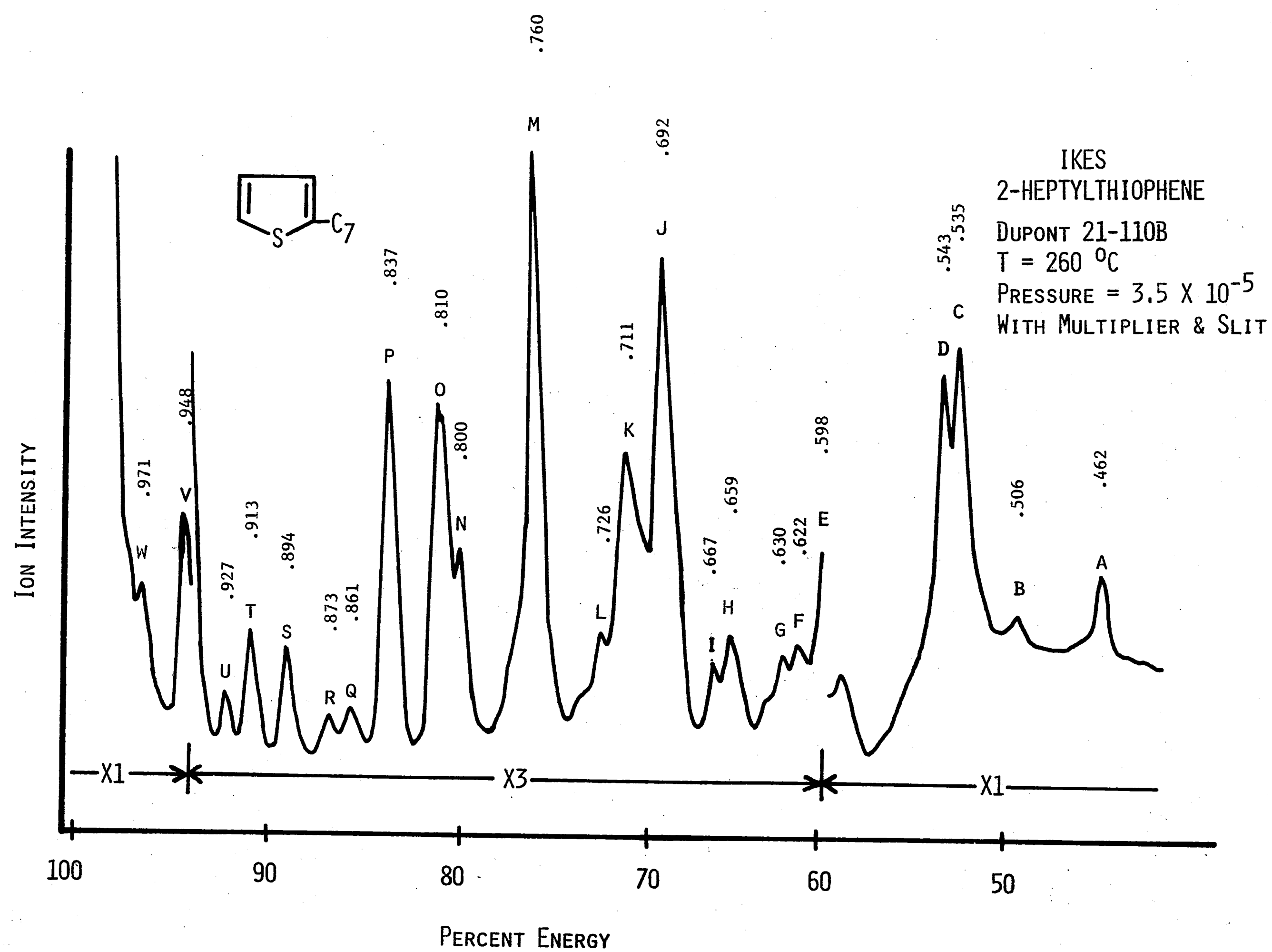

Figure 13. Ion Kinetic Energy Spectrum of 2-heptylthiophene Using the Adjustable β-slit and the Electron Multiplier

recorded with the bilateral ion source slits opened for maximum sensitivity. In Figure 13, although the source slits were left open the adjustable β-slit, electron multiplier, and electrometer were all reduced to bring the peaks on scale. The additional energy resolution in Figure 13 is apparent in the C-D doublet as well as many of the lower intensity peaks. The electron multiplier-adjustable slit assembly was removed from the beam and the apparent masses, m*, of the daughter ions were obtained from the photographic plate. Plate exposures of approximately 10^{-12} - 10^{-11} coulombs were taken. Using Equations (I-4) and (I-5) the metastable transitions in Table II were assigned. No attempt was made to quantify the metastable transitions since generally several daughter ions were present in a recorded metastable peak and the photographic plate was exposed at the metastable peak maximum. The metastable peak maximum corresponds to the maximum intensity resulting from superposition of all metastable peak contributions at that point.

The IKE spectra of the remaining thiophene compounds are reported in Figures 14-26. The metastable transitions were assigned on a basis of the electrostatic sector voltage; however, for major and pertinent peaks for the discussion the apparent mass of the daughter ions were checked with the photographic plate or the electron multiplier following magnetic deflection. The percent electrostatic sector energies indicated are the experimentally determined values. The IKES of thiophene in Figure 14 illustrates the fragmentation of the unsubstituted ring. The molecular ion undergoes multiple bond rupture to lose mass 45, $84^+ \rightarrow 39^+ + 45$, as well as hydrocarbon loss from the molecular ion to form the daughter ion at m/e 45. Loss of sulfur, m/e 32, is common from the molecular or fragment ions as are rearrangements or multiple bond rup-

TABLE II

METASTABLE PEAKS AND TRANSITIONS IN THE IKES OF 2-HEPTYLTHIOPHENE

Metastable Peak	Assigned Transition	Calculated m_2/m_1
a	97 → 45	.464
b	85 → 43	.506
c	182 → 97	.533
	183 → 98	.536
	84 → 45	.536
	55 → 29	.527
d	180 → 98	.544
	97 → 53	.546
e	65 → 39	.600
	111 → 67	.604
	110 → 66	.600
	108 → 65	.602
	97 → 58	.598
f	67 → 41	.612
	182 → 111	.610
	182 → 110	.604
g	43 → 27	.628
h	71 → 45	.634
	153 → 97	.634
i	97 → 63	.649
j	84 → 58	.690
	181 → 125	.691
	111 → 77	.694
k	55 → 39	.709
	97 → 69	.711
l	153 → 111	.726
m	182 → 139	.764
	139 → 105	.755
	110 → 84	.764
n	148 → 119	.804
	149 → 120	.805

TABLE II (Continued)

Metastable Peak	Assigned Transition	Calculated m_2/m_1
o	182 → 148	.813
	183 → 149	.814
p	182 → 153	.841
	183 → 154	.842
q	97 → 84	.866
r	110 → 96	.873
s	29 → 26	.897
t	43 → 39	.907
u	27 → 25	.926
	28 → 26	.929
	29 → 27	.931
	41 → 38	.927
	57 → 53	.930
v	29 → 27	.931
	30 → 28	.933
	43 → 41	.953
	42 → 40	.952
	47 → 45	.957
	41 → 39	.951
	44 → 42	.955
w	27 → 26	.963
	28 → 27	.964
	30 → 29	.967
	39 → 38	.974
	40 → 39	.975
	44 → 43	.977
	46 → 45	.978
	55 → 53	.964
	53 → 51	.962
	67 → 65	.970
	68 → 66	.971
	69 → 67	.971

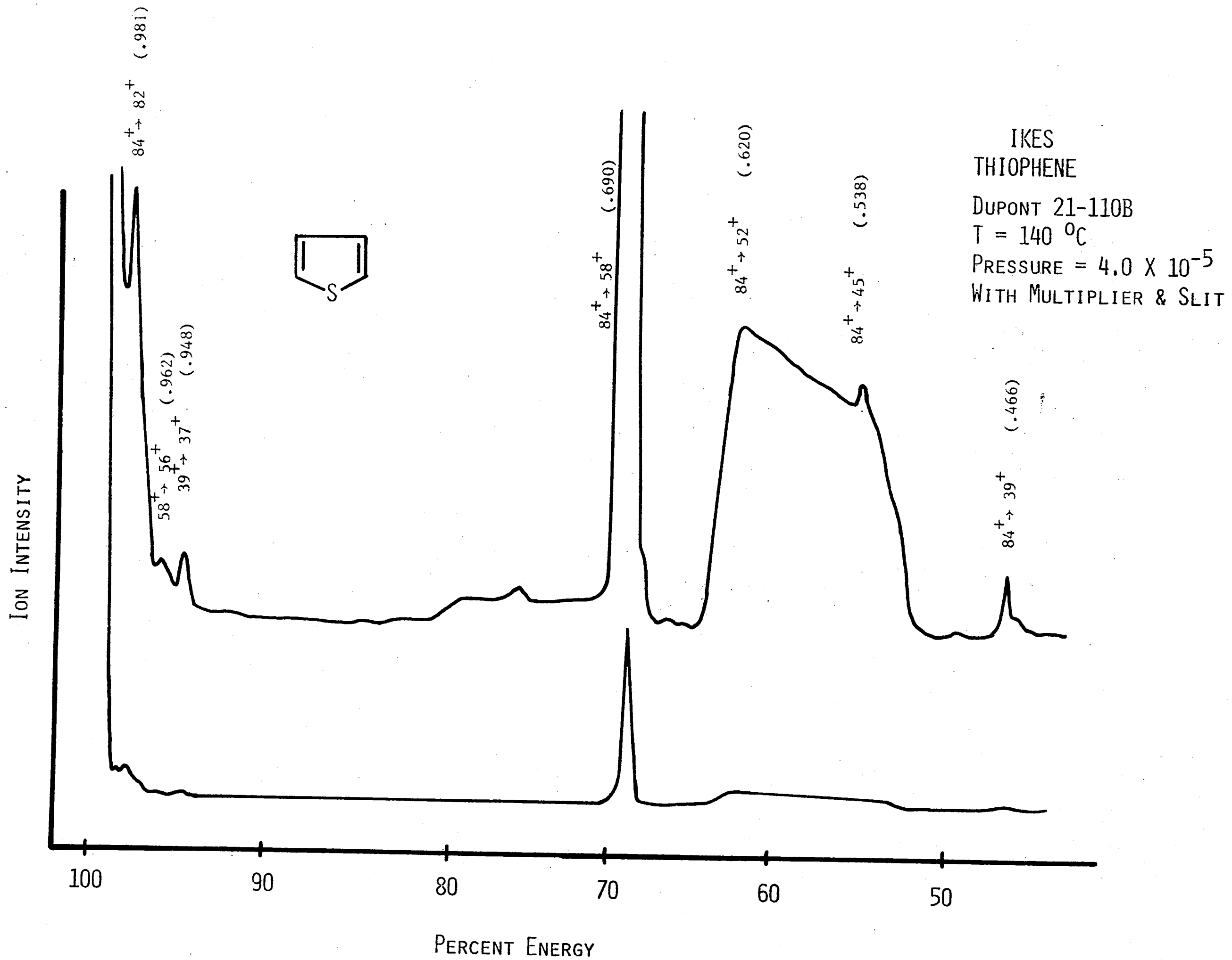

Figure 14. Ion Kinetic Energy Spectrum of Thiophene

tures to lose m/e 34 and m/e 26.

The mass spectra of 2-(2-methylpropyl)thiophene and 2-butylthiophene are similar (36). The differences that do exist in the mass spectra are in intensities at m/e 125 (1.23 vs. .17), m/e 111 (.42 vs. 3.66), m/e 110 (.64 vs. 1.19), m/e 85 (.61 vs. 1.66), m/e 84 (1.11 vs. 2.59), and m/e 77 (.95 vs. 1.72). The numbers in parentheses are the percent of the base peak, m/e 97, contributed to a given ion fragment by 2-(2-methylpropyl)thiophene and 2-butylthiophene respectively.

The differences in the mass spectral intensities can be explained by the metastable transitions in their respective IKE spectra, Figures 15 and 16. The loss of m/e 29 from the molecular ions to form m/e 111 is observed in the IKES at 79.3% of the electrostatic sector energy. The 79.3% peak in the IKES of 2-butylthiophene is a significant metastable transition. The m/e 111 peak is small in the 2-(2-methylpropyl) thiophene mass spectra since it is probably not a simple fragmentation but requires at least one rearrangement; however, daughter ions at m/e 111 do occur in the IKES at 79.3% and 88.8% of the electrostatic sector energy. These fragmentations, although they do occur in 2-(2-methylpropyl)thiophene, do not have sufficiently large rate constants to be of any consequence in the time frame of the mass spectra. The metastable transition indicating the loss of a methyl group from the 2-(2-methylpropyl)thiophene molecular ion is present in the IKES as is the large peak indicating the loss of m/e 41 at 71.2% of the electrostatic sector energy. At an electron energy of 70 eV fragment ions resulting from rearrangements will be observed in the mass spectra; however, they may be minor peaks. In the IKES daughter ions resulting from transitions requiring rearrangements will generally account for a

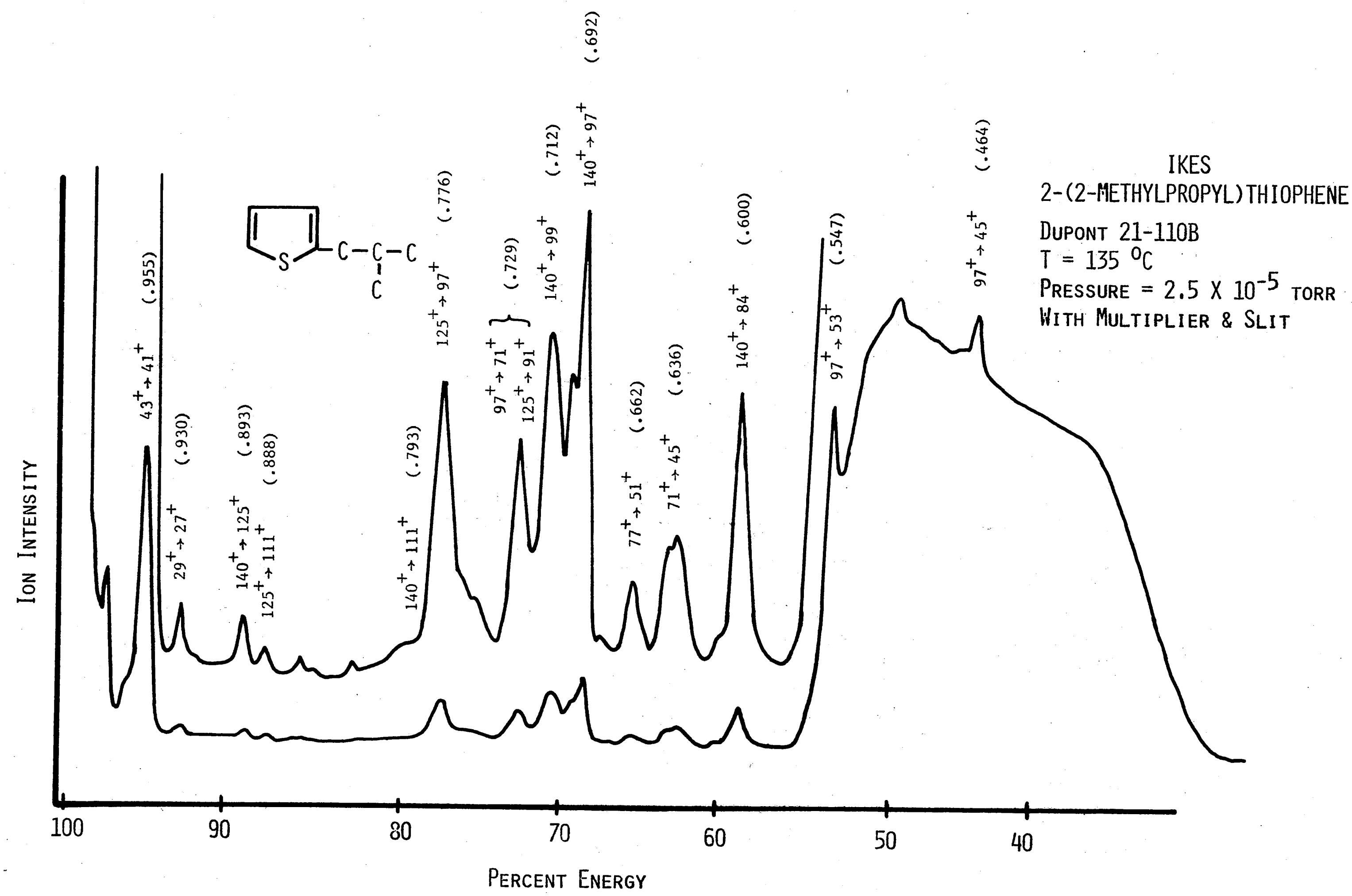

Figure 15. Ion Kinetic Energy Spectrum of 2-(2-methylpropyl)thiophene

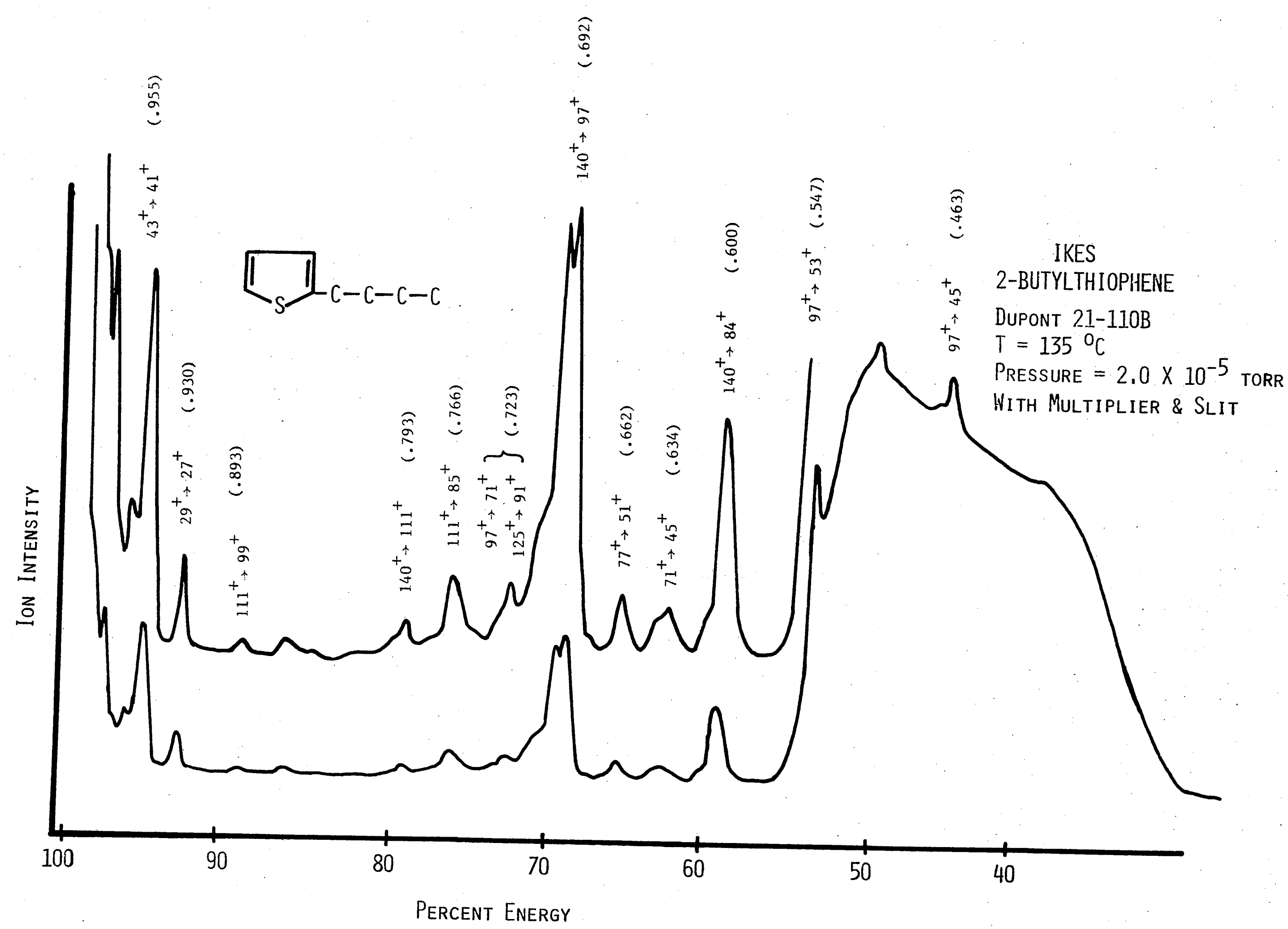

Figure 16. Ion Kinetic Energy Spectrum of 2-butylthiophene

larger part of the total ion current than the ions in the mass spectra. Examples of large metastable peaks in the IKES resulting from rearrangements are $140^+ \rightarrow 84^+$ and $97^+ \rightarrow 53^+$ in both 2-butylthiophene and 2-(2-methylpropyl)thiophene as well as $140^+ \rightarrow 99^+$, $125^+ \rightarrow 91^+$, and $140^+ \rightarrow 111^+$, in 2-(2-methylpropyl)thiophene and $110^+ \rightarrow 77^+$, $140^+ \rightarrow 84^+$, and $97^+ \rightarrow 53^+$ in 2-butylthiophene.

Analysis of mixtures of small amounts (a few percent) of either 2-butylthiophene in 2-(2-methylpropyl)thiophene or 2-(2-methylpropyl)-thiophene in 2-butylthiophene can be done on any mass spectrometer which has good reproducibility of peak intensities (e.g. a Dempster mass spectrometer). The analysis could be done with the intensity variation at m/e 125 for the first mixture and m/e 111 for the second. The analysis using IKES could be done on small amounts of 2-butylthiophene in 2-(2-methylpropyl)thiophene using the $140^+ \rightarrow 111^+$ transition if it is shown to be a true first order decomposition. The analysis of small amounts of 2-(2-methylpropyl)thiophene in 2-butylthiophene using IKES would be more difficult. With higher energy resolution (.1% or better) the metastable decomposition, $111^+ \rightarrow 99^+$, in 2-butylthiophene could be separated from $140^+ \rightarrow 125^+$ in 2-(2-methylpropyl)thiophene; the $111^+ \rightarrow 99^+$ transition could then be used for the analysis.

The IKES of the 2-(1,1-dimethylethyl)thiophene, Figure 17, is significantly different from that of either 2-(2-methylpropyl)thiophene or 2-butylthiophene; however, these mass spectra are also different. The base peak is at m/e 125 with large fragment ions at m/e 140 (25%), m/e 97 (17%), and m/e 85 (12.3%).

Figures 18-23 are IKES of alkylthiophenes substituted in the 2 or 2,5 positions. The daughter ions observed result in large part from

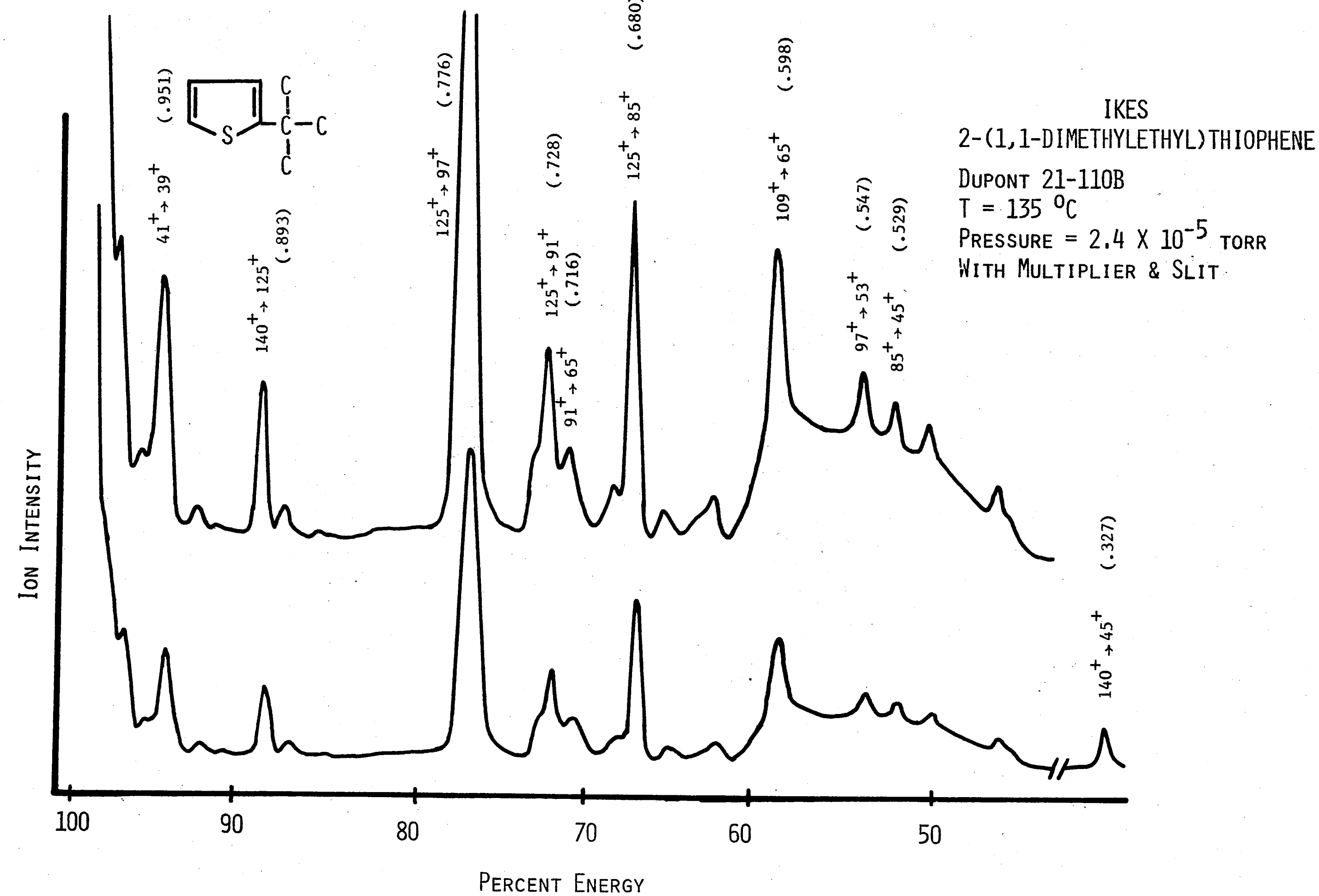

Figure 17. Ion Kinetic Energy Spectrum of 2-(1,1-dimethylethyl)thiophene

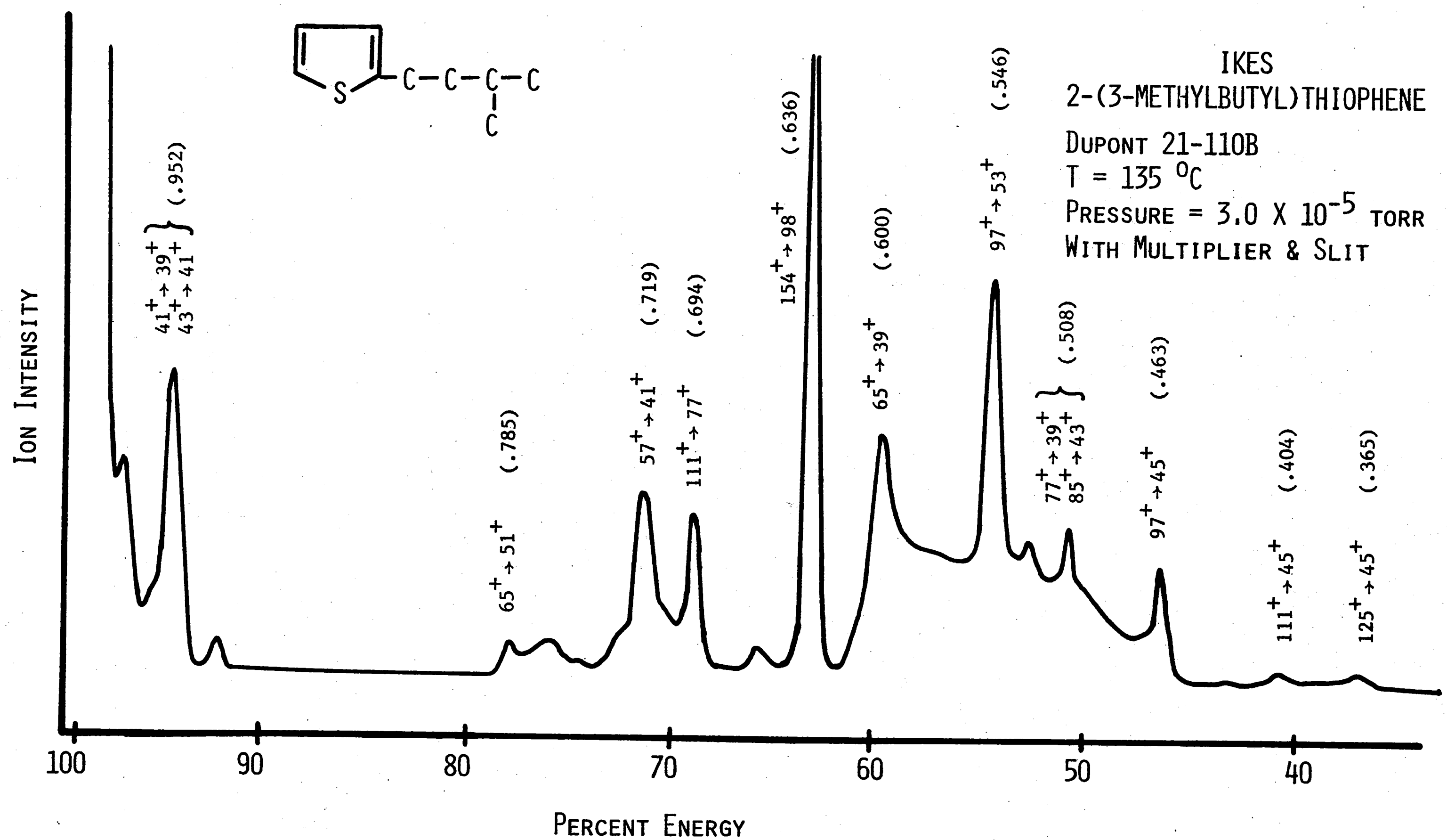

Figure 18. Ion Kinetic Energy Spectrum of 2-(3-methylbutyl)thiophene

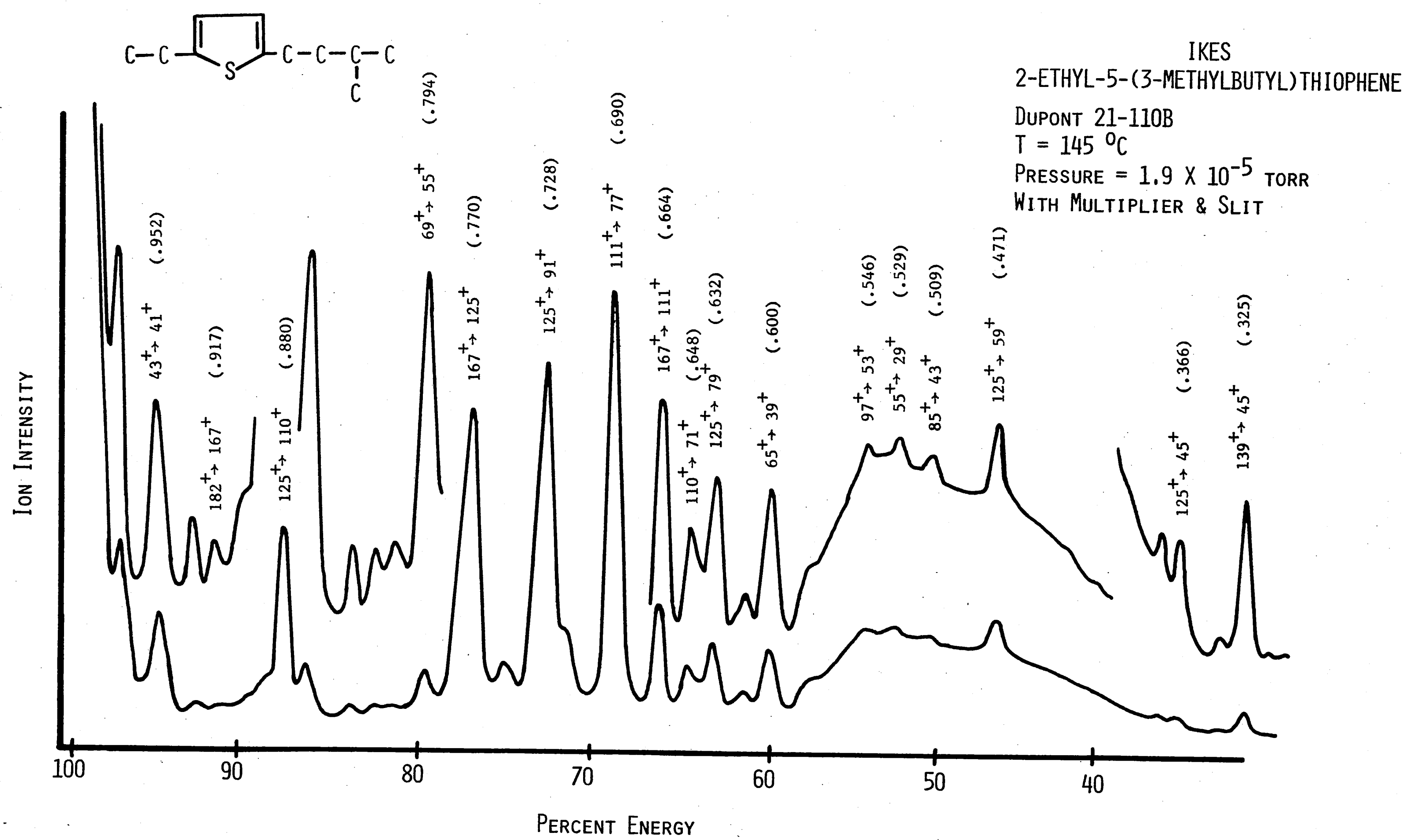

Figure 19. Ion Kinetic Energy Spectrum of 2-ethyl-5-(3-methylbutyl)thiophene

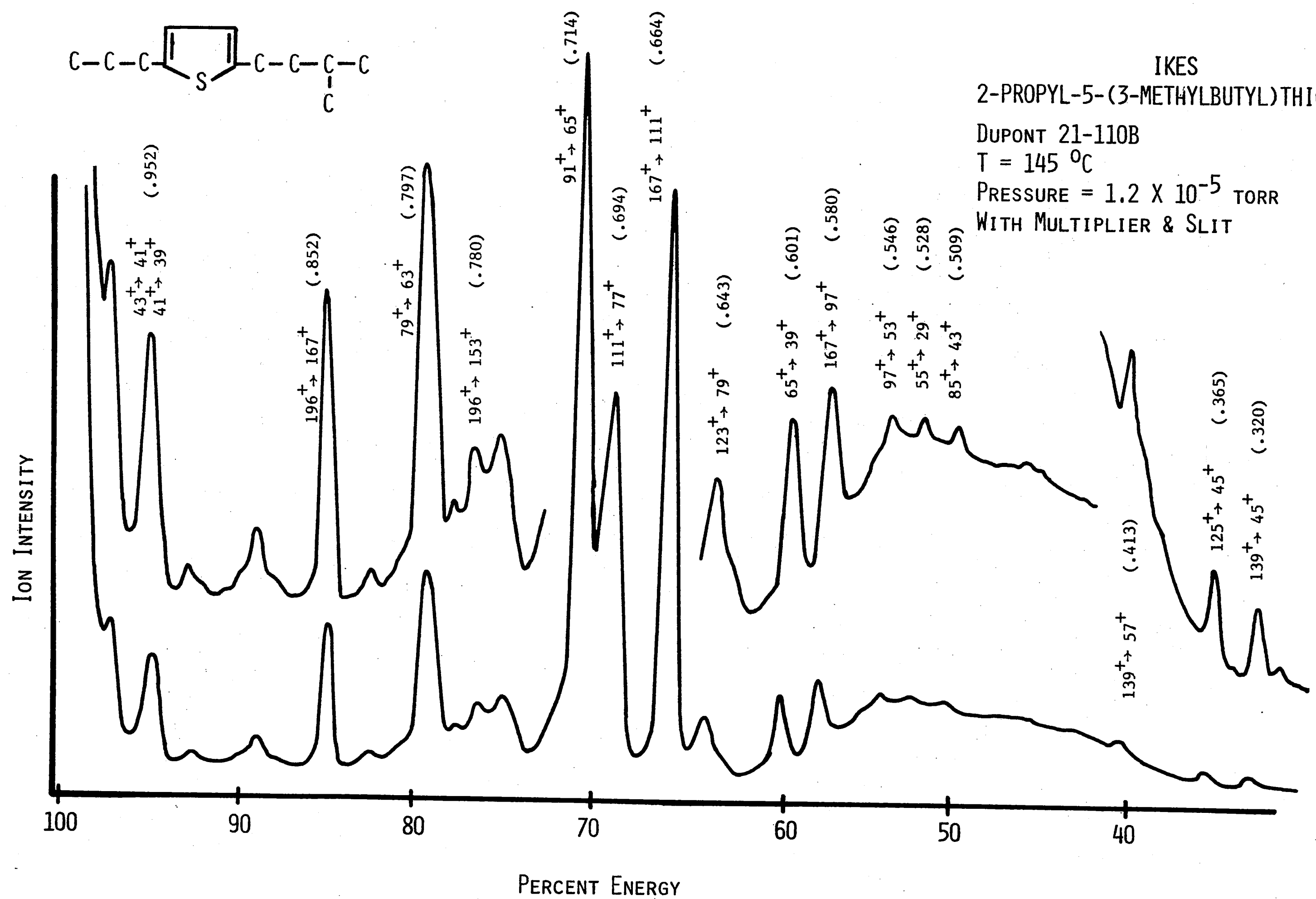

Figure 20. Ion Kinetic Energy Spectrum of 2-propyl-5-(3-methylbutyl)thiophene

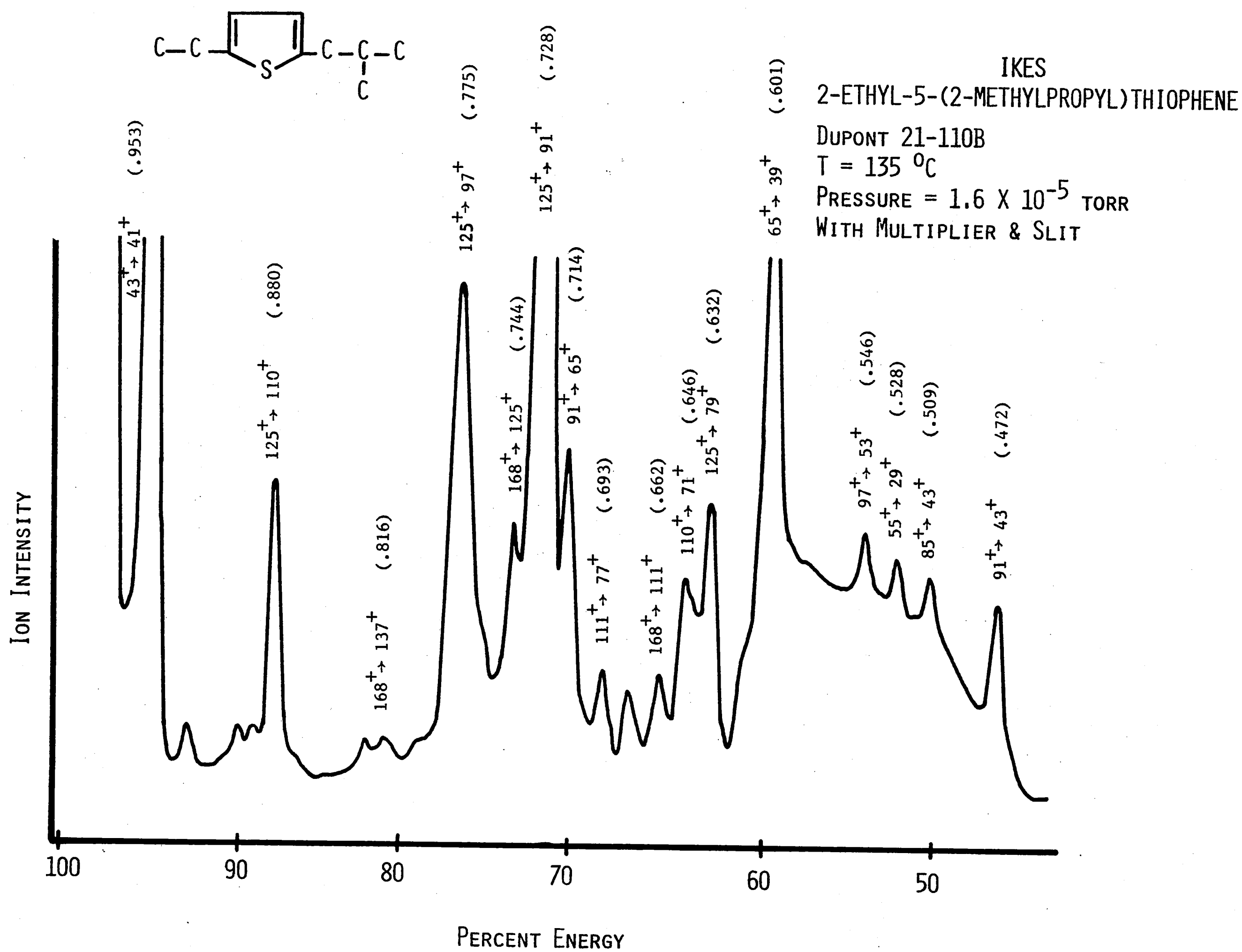

Figure 21. Ion Kinetic Energy Spectrum of 2-ethyl-5-(2-methylpropyl)thiophene

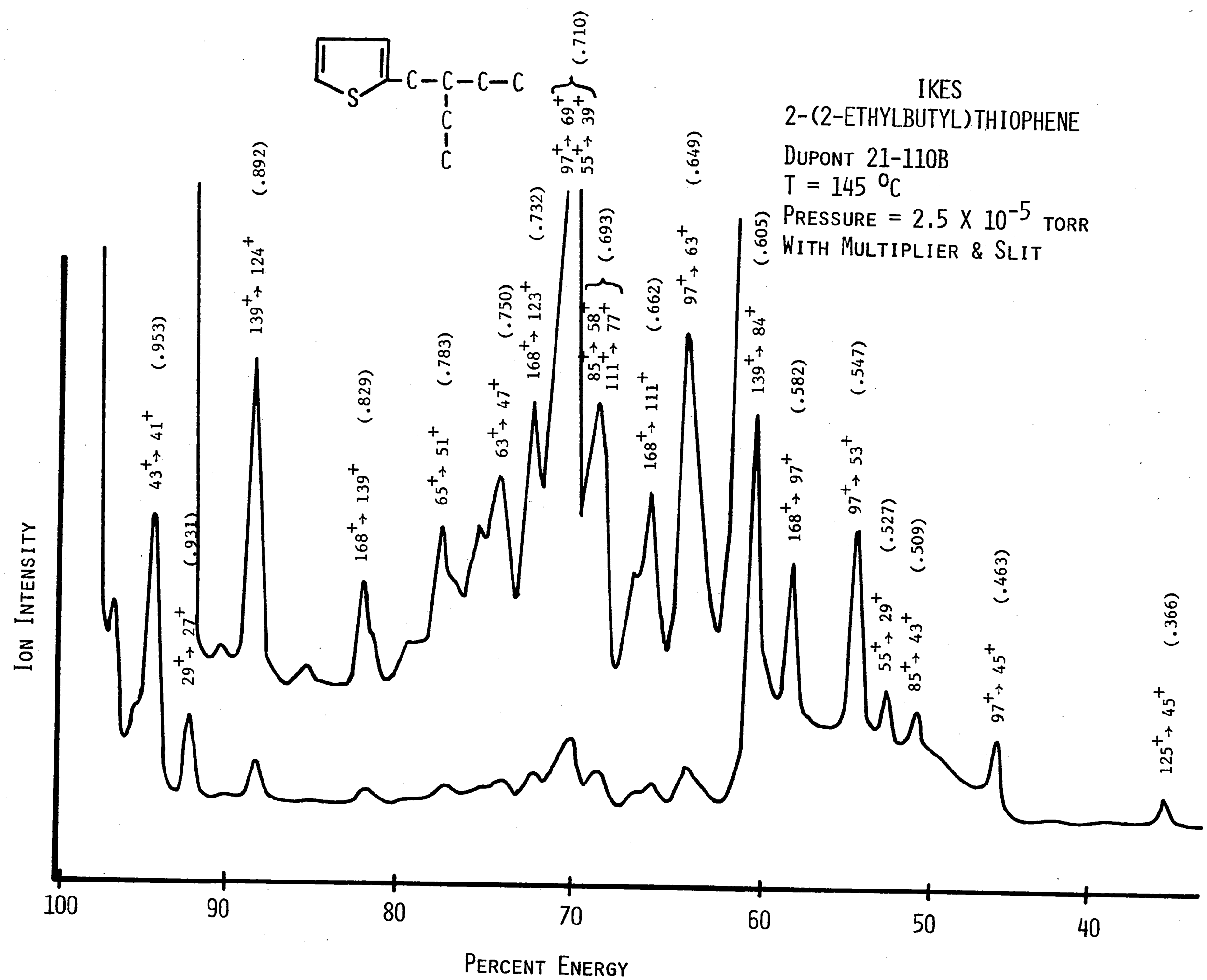

Figure 22. Ion Kinetic Energy Spectrum of 2-(2-ethylbutyl)thiophene

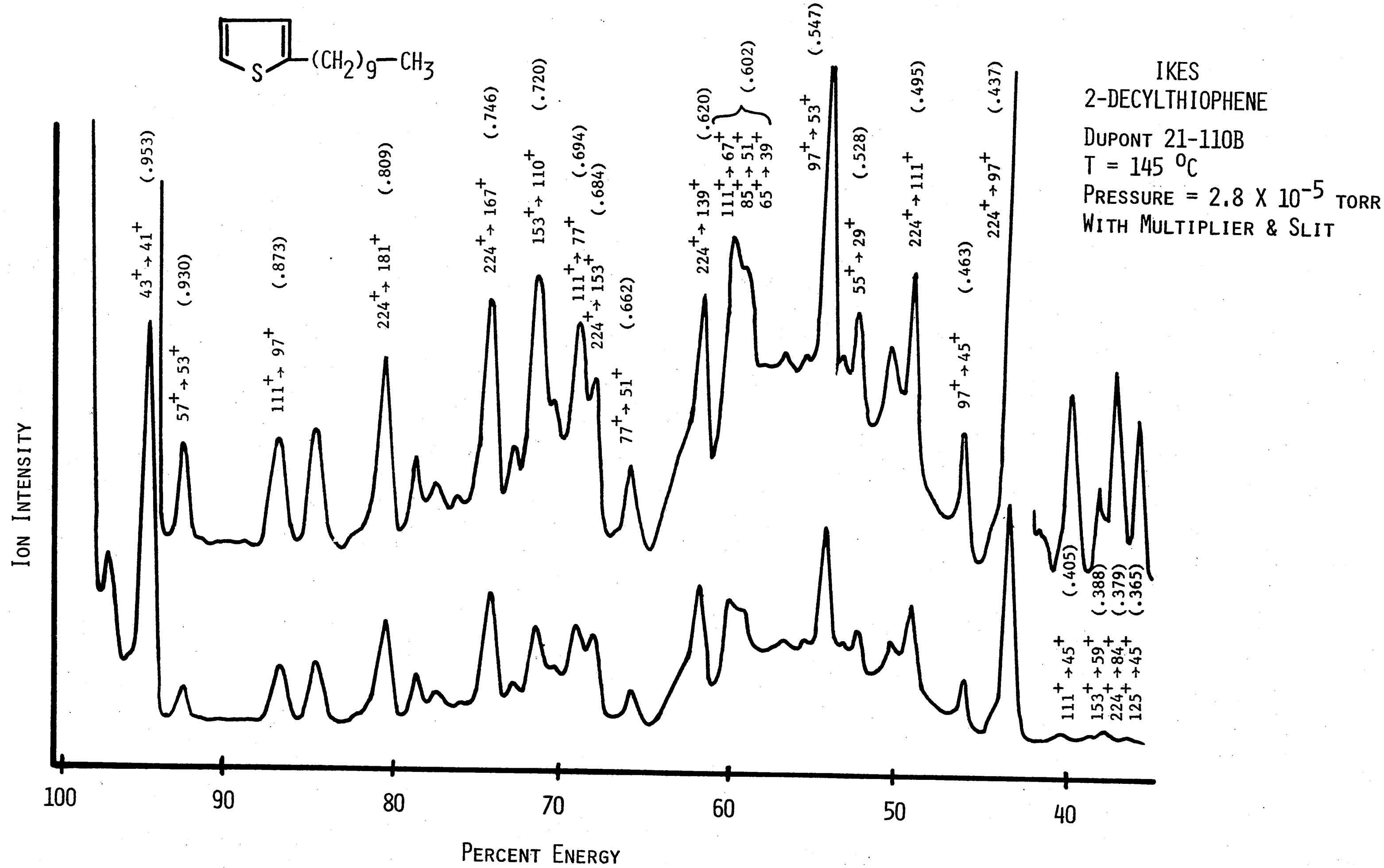

Figure 23. Ion Kinetic Energy Spectrum of 2-decylthiophene

decompositions of hydrocarbon fragment ions (e.g. $91^+ \rightarrow 65^+$, $65^+ \rightarrow 39^+$, $43^+ \rightarrow 41^+$, etc.) and loss of sulfur fragments (HS, H_2S, HCS, H_3C_2S, etc.) from the molecular ions and large fragments. Metastable decompositions from the molecular ions give daughter ions which predominately contain the sulfur atom. The alkylthiophenes substituted in the 2-position have large metastable transitions from the molecular ion to the base peak of the mass spectra, Figures 13-18, 22, and 23. The mono-substituted thiophenes which have large or branched alkyl groups have significant transitions from the molecular ion to m/e 111 (97+14) and m/e 125 (97+28).

The IKES of the 2,5-dialkylthiophenes rich in transitions usually exhibit significant transitions from the molecular ions. For example, 2-propyl-5-(3-methylbutyl)thiophene, Figure 20, and 2-ethyl-5-(2-methylpropyl)thiophene, Figure 21, unlike 2-ethyl-5-(3-methylbutyl)thiophene, Figure 19, have prominent metastable peaks from the molecular ions. A characteristic transition of dialkylthiophenes with molecular weights greater than 168 is $167^+ \rightarrow 111^+$.

The IKES of benzo[b]thiophene, Figure 24, contains several intense metastable peaks which result from fragmentation of the molecular ion by multiple bond ruptures and/or rearrangements. The most intense metastable peak results from the loss of m/e 45 from the molecular ion. A similar fragmentation pattern occurs in 6-methylbenzo[b]thiophene and 2-benzylthiophene, Figures 25 and 26, with major metastable peaks resulting from the loss of m/e 45, 26, 32, 59, and 71 from the molecular ion.

As indicated previously, high mass resolution is required to separate the molecular ions of the large thiophene compounds from those of hydrocarbons at the same nominal mass. Specifically, 2-heptylthiophene

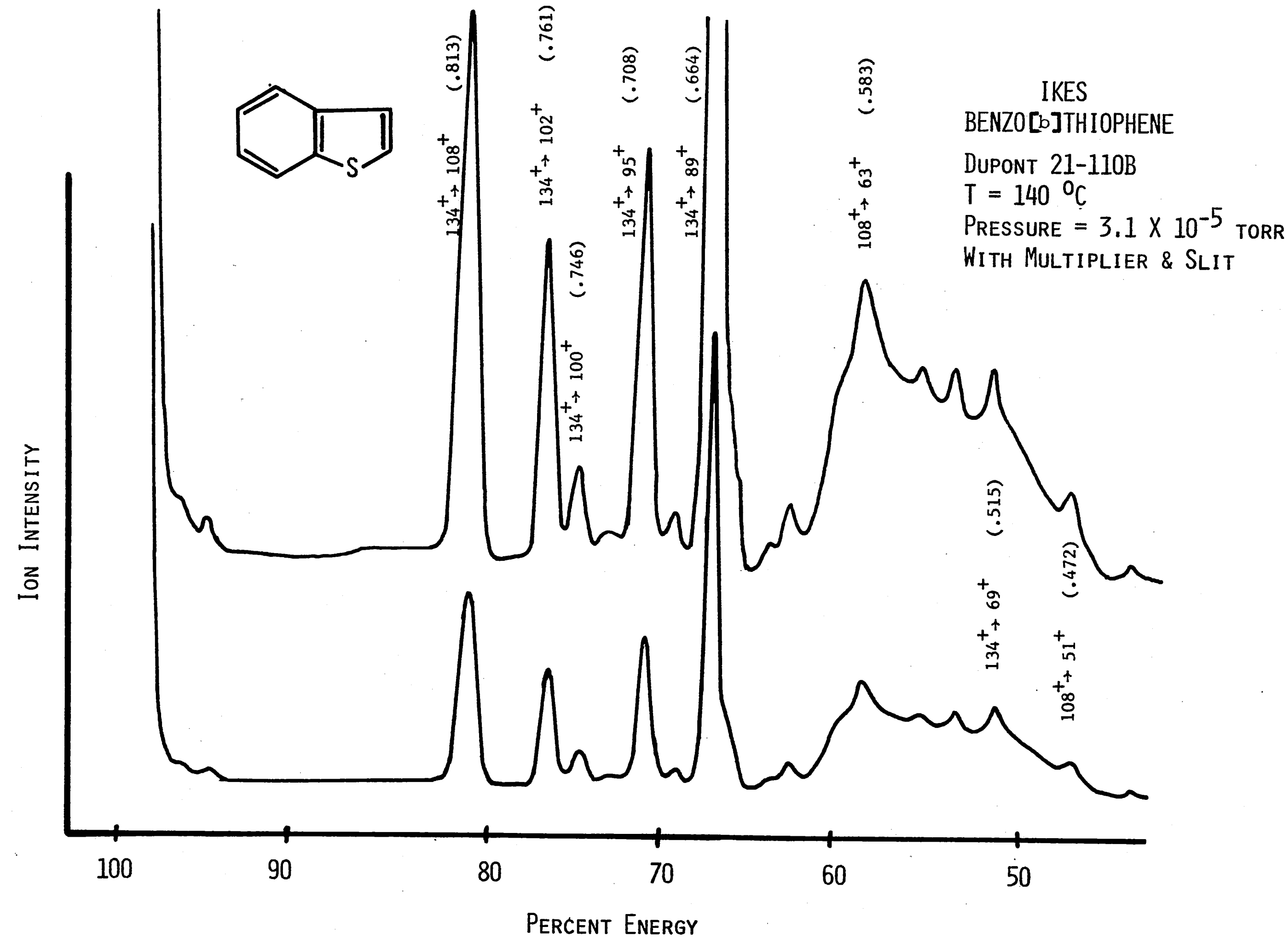

Figure 24. Ion Kinetic Energy Spectrum of Benzo[b]thiophene

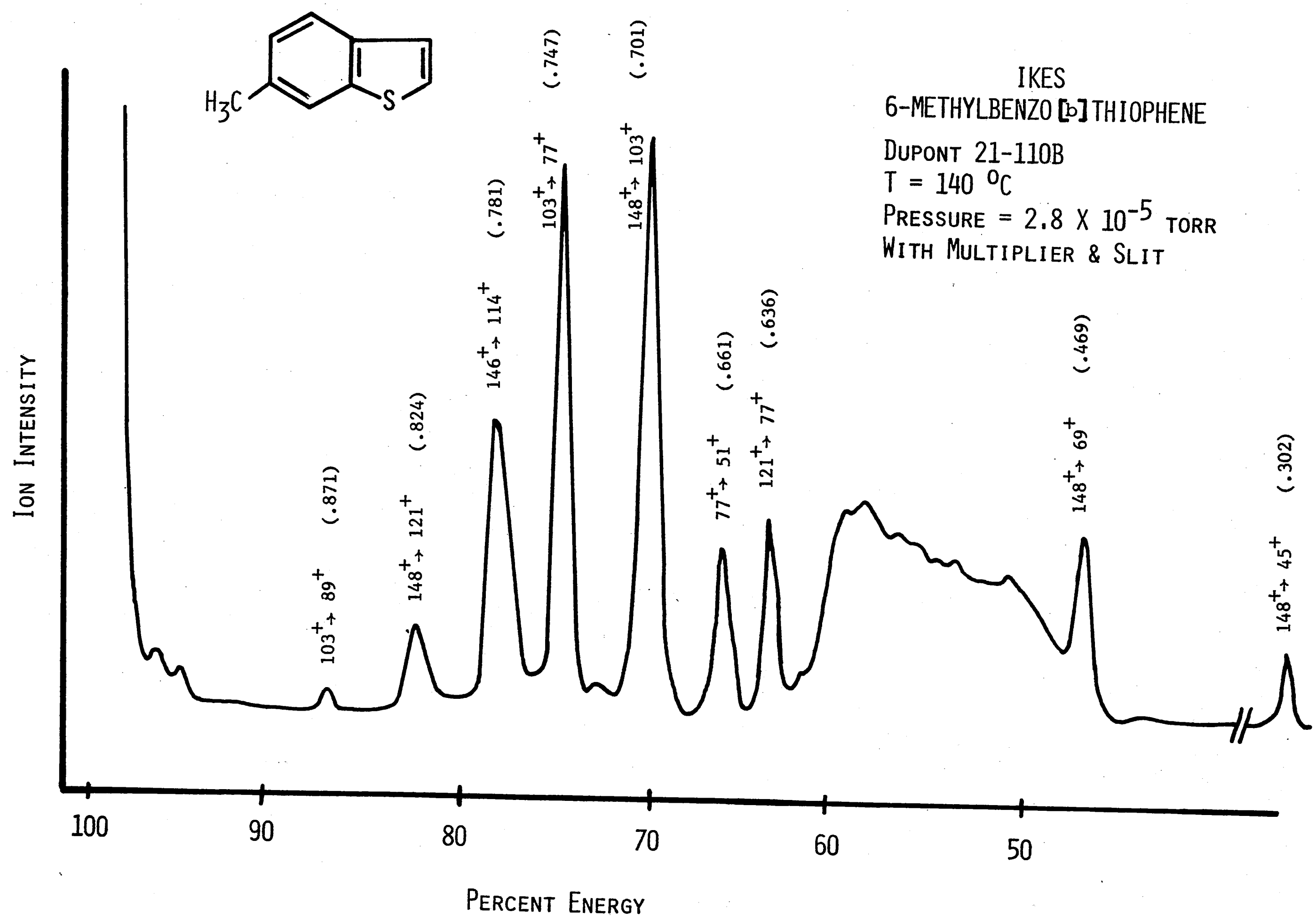

Figure 25. Ion Kinetic Energy Spectrum of 6-methylbenzo[b]thiophene

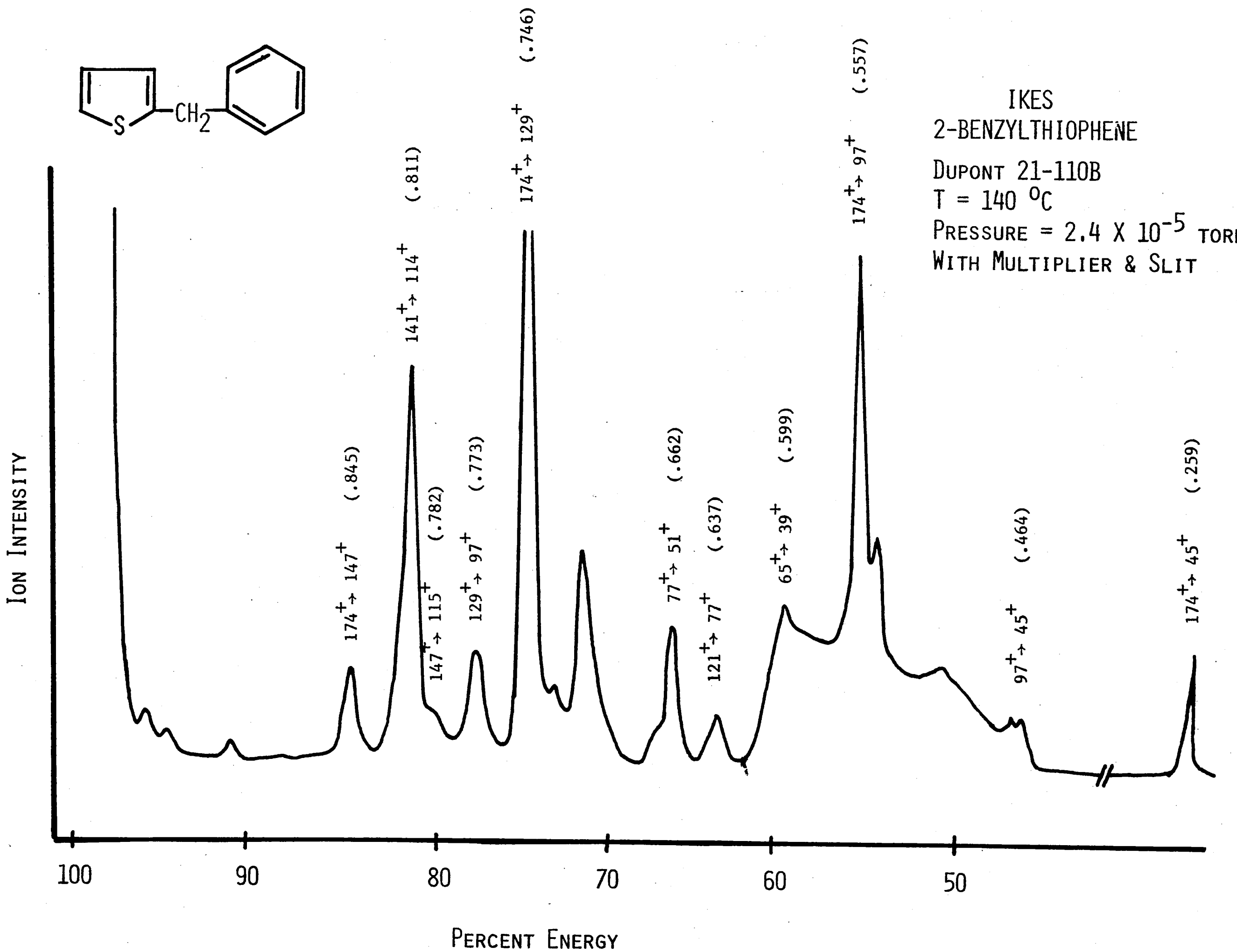

Figure 26. Ion Kinetic Energy Spectrum of 2-benzylthiophene

has a molecular weight of 182.1129 and bibenzyl has a molecular weight of 182.1095. The mass resolution required to separate the molecular ions would be in excess of 53,000. Although the fragmentation patterns are quite different for the two compounds, in mixtures containing homologous compounds common ions would make identification difficult. The IKES could be helpful in identification of the two compounds in the mixture. The IKES of 2-heptylthiophene, Figure 13, has several transitions from the molecular ion (peak c, m, o, and p). In the IKES of bibenzyl, Figure 27, there are two transitions from the molecular ion. Whereas in the mass spectra identification of m/e 182 in the mixture would be difficult, requiring high mass resolution, the same problem is not present in the IKES. If sufficient energy resolution is not possible to resolve the transitions at the β-slit, the daughter ions at the specific electric sector voltage can be mass analyzed giving a unique assignment to each transition.

To explore the uses of IKES further, higher energy resolution and increased sensitivity would be beneficial. The increase in energy resolution and sensitivity was explored by theoretical modification of the ion optical path.

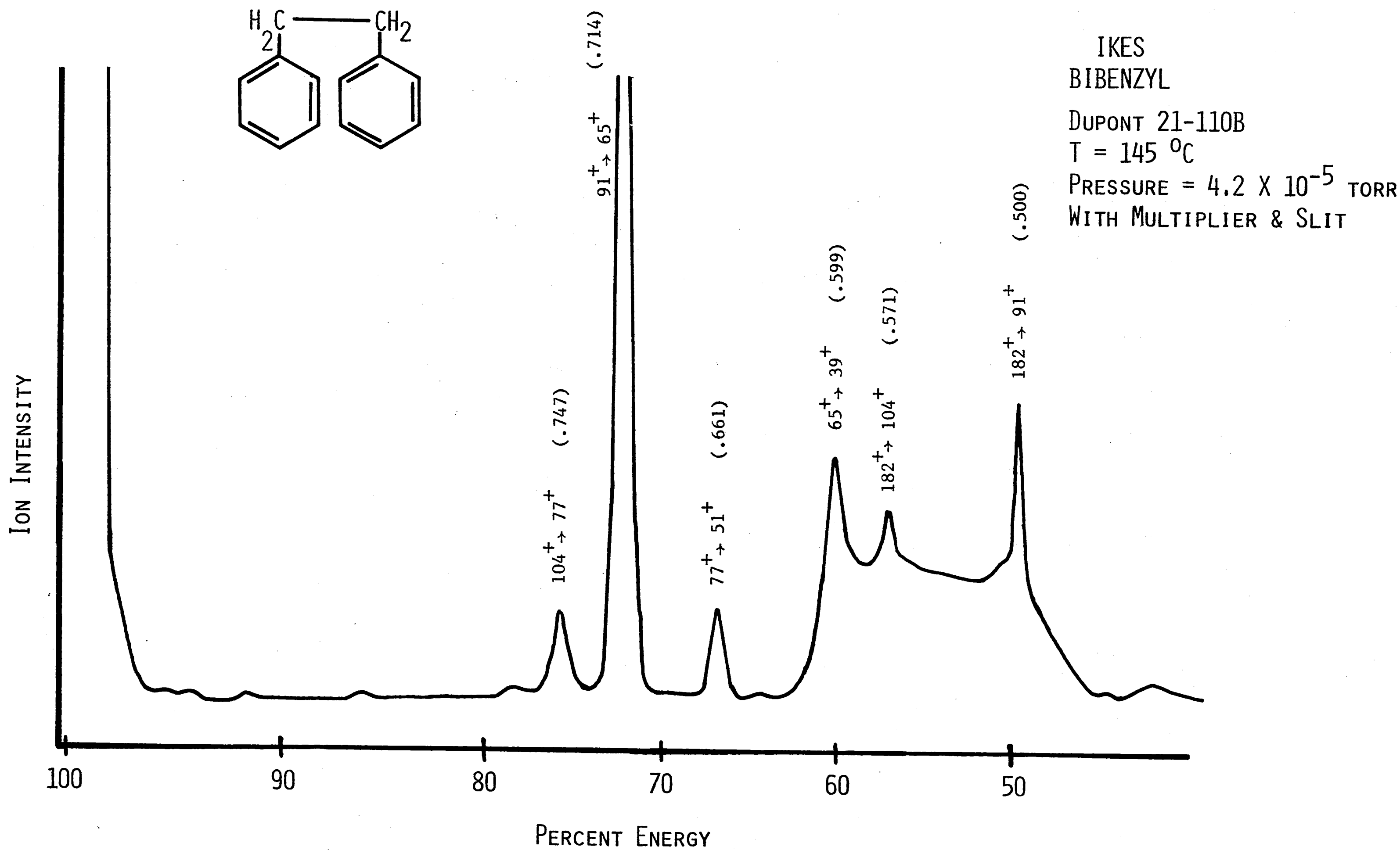

Figure 27. Ion Kinetic Energy Spectrum of Bibenzyl

CHAPTER IV

FURTHER IMPROVEMENTS IN ENERGY RESOLUTION FOR A MATTAUCH-HERZOG MASS SPECTROMETER

In the Mattauch-Herzog geometry the ion source is placed at the focal point of the electric sector giving rise to ions whose trajectories in the second field-free region are parallel to each other (38). The interdependence of the solid angle and energy bandwidth which was discussed quantitatively in Chapter II is represented in Figure 28. (39) In Figure 28(a), the β-slit is opened to transmit all ions of energy eU_o that have passed the α-slit. The ions with energy $e(U_o + \Delta U)$ exiting the electric sector also form a parallel beam but make a small angle with the beam of ions with energy eU_o. The ions with the higher energy $e(U_o + \Delta U)$ are partially cut off by the β-slit; for these ions the β-slit acts as a one-sided α-stop. In Figure 28(b) the β-slit is closed to allow only the ions at the extremes of the beams with energy $e(U_o + \Delta U)$ and $e(U_o - \Delta U)$ to pass. In this second case the energy pass of the β-slit increases with the width of the α-slit.

A proposed solution to this problem of interdependence has been to use two radial electrostatic sectors instead of one (40). The β-slit could then be placed between the first and second electrostatic sector; if proper geometry is maintained, excellent energy resolution would be achieved. Although this solution is no doubt possible, it was not considered for two reasons: (1) it would require severe modification of

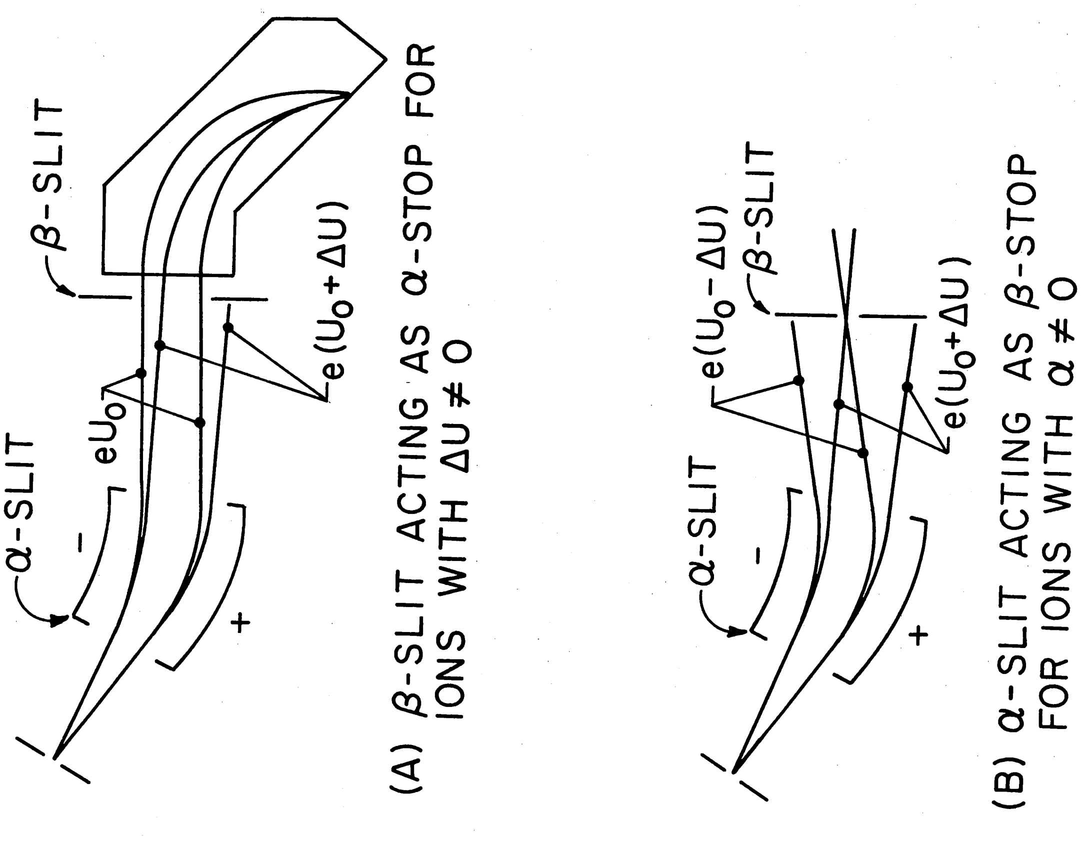

Figure 28. Interdependence of Solid Angle and Energy Bandwidth in a Mattauch-Herzog Mass Spectrometer

the optical bench and expense in obtaining an appropriate electrostatic sector; and (2) it would effectively exclude the Mattauch-Herzog portion of the instrument from the energy focusing for ion kinetic energy spectra.

A second approach to the problem of interdependence of the solid angle and energy bandwidth was that of Liebl (39). He had suggested the incorporation of a single linear three-element electrostatic lens in the second field-free region as indicated in Figure 29. Such lenses are often called *Einzel* lenses. There is one additional characteristic this electrostatic lens must have for ion kinetic energy spectra not considered by Liebl in his application to conventional mass spectrometry. With IKES, as the radial electrostatic voltage is decreased to pass daughter ions of lower energy, the voltage on the three-element electrostatic lens would also have to be changed. The voltage on the lens must be changed in such a way as to maintain a constant focal length for the ions with the proper energy (those ions whose energies are in the proper ratio to the radial electrostatic sector voltage). To avoid having to design a power supply for the three-element lens which would be scanned as some non-linear function of the radial electrostatic sector voltage, it would be desirable to design the lens such that its focal length would be constant as its applied voltage maintains a constant-ratio to the radial electrostatic sector voltage, i.e.

$$\frac{\text{Voltage}_{\text{(lens)}}}{\text{Voltage}_{\text{(radial electrostatic sector)}}} = \text{constant} \qquad \text{(IV-1)}$$

In this way as two daughter ions enter the lens system with kinetic

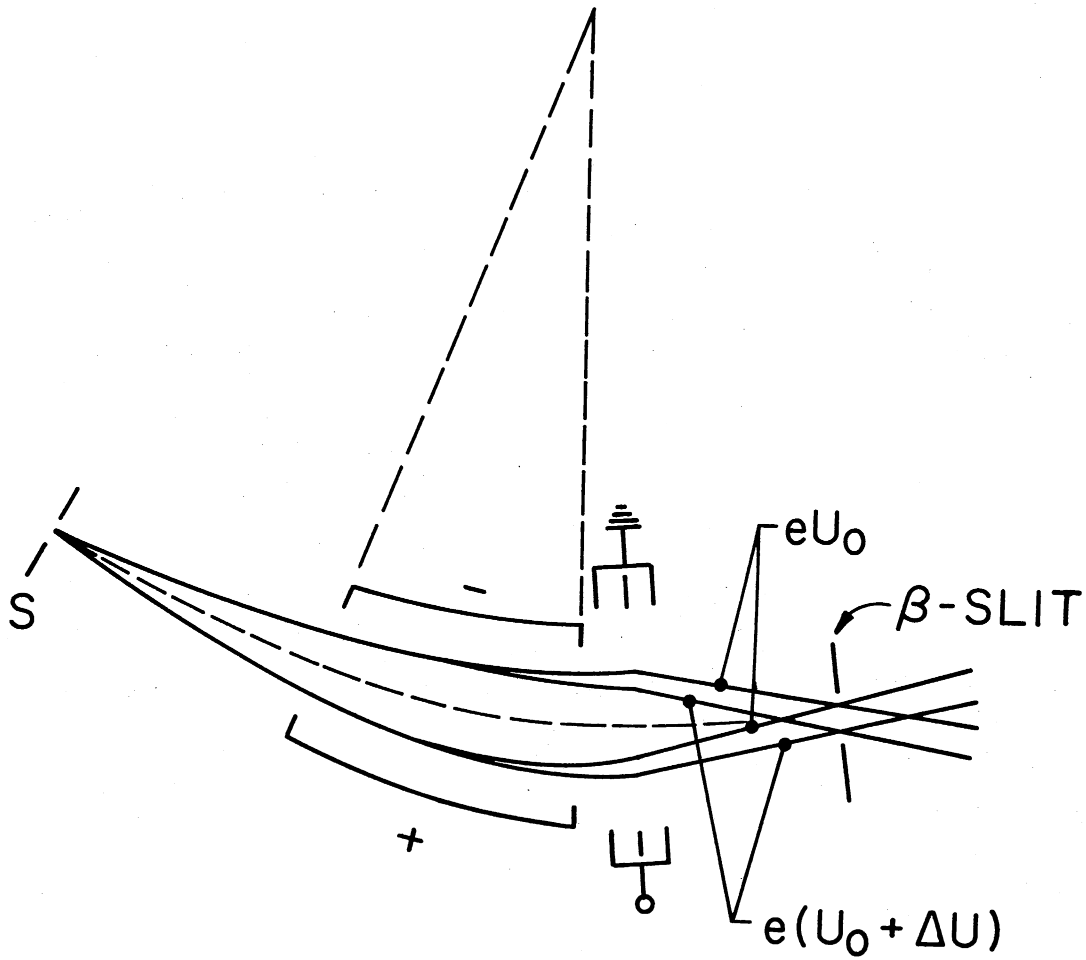

Figure 29. Incorporation of an *Einzel* Lens After a $\Pi/4\sqrt{2}$ Radial Electric Sector

energies eU_o and $e(U_o + \Delta U)$, their focal length and hence their image size at the β-slit would be a function only of their kinetic energy. Although this modification would improve ion kinetic energy discrimination at the β-slit, the double focusing properties of the instrument would be lost if this lens were energized during conventional mass spectra analysis.

Experimental focal properties of linear three-element electrostatic lenses have been compiled and discussed by Septier (41), the essential properties of which are illustrated in Figure 30. The ratio of potentials for the single lens, R_{sl}, contains the potentials of the two outer and the inner electrodes as well as the kinetic energy of the incident particle, U_a, U_i, and U_o respectively. The inverse of the focal length of the lens, K, is given as a function of lens potentials, R_{sl}. For given U_a and U_i particles entering the lens normal, with a range of kinetic energies sufficient to give rise to R_{sl} values of .5 - .6 are focused to approximately equal focal lengths. However, if the potentials on the lens are adjusted to yield R_{sl} values of -0.1 to 0.1 (actual values depending upon the specific lens chosen), a small difference in ion energies yields a large difference in focal lengths. It is this later case that is of most interest in increasing the energy discrimination of the Mattauch-Herzog instrument for ion kinetic energy spectra.

Due to the demand on our instrument for conventional mass analysis, it was decided that the proposed incorporation of a linear three-element electrostatic lens be investigated computationally prior to any experimental modification. For computational purposes the ions were considered as point particles, and the influence of their charges on those of the electrodes, as well as other ions, was ignored so the focusing

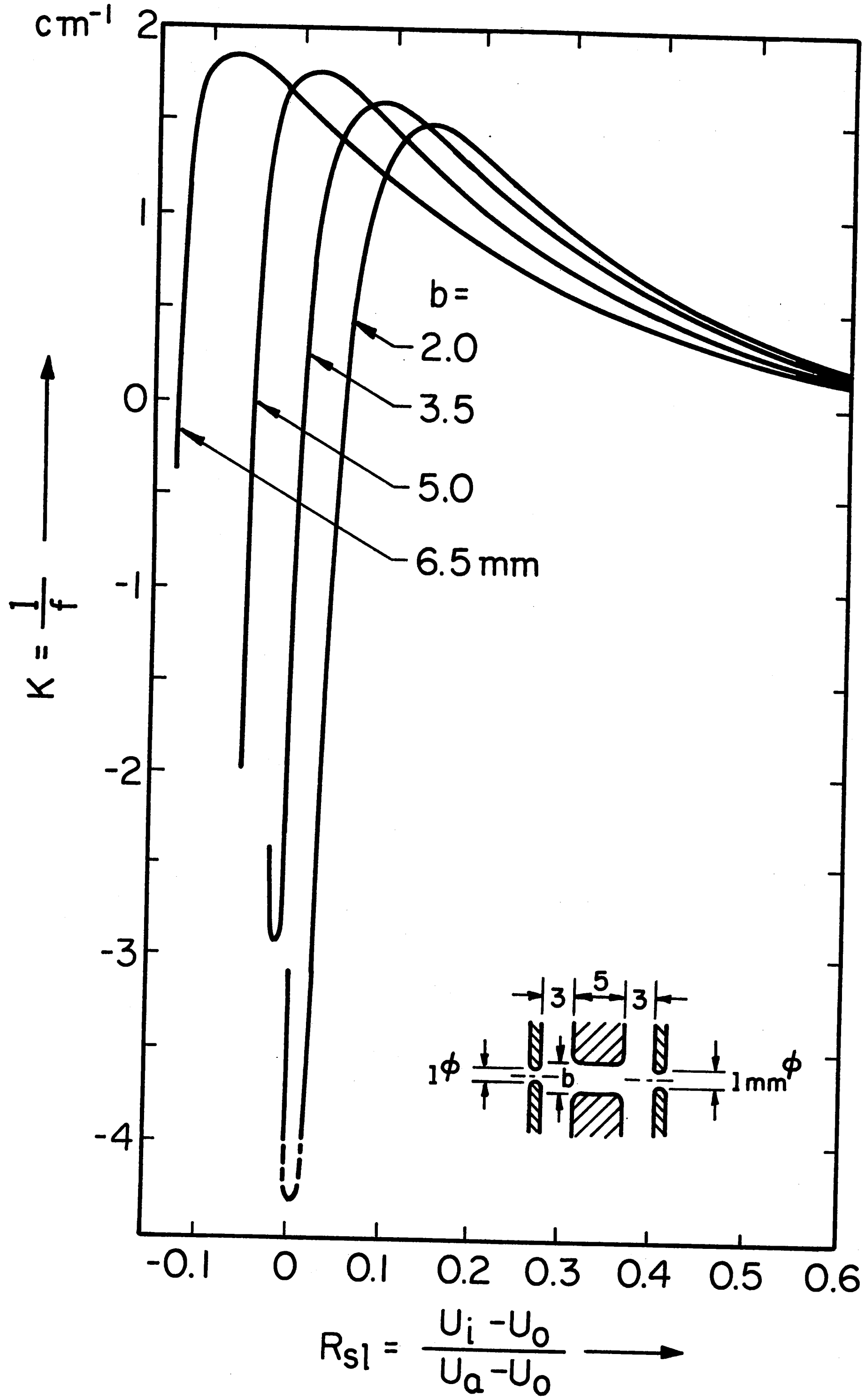

Figure 30. Power Characteristics of Three Element Electrostatic Lenses. (Taken From Reference 41)

field could be calculated independently of the beam it is to focus. This approximation is acceptable in the case of low particle flux beams. Furthermore, all electrode surfaces were treated as ideal in that no charge build-up or screening was considered at the electrode surfaces (42).

In the calculation of the ion focal properties of slit-aperture electrostatic lenses, it is usually necessary to first determine accurately the potential distribution within the lens system. At present, the most widely used method involves computation of tens of thousands of potentials at mesh points by numerical relaxation and interpolation between points by either Lagrange formulas (43) or cubic splines (44). The present experimental methods, such as the electrolytic plotting tank (45) and the resistor network (46), require special equipment and are very time consuming if one is to obtain potentials of sufficient accuracy for trajectory analysis.

Despite the popularity of the numerical relaxation method, it requires substantial computer time and generates potentials at a large number of points outside the region of interest (47). For this reason the method of Conformal Mapping was used. With the knowledge of potentials and potential gradients throughout the lens system, ions with known mass and initial momentum were traced through the lens.

If the electrodes and slits of the three-element lens in Figure 31 are treated as infinite in the x and z directions, then the lens can be treated as two dimensional in the xy plane. The electrode system is now considered mathematically as a degenerate polygon in the complex z-plane (x + iy). As the boundary of the electrode system and the associated electrostatic field can be rather complicated, the region

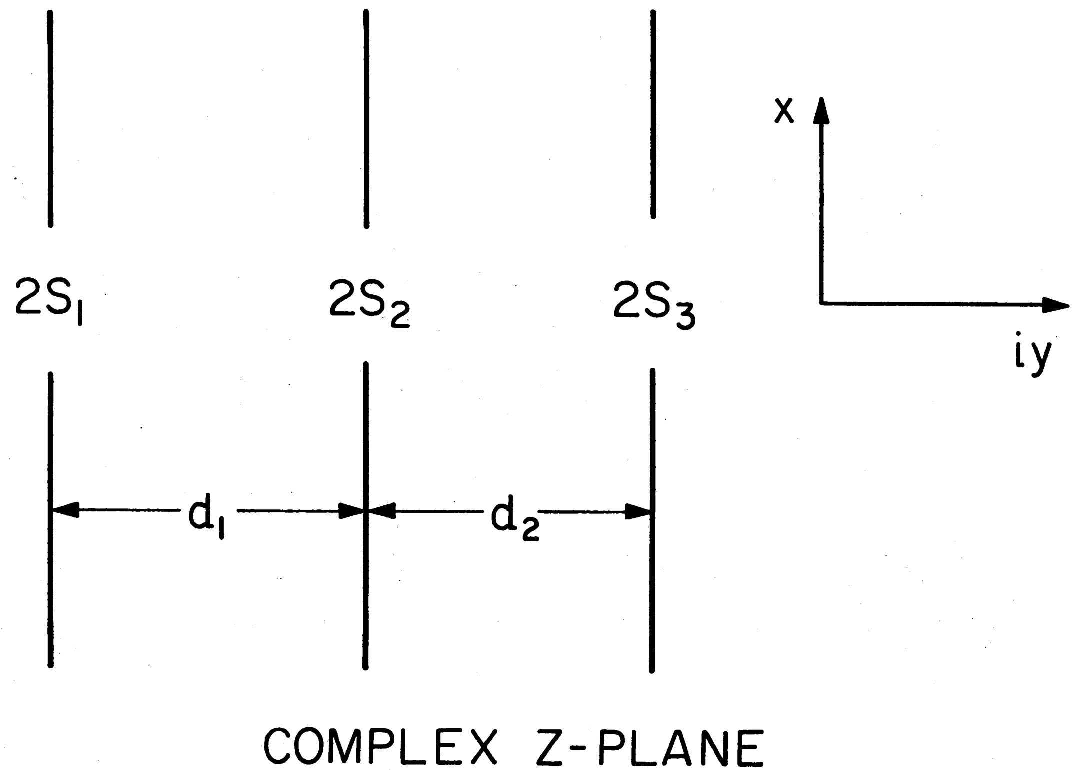

Figure 31. XY Cross-sectional Plane of a Three Apertured Planes Lens System (Six Electrodes)

between the projections of the slits was mapped on the positive imaginary half of a complex w-plane (u + iv) Figure 32. This conformal mapping is best accomplished by the Schwarz-Christoffel transformation (48,49) which is applicable to bounded polygons. In this transformation LaPlace's equation is invariant; so the same equation must be solved in the w-plane but with simplier boundary conditions.

The potential distribution along the center line of the lens system can be obtained in closed form (Appendix A) whereas off-axis potentials near the main axis are computed by series expansion (48).

$$V(x,y) = V(o,y) + \left(\frac{\partial V}{\partial x}\right)_{o,y} x + \frac{1}{2}\left(\frac{\partial^2 V}{\partial x^2}\right)_{o,y} x^2 + \cdots \qquad \text{(IV-2)}$$

For the case of a symmetrical potential distribution all odd derivatives are zero.

$$V(x,y) = V(-x,y) \qquad \text{(IV-3)}$$

The partials of the potential with respect to x are not easily obtainable; however, by differentiation of LaPlace's equation all even derivatives can be found

$$\frac{\partial^2 V}{\partial x^2} = -\frac{\partial^2 V}{\partial y^2}, \text{ (LaPlace Equation)} \qquad \text{(IV-4)}$$

$$\frac{\partial^4 V}{\partial x^4} = \frac{\partial^4 V}{\partial y^4},$$

etc.

From knowledge of the potential distribution along the center line, potentials near this line are given by:

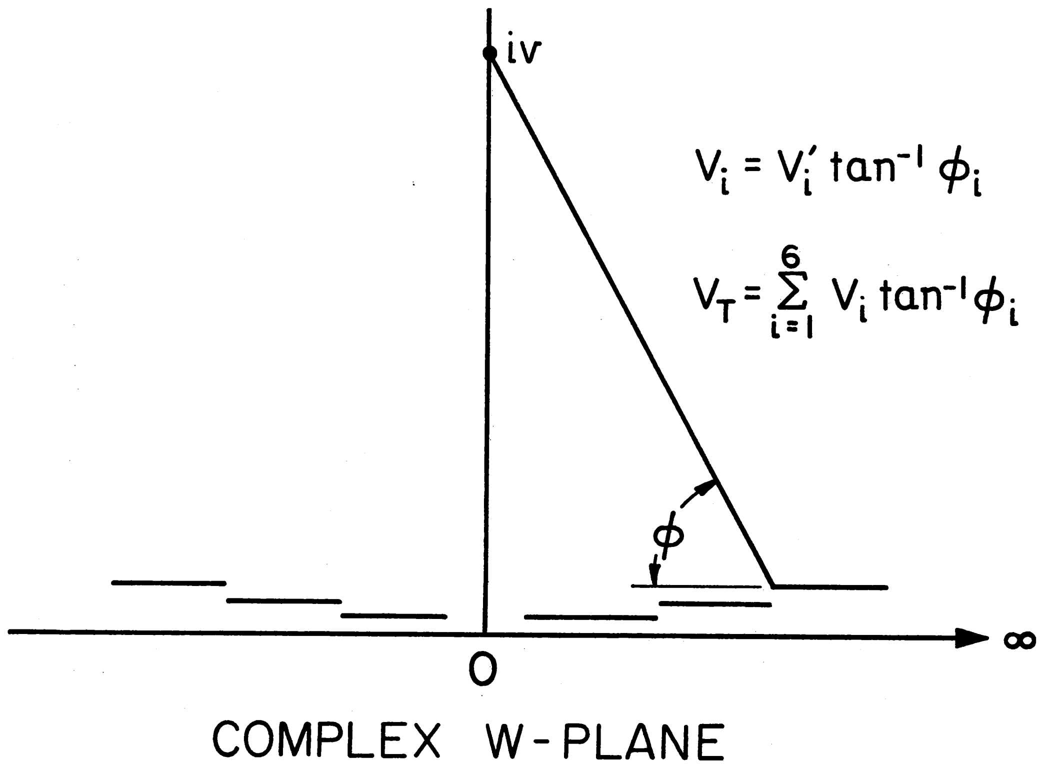

Figure 32. Electrode System in Complex w-plane

$$V(x,y) = V(o,y) - \frac{x^2}{2!}\left(\frac{\partial^2 V}{\partial y^2}\right)_{o,y} + \frac{x^4}{4!}\left(\frac{\partial^4 V}{\partial y^4}\right)_{o,y} - + \cdots \quad \text{(IV-5)}$$

Numerically, the ray tracing can be simplified by calculating the gradients of the potential at the points of interest. Equations (IV-6) and (IV-7) are obtained by differentiation of Equation (IV-5).

$$\left(\frac{\partial V}{\partial x}\right) = - x \left(\frac{\partial^2 V}{\partial y^2}\right)_{o,y} + \frac{x^3}{6}\left(\frac{\partial^4 V}{\partial y^4}\right)_{o,y} - \frac{x^5}{120}\left(\frac{\partial^6 V}{\partial y^6}\right)_{o,y} + - \cdots \quad \text{(IV-6)}$$

$$\left(\frac{\partial V}{\partial y}\right) = \left(\frac{\partial V}{\partial y}\right)_{o,y} - \frac{x^2}{2}\left(\frac{\partial^3 V}{\partial y^3}\right)_{o,y} + \frac{x^4}{24}\left(\frac{\partial^5 V}{\partial y^5}\right)_{o,y} - \frac{x^6}{720}\left(\frac{\partial^7 V}{\partial y^7}\right)_{o,y} + - \cdots \quad \text{(IV-7)}$$

It is thus possible to calculate the potential (Equation IV-5) or the gradients of the potential (Equations IV-6 and IV-7) at any point in the lens system with only the knowledge of the potential as well as the derivatives of the potential at that y-coordinate on the central axis.

The principle of the Schwarz-Christoffel method is to treat the electrode array as the limiting case of a polygon; in so doing no provisions are made to calculate potential distributions on the outer sides of the electrode system, Figure 31. Since it is intended to ground the outer electrodes, field penetration of the center electrode potential out of the lens system is of concern. By incorporation of two extra apertured planes as in Figure 33, ion trajectories into and out of the central three apertured planes can be considered. The conformal mapping of this larger lens follows identically that of the three apertured case; however, the size and number of the actual equations for the transformation increase.

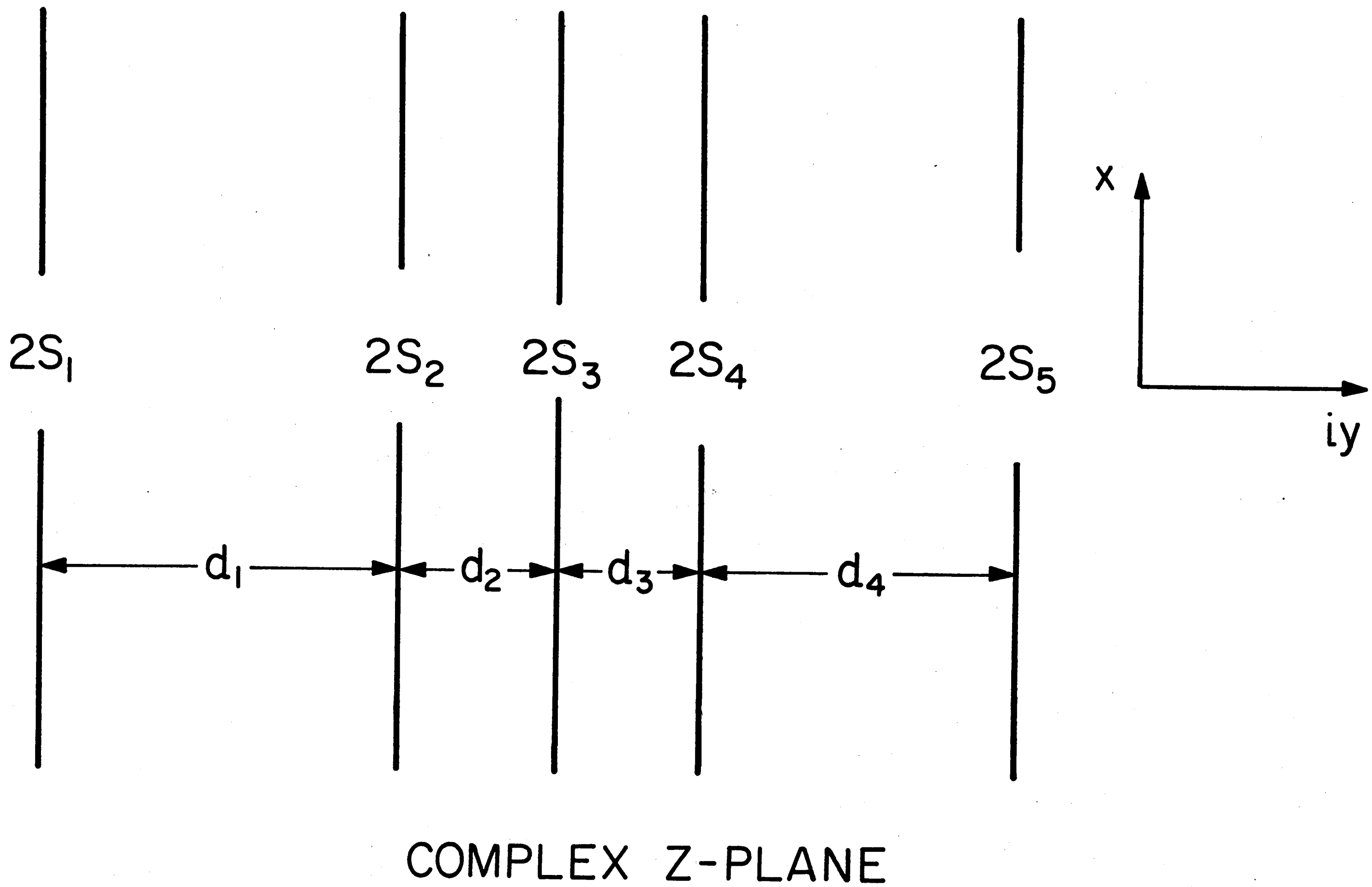

Figure 33. Five Apertured Plane Linear Electrostatic Lens

The thickness of each electrode must be considered if the lens is to be realistic. In the Schwarz-Christoffel transformation the electrodes are represented as infinitely thin. Wallington (50) has found that accurate theoretical representation of an electrode requires the use of two or more planes of infinitesimal thickness with the outermost planes separated by distances equal to the real thickness of the electrode. The potential on each plane is the same as the real electrode. In the case of *Einzel* lenses (three-element electrostatic lenses in which the outer two electrodes are at the same potential; usually ground) the thickness of the center electrode is most important for the lens properties (50,51).

To simulate trajectories of ions leaving the exit slit of the radial electrostatic sector in the mass spectrometer and entering an *Einzel* lens, the potentials and notation indicated in Figure 34 are used. Four electrodes are used to represent the "thick" electrode instead of two; so a wide range of electrode thickness can be investigated without adversely affecting potentials near the center line between the "thick" electrodes. The potentials at x-positions up to 30% of the slit widths were plotted as a function of y in the vicinity of the "thick" electrode; no effects of multiple thin electrodes were apparent.

The conformal map constants as well as calculated geometry (using Program #3, Appendix B, Statement #40-69) are given in Table III for the electrostatic lens in Figure 34. The calculated geometry compares to better than 1 part in 10^5 to the initial geometry which was used to compute the conformal mapping constants. This is well within machining tolerances for construction of lenses.

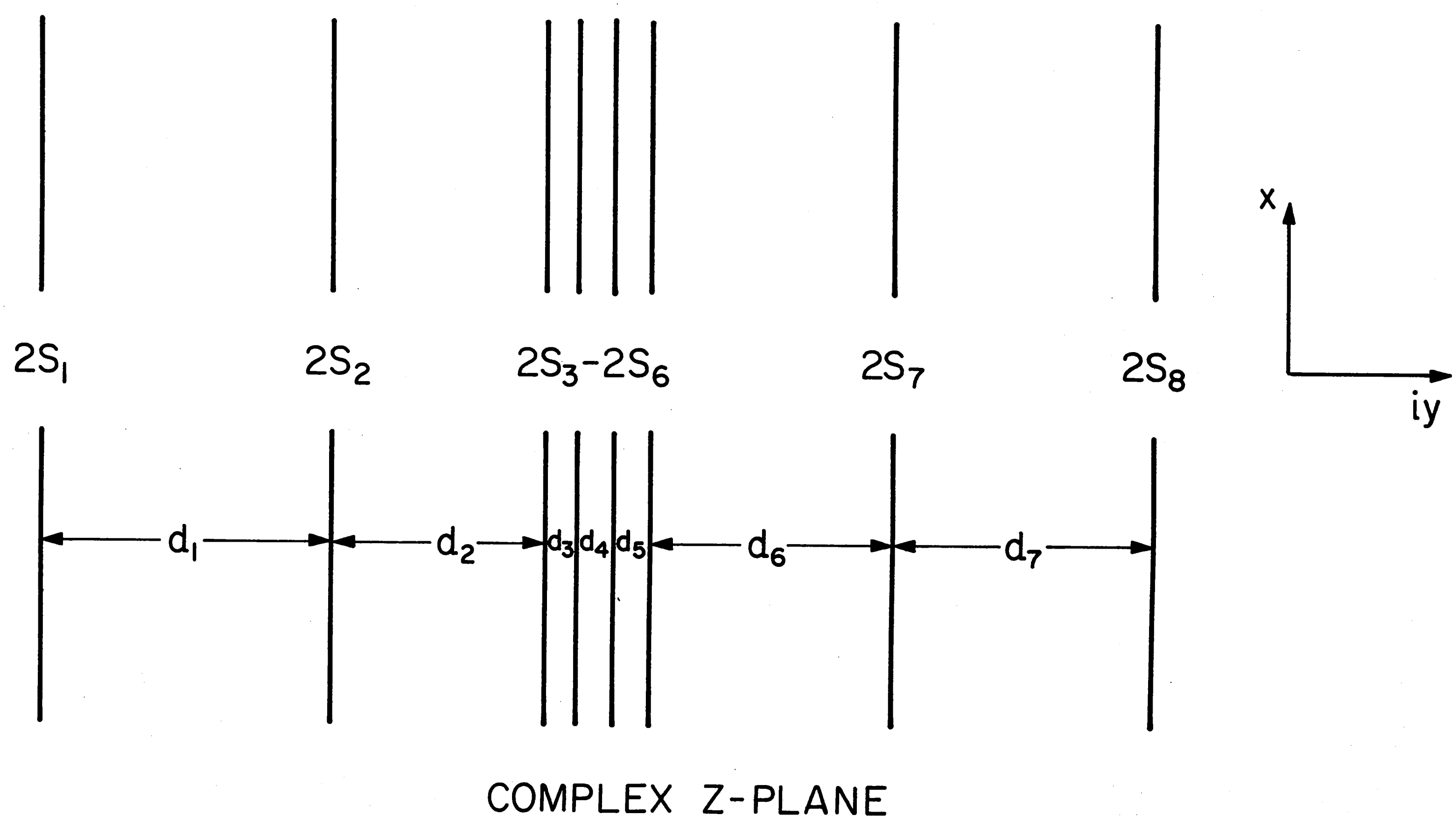

Figure 34. Eight Apertured Plane Linear Electrostatic Lens With a "Thick" Center Plane

TABLE III

CONFORMAL MAPPING CONSTANTS AND CALCULATED GEOMETRY
FOR AN EIGHT APERTURED ELECTROSTATIC LENS

Conformal Map Constants

$a = .50024775480706 \times 10^{-1}$	$o = .18082807808053 \times 10^{-6}$
$b = .19300864069821 \times 10^{-2}$	$p = .10108731694186 \times 10^{-6}$
$c = .75029876030201 \times 10^{-4}$	$q = .54139569185460 \times 10^{-7}$
$d = .11355285860026 \times 10^{-4}$	$r = .90256235746935 \times 10^{-8}$
$e = .18930615960949 \times 10^{-5}$	$s = .13659682395425 \times 10^{-8}$
$f = .10138808939371 \times 10^{-5}$	$t = .53100422724127 \times 10^{-10}$
$g = .56679183410157 \times 10^{-6}$	$u = .20487528999131 \times 10^{-11}$
$h = .32014561619614 \times 10^{-6}$	

Calculated Geometry (cm)

S1 = 0.1000	S6 = 0.1000	D3 = 0.0872
S2 = 0.1000	S7 = 0.1000	D4 = 0.0871
S3 = 0.1020	S8 = 0.1000	D5 = 0.0872
S4 = 0.1020	D1 = 2.0306	D6 = 0.5000
S5 = 0.1020	D2 = 0.5000	D7 = 2.0306

Computed trajectories were carried out on monoenergetic positive ions entering the lens system parallel to the y-axis. The time step (δt) used in all calculations was determined by first selecting a large time interval and calculating the final position of the particle at the seventh apertured slit. The time interval was then reduced in steps until the position of the ion at the seventh electrodes remained constant to five significant figures with successive changes in δt. Consistency in the final position was obtained with δt values of approximately .75 nanoseconds; however, time intervals of .1 nanoseconds were typically used to insure that the trajectories would be well within achievable experimental accuracy.

The final x-coordinates of the ions are indicated as a function of initial ion kinetic energy as well as initial x-coordinates in Figure 35. All ions enter the lens system parallel to the y-axis. The final x-coordinates for the 7300 eV ions form a sharp image at the seventh apertured plane at -0.0004 cm, -0.0005 cm, -0.0004 cm, and +0.0006 cm for ions with initial x-coordinates of +0.0025 cm, +0.0050 cm, +0.0075 cm, and +0.0100 cm respectively. The apparent discrepancy of the fourth final x-position from the previous three is an artifact of the calculation. The symmetry of the lens system about the y-axis was tested by using initial values for the ions of -0.0025 cm, -0.0050 cm, -0.0075 cm, and -0.0100 cm; the final x-coordinates at the seventh apertured plane agreed in magnitude but differed in sign from the previous results.

In using the conformal transformation method for calculations of the forces acting on the ions, the series expansion for the gradients of the potentials given in Equations (IV-6) and (IV-7) were used. Wallington (50) has found that by including terms up to and including

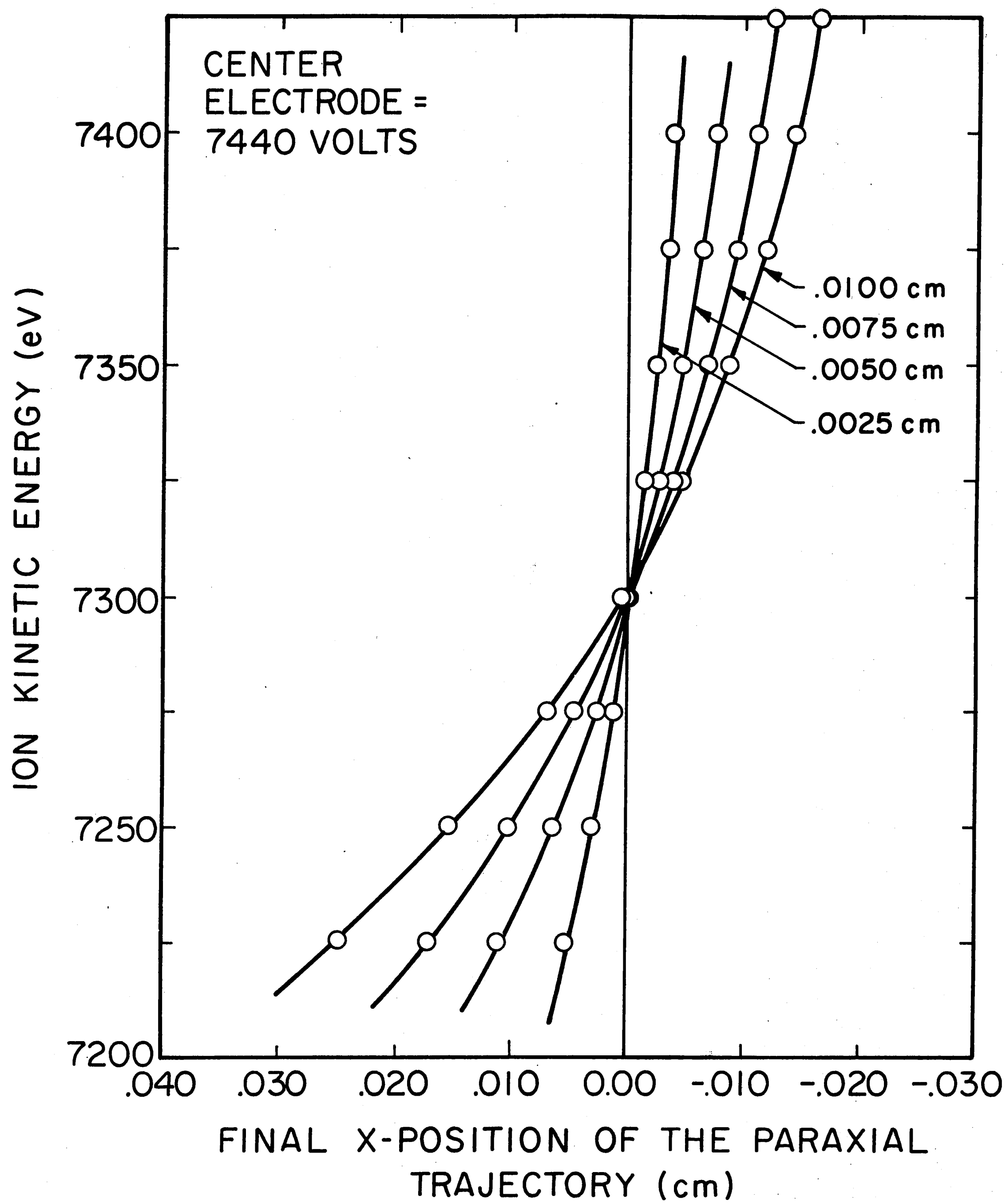

Figure 35. Trajectory Analysis of 7300 eV Ions in an Eight Apertured Symmetric Lens

the fourth partial of the potential, the paraxial trajectories calculated are good approximations to the true trajectories only when the starting x-coordinates of the trajectories are less than approximately 1/10 of the width of the apertures. Therefore, in the present calculations a starting position of ± 0.0100 cm for the ions represents the x-coordinates extrema as partial derivatives up to and including only the fourth were included. The calculations of paraxial trajectories with starting positions greater than 0.0100 cm were considered for purposes of comparison. Figure 36 is a point-by-point ray trace of 7300 eV positively charged ions through the eight apertured lens with +7440 volts on the "thick" electrodes. With starting positions of ± 0.0100 cm the ions reach maximum off-axis values of ∓ 0.0181 cm. At this off-axis point the second term in Equation (IV-7) was less than 1% of the first term. If the starting x-coordinate of the paraxial trajectory is increased to ± 0.015 cm or ± 0.020 cm (the ions reaching maximum off-axis x-coordinates of ∓ 0.0276 cm and ∓ 0.0378 cm), the second term in the series expansion (Equation (IV-7) now represents 4% and 9% respectively of the first terms. Because $\left(\frac{\delta^5 V}{\delta y^5}\right)_{o,y}$ is positive in the vicinity of the maximum x-coordinates of a trajectory in Figure 36, the calculated $\left(\frac{\delta V}{\delta y}\right)$ and hence the force in the y-direction is smaller than it should be. The ion therefore spends too much time in the lens system subject to the forces acting in the x-direction and appears at increasingly larger final x-coordinates at the seventh apertured plane with increasing starting x-coordinates. The second term in Equation (IV-6) approaches only 1% of the first term as the starting x-coordinate for the paraxial trajectory is increased to ± 0.0200 cm. To use starting x-coordinates for the paraxial trajectories in the range 0.010 to

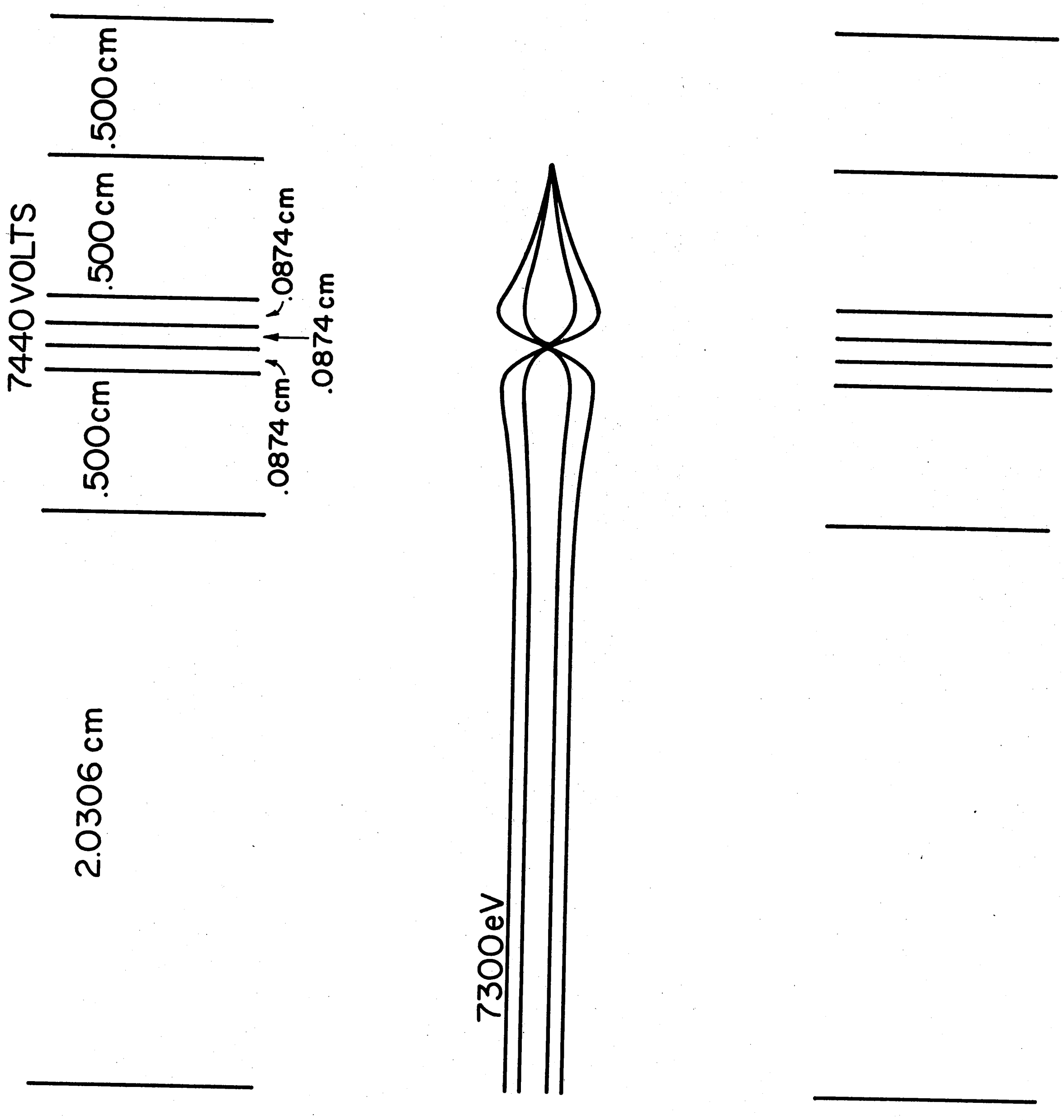

Figure 36. Ray Trace of a 7300 eV Positive Ion Through the Eight Apertured Lens

0.020 would therefore require the inclusion of an additional term in Equation (IV-6) as it must be significant. Starting x-positions greater than 0.0200 cm would no doubt require additional terms in both Equations (IV-6) and (IV-7).

The introduction of an apertured plane with an adjustable slit into the *Einzel* lens was considered in order to determine whether this would adversely affect the final positions of the trajectories or the image size. A second lens was conformally mapped to give the constants and calculated geometry in Table IV. This second lens is identical in calculated geometry to the first lens (Table III) except for the much smaller aperture in the seventh plane (S_7). Ray traces were carried out for positive ions with paraxial trajectories as previously described. The results of the final x-coordinates of the ions are illustrated in Figure 37 as well as trajectory analysis in Figure 38 through Figure 40. Figure 37 illustrates the path of ions with the proper as well as improper energy to pass the lens at a given potential on the "thick" electrodes. Figure 38 when compared to Figure 35 illustrates the minor focusing change when the seventh aperture is changed from a large to a narrow slit. The image size of a 7300 eV beam of ions compares favorably with the image size of the first lens. The final x-coordinates at the seventh apertured plane for the second lens are -0.0004 cm, -0.0004 cm, -0.0005 cm, and +0.0006 cm for initial x-coordinates of 0.0025 cm 0.0050 cm, 0.0075 cm, and 0.0100 cm respectively. Therefore, changes in the size of the collector slit do not significantly change focal properties of the *Einzel* lens.

It was previously established that in order for the *Einzel* lens to be useful as an energy selective device for ion kinetic spectra,

TABLE IV

CONFORMAL MAP CONSTANTS AND CALCULATED GEOMETRY FOR AN EIGHT APERTURED LENS WITH A NARROW SEVENTH APERTURE

Conformal Map Constants

$a = .50024774723523 \times 10^{-1}$	$o = .17963624022968 \times 10^{-6}$
$b = .19300862635880 \times 10^{-2}$	$p = .10027910788180 \times 10^{-6}$
$c = .75028372396914 \times 10^{-4}$	$q = .53657306727246 \times 10^{-7}$
$d = .11354848732495 \times 10^{-4}$	$r = .91460386857642 \times 10^{-8}$
$e = .18924732492200 \times 10^{-5}$	$s = .28076474096165 \times 10^{-10}$
$f = .10121472509559 \times 10^{-5}$	$t = .86093522158906 \times 10^{-13}$
$g = .56494427727956 \times 10^{-6}$	$u = .13306465669631 \times 10^{-13}$
$h = .31856328547029 \times 10^{-6}$	

Calculated Geometry (cm)

S1 = 0.1000	S6 = 0.1020	D3 = 0.0874
S2 = 0.1000	S7 = 0.0020	D4 = 0.0874
S3 = 0.1020	S8 = 0.1000	D5 = 0.0874
S4 = 0.1020	D1 = 2.0306	D6 = 0.5000
S5 = 0.1020	D2 = 0.5000	D7 = 0.5000

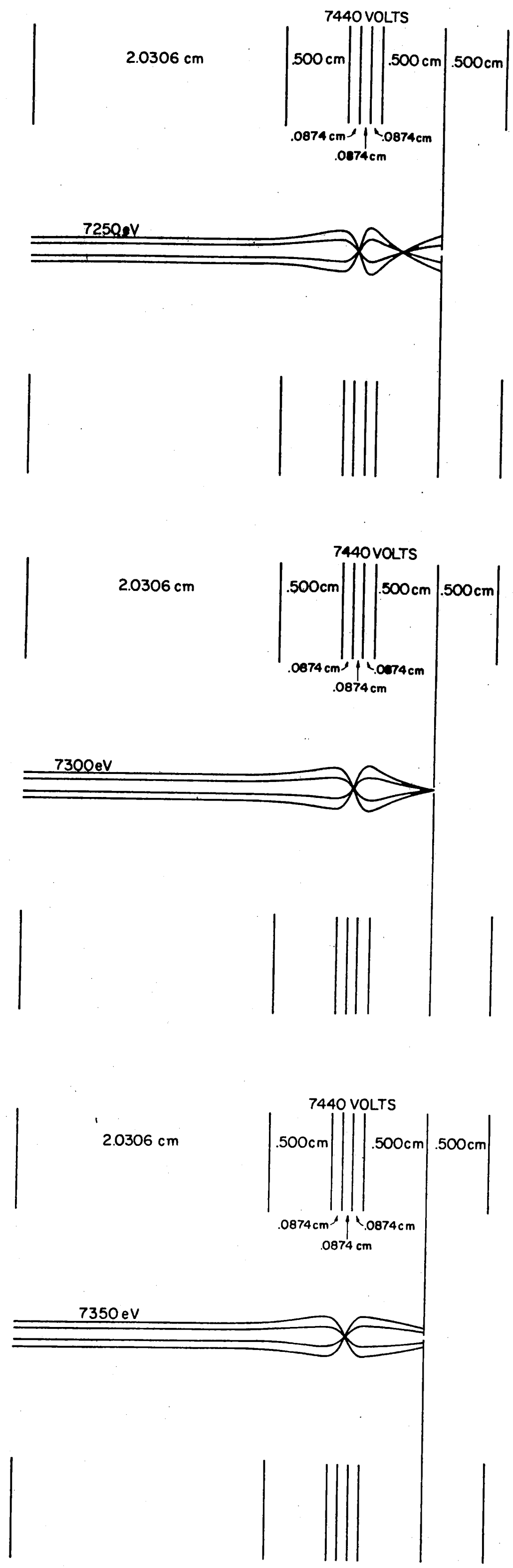

Figure 37. Ray Trace of Ions Focused (a) in Front, (b) at, and (c) Behind a Narrow Slit in an Eight Apertured Lens

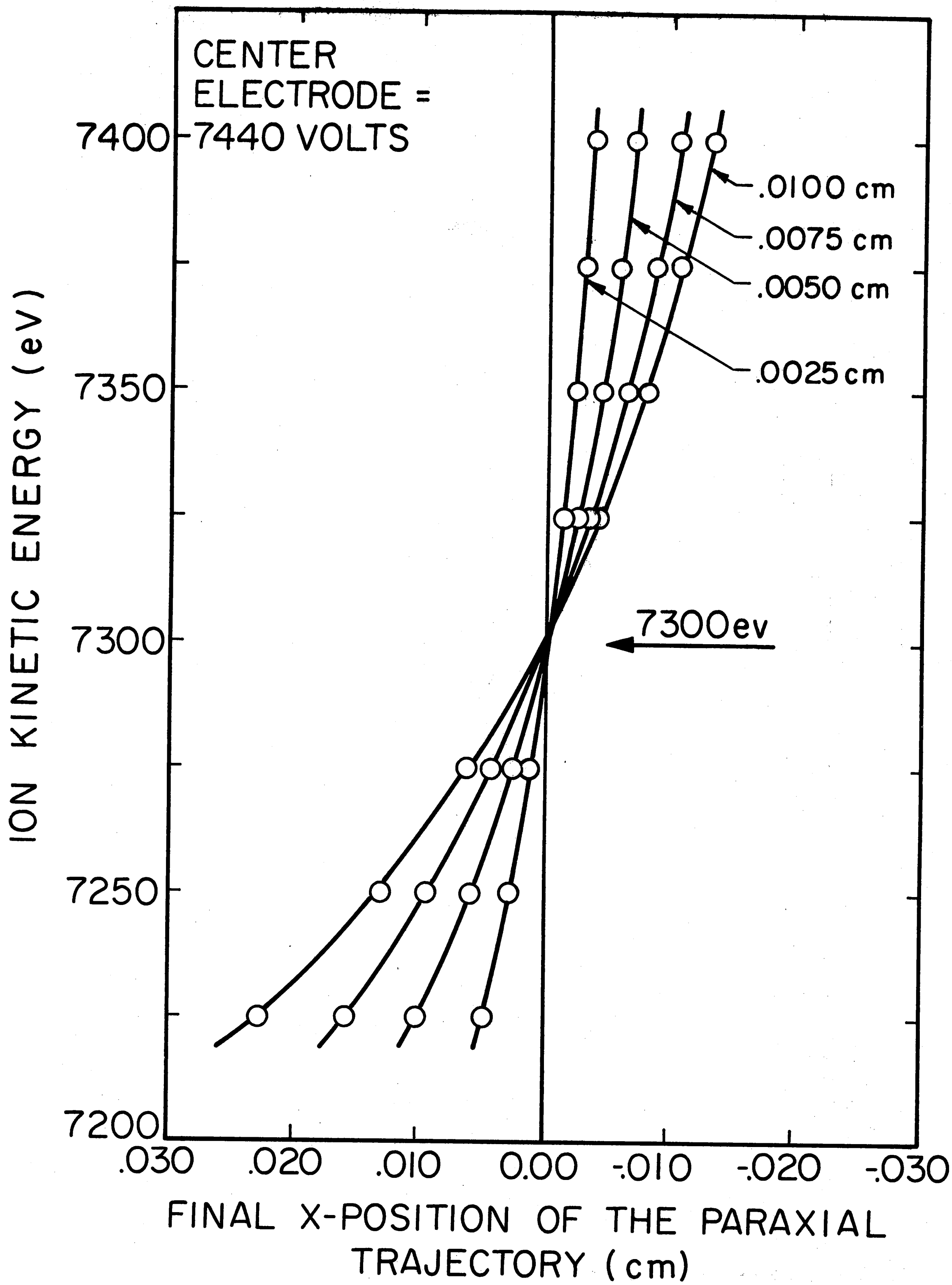

Figure 38. Trajectory Analysis of an Eight Apertured Lens With a Center Electrode Potential of 7440 Volts and a Narrow 7th Slit

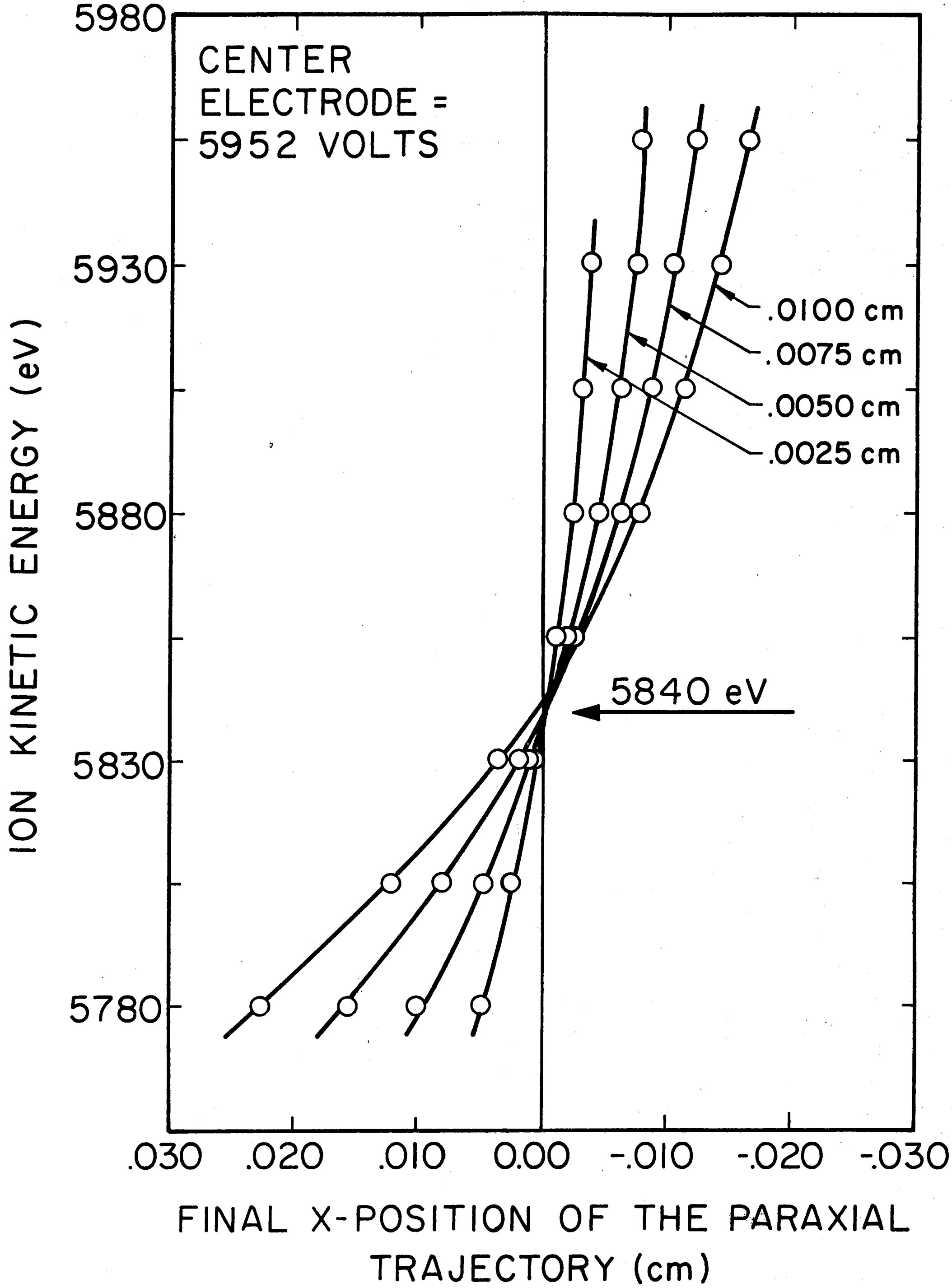

Figure 39. Trajectory Analysis of an Eight Apertured Lens With a Center Electrode Potential of 5952 Volts and a Narrow 7th Slit

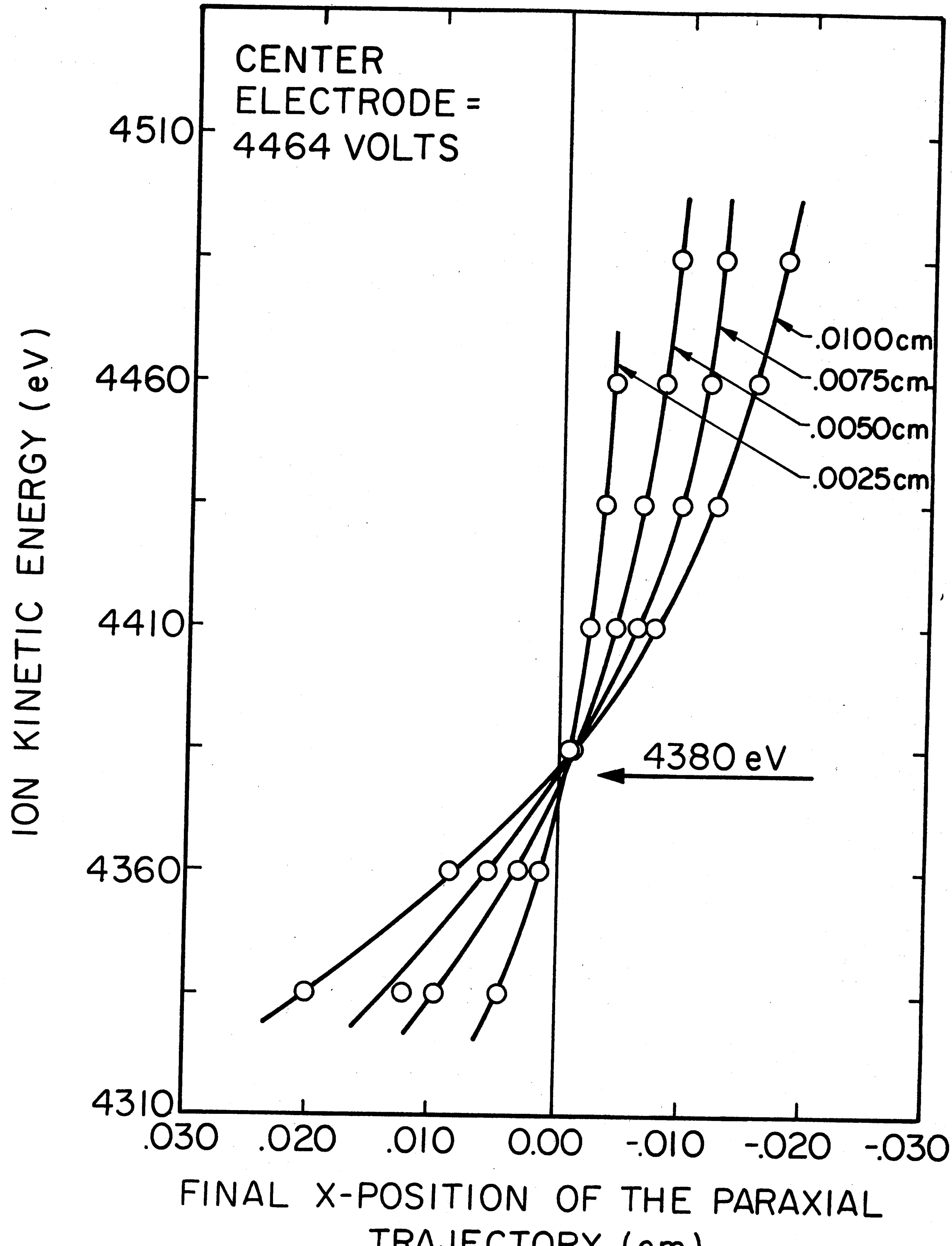

Figure 40. Trajectory Analysis of an Eight Apertured Lens With a Center Electrode Potential of 4464 Volts and a Narrow 7th Slit

there must exist a linear relationship between the energy of the ions focused and the voltage on the "thick" electrodes. This relationship is illustrated in Figure 39 and Figure 40 where the potential on the "thick" electrodes is reduced to 5952 volts and 4464 volts respectively. The arrow in the figures indicates the required focal point for a linear relationship; i.e. V(center electrode)/V(focus) = 1.0192.

The final problem is to calculate the energy resolution of the combination $\Pi/4\sqrt{2}$ radial electrostatic analyzer followed by the linear electrostatic lens. The method used in calculation of trajectories restricted analysis of the three element electrostatic lens to the center 10%. Fortunately, when two beams of ions with similar energy exit the radial electric sector, the width of the combined beam is only 0.139 cm (Chapter II); thus the analysis uses approximately 15% of the combined beam in the calculated trajectories through the three element lens. The ions entering the *Einzel* lens have initial trajectories parallel to each other and perpendicular to the plane of each of the apertures. The ions entering the lens along the center line (x = 0.0) experience no deflection regardless of their energy or the potential on the "thick" electrodes of the lens. The further off-axis an ion of a given energy enters the lens, the more deflection it experiences at the energy resolving slit. To obtain the energy resolution of the *Einzel* lens, the final x-coordinates at the seventh apertured plane were plotted as a function of the initial x-coordinates for various energy paraxial trajectories, Figure 41. Linear extrapolations were then made to the full beam width. The energy resolution calculated will serve only as an approximation to the true energy resolving power of the lens due to the uncertainty in the extrapolation beyond the data points.

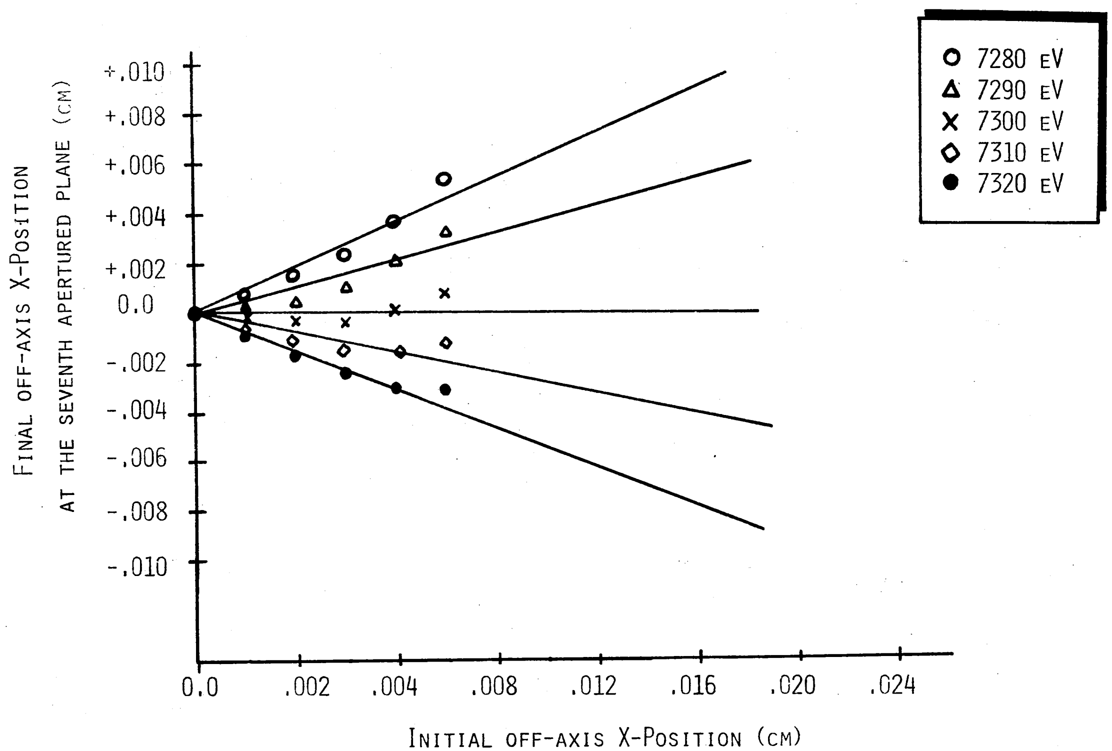

Figure 41. Energy Discriminating Properties of an Eight-apertured Electrostatic Lens With a Narrow Seventh Slit

The calculations indicate that the energy resolution using the *Einzel* lens described would be approximately .13% with a .0005 inch β-slit and .26% with a .002 inch β-slit and a 10% valley. No attempt has been made to optimize the energy resolution of the *Einzel* lens by changing geometries.

The energy resolution of the Mattauch-Herzog mass spectrometer without the β-slit modification was approximately 3-5%. It has been shown that because of the poor energy resolution and sensitivity the instrument is limited as a research tool for the study of first field-free region metastable decompositions. Modification of the β-slit and insertion of an electron multiplier increased the energy resolution to .6% while also increasing the detectibility and sensitivity of the instrument. Calculations have shown the feasibility of using an *Einzel* lens to further increase the energy resolution of the instrument while maintaining its utility as a general purpose mass spectrometer. The use of such a lens would give an energy dispersed intermediate energy image in the second field-free region at the β-slit and would thus circumvent the inherent low energy resolution associated with the Mattauch-Herzog geometry mass spectrometer by providing an independent adjustment of the aperture and energy bandwidth for Ion Kinetic Energy Spectra.

BIBLIOGRAPHY

1. H. M. Rosenstock, M. B. Wallenstein, A. L. Wahrhaftig, and H. Eyring, Proc. Natl. Acad. Sci. (U.S.), 38, 667 (1952).

2. Wendell Forst, Theory of Unimolecular Reactions, Academic Press, New York (1973), pg. 263. Peter J. Derrick, Roger P. Morgan, John T. Hill, M. A. Baldwin, Int. J. Mass. Spectrom. Ion Phys., 18, 393 (1975).

3. K. R. Jennings, Mass Spectrometry: Techniques and Applications, Ed., George W. A. Milne, Wiley Interscience, 1971, pg. 420.

4. J. A. Hipple, E. U. Condon, Phys. Rev., 68, 54 (1945).

5. J. A. Hipple, R. E. Fox, E. U. Condon, Phys. Rev., 69, 347 (1946).

6. J. H. Beynon, R. A. Saunders, A. E. Williams, Nature, 204, 67 (1967); J. H. Beynon, A. E. Fontaine, Z. Naturforschg., 22a, 334 (1967).

7. D. T. Terwilliger, J. F. Elder, Jr., J. H. Beynon, R. G. Cooks, Int. J. Mass Spectrom. Ion Phys., 16, 225 (1975).

8. J. H. Beynon, R. M. Caprioli, W. E., Baitinger, J. W. Amy, Org. Mass Spectrom., 3, 455 (1970).

9. N. R. Daly, A. McCormick, R. E. Powell, Rev. Sci. Instrum., 39, 1163 (1968).

10. M. Barber, R. M. Elliot, "Comparison of Metastable Spectra from Single and Double-Focussing Mass Spectrometers", ASTM Committee E-14, 12th Annual Conference on Mass Spectrometry and Allied Topics, Montreal, Canada, 7th to 14th June, 1964. J. H. Beynon, R. A. Saunders, A. E. Williams, Nature, 204, 67 (1964).

11. T. W. Shannon, F. W. McLafferty and C. R. McKinney, Chem. Commum., 478 (1966); J. H. Futrell, K. R. Ryan, L. W. Lieck, J. Chem. Phys., 43, 1832 (1965).

12. J. H. Beynon, R. M. Caprioli, W. E. Baitinger, J. W. Amy, Int. J. Mass Spectrom. Ion Phys., 3, 313 (1969).

13. R. G. Cooks, J. H. Beynon, R. M. Caprioli, G. R. Lester, Metastable Ions, Elsevier, 1973.

14. Lorin P. Hills, Jean H. Futrell, Austin L. Wahrhaftig, J. Chem. Phys., 51, 5255 (1969); K. R. Jennings, Chem. Commum., 283 (1966).

15. F. W. McLafferty, R. Venkataraghavan, P. Irving, Biochem. Biophys. Res. Commun., 39, 274 (1970).

16. J. H. Beynon, D. F. Brothers, R. G. Cooks, Anal. Chem., 46, 1299 (1974).

17. Charles Reichert, Robert E. Fraas, Robert W. Kiser, Int. J. Mass Spectrom. Ion Phys., 5, 457 (1970). J. H. Beynon, R. M. Caprioli, W. E. Baitinger, J. W. Amy, Org. Mass Spectrom., 3, 661 (1970).

18. T. Ast, J. H. Beynon, R. G. Cooks, J. Am. Chem. Soc., 94, 6611 (1972).

19. J. H. Beynon, R. M. Caprioli, T. Ast, Org. Mass Spectrom., 5, 229 (1971).

20. J. H. Beynon, J. A. Hopkinson, G. R. Lester, J. Mass Spectrom. Ion Phys., 2, 291 (1969).

21. E. G. Jones, J. H. Beynon, R. G. Cooks, J. Chem. Phys., 57, 2652 (1972); R. G. Cooks, M. Bertrand, J. H. Beynon, M. F. Rennekamp, D. W. Setser, J. Am. Chem. Soc., 95, 1732 (1973).

22. R. G. Cooks, K. C. Kim, J. H. Beynon, Chem. Phys. Lett., 23, 190 (1973); T. Ast, D. T. Terwilliger, R. G Cooks, J. H. Beynon, J. Phys. Chem., 79, 708 (1975).

23. N. R. Daly, A. McCormick, R. E. Powell, Org. Mass Spectrom., 1, 169 (1968).

24. R. M. Caprioli, J. H. Beynon, T. Ast, Org. Mass Spectrom., 5, 417 (1971).

25. E. M. Chait, W. B. Askew, Org. Mass Spectrom., 5, 147 (1971).

26. Harold W. Major Jr., U.S. Patent 3,673,404, 27 Jun 1972.

27. S. Safe, O. Hutzinger, W. D. Jamieson, Org. Mass Spectrom., 7, 167 (1973).

28. A. O. Nier, T. R. Roberts, Phys. Rev., 81, 507 (1951).
E. G. Johnson, A. O. Nier, Phys. Rev., 91, 10 (1953).

29. J. Mattauch, R. Herzog, Z. Physik, 89, 786 (1934).

30. R. D. Craig, B. N. Green, J. D. Waldron, Chimia, 17, 33 (1963).

31. J. H. Beynon, W. E. Baitinger, J. W. Amy, T. Komatsu, Int. J. Mass Spectrom. Ion Phys., 3, 47 (1969); J. H. Beynon, W. E. Baitinger, J. W. Amy, Int. J. Mass Spectrom. Ion Phys., 3, 55 (1969).

32. J. H. Beynon, R. G. Cooks, J. W. Amy, W. E. Baitinger, T. Y. Ridley, Anal. 45, 1023A (1973).

33. J. H. Beynon, J. W. Amy, W. E. Baitinger, Chem. Commun., 723 (1969).

34. Y. Petet-Clere et J. D. Carette, ASTM Committee E-14, 16th Annual Conference on Mass Spectrometry and Allied Topics, Pittsburgh, Pennsylvania, 12th to 17th May, 1968, Paper No. 93.

35. Colin T. Kyte, George H. Jeffery, Arthur I. Vogel, J. Chem. Soc. (London), 4454 (1960); G. H Jeffery, R. Parker, A. I. Vogel, J. Chem. Soc. (London), 570 (1961).

36. I am indebted to Mr. Gil Greenwood for the Field Ionization analysis.

37. Norman G. Foster, D. E. Hirsch, R. F. Kendall, B. H. Eccleston, U.S. Bur. Mines. Invest. Rept. #6433; Rossini, Frederick, et. al., "Table of the American Petroleum Institute Research Project 44". Carnegie Press, Carnegie Institute of Tech., Pittsburgh, Pa. 1959.

38. J. Mattauch, R. Herzog, Z. Physik., 89, 786 (1934).

39. H. Liebl, Recent Developments in Mass Spectrometry, 1970, pg. 188-193.

40. Isao Takeshita, Z. Naturforschg, 21a, 14 (1966).

41. Albert Septier, Focusing of Charged Particles, Vol. I, Academic Press 1967, pg. 274.

42. S. Natali, D. DiChio, C. E. Kuyatt, J. Research NBS, Vol. 76A(1), 27 (1972).

43. A. Galejs, C. E. Kuyatt, J. Vac. Technol., 10, 1114 (1973). D. DiChio, S. V. Natali, Rev. Sci. Instrum., 45(4), 559 (1974).

44. R. Mock, E. Roth, J. Solmon, J. Phys. Rad., 11, 524 (1950).

45. G. Liebmann, J. Appl. Phys., 1, 92 (1950).

46. M. J. Wallington, J. Phys. E., 3, 599 (1970).

47. A. J. H. Boerboom, Z. Naturforschg., 14a, 809 (1959).

48. Michel Laudet, Cah. Phys., 41-72, 1 (1953).

49. K. Shimizer, H. Kanakatsu, J. Phys. E., 7, 472 (1974).

50. M. J. Wallington, J. Phys. E., 4, 1 (1974).

51. P. Grivet, Electron Optics, Pergamon Press, 1965, pg. 455.

52. A. I. Markushevich, Theory of Functions of a Complex Variable Vol. III, translated by Richard A. Silverman, Prentice-Hall, Inc., 1967, pg. 320.

53. A. J. H. Boerboom, Z. Naturforschg., 15a, 244 (1960).
A. J. H. Boerboom, Z. Naturforschg., 15a, 253 (1960).

APPENDIX A

NUMERICAL CALCULATION OF THE POTENTIAL DISTRIBUTION IN AN EIGHT APERTURED PLANE LENS

APPENDIX A

NUMERICAL CALCULATION OF POTENTIAL DISTRIBUTION IN AN EIGHT APERTURED PLANE LENS

The region between the projections of the electrodes was mapped conformally on the positive imaginary half of the complex w-plane. The Schwarz-Christoffel transformation was used because of its general applicability to regions bounded by straight lines (52). For the calculations in Appendices A and B, the variable names a,b,c,...,u (excluding i-n) are attributed successively to the internal and infinite ends of the electrodes as indicated in Figure 42. The conformal mapping of the planar lens system from the complex z-plane ($z = x + iy$) to the complex w-plane ($w = u + iv$) was performed by the inverse of the function (47, 53)

$$z = \int_{w_0}^{w} \frac{(x^2-a^2)(x^2-c^2)(x^2-e^2)(x^2-g^2)(x^2-o^2)(x^2-q^2)(x^2-s^2)(x^2-u^2)}{(x^2-b^2)(x^2-d^2)(x^2-f^2)(x^2-h^2)(x^2-p^2)(x^2-r^2)(x^2-t^2)}\,dx \tag{A-1}$$

The function was decomposed into partial fractions, integrated, and the boundary conditions ware applied (48). The resulting equations contain the physical constants of the lens and the parameters governing the conformal mapping, Table V. From the nature of the problem the conformal mapping constants a,b,c,...,u are real and subject to the constraints $a>b>c>d>e>f>g>h>o>p>q>r>s>t>u$. The restrictions limit the solutions to one which is not obvious without further approximations.

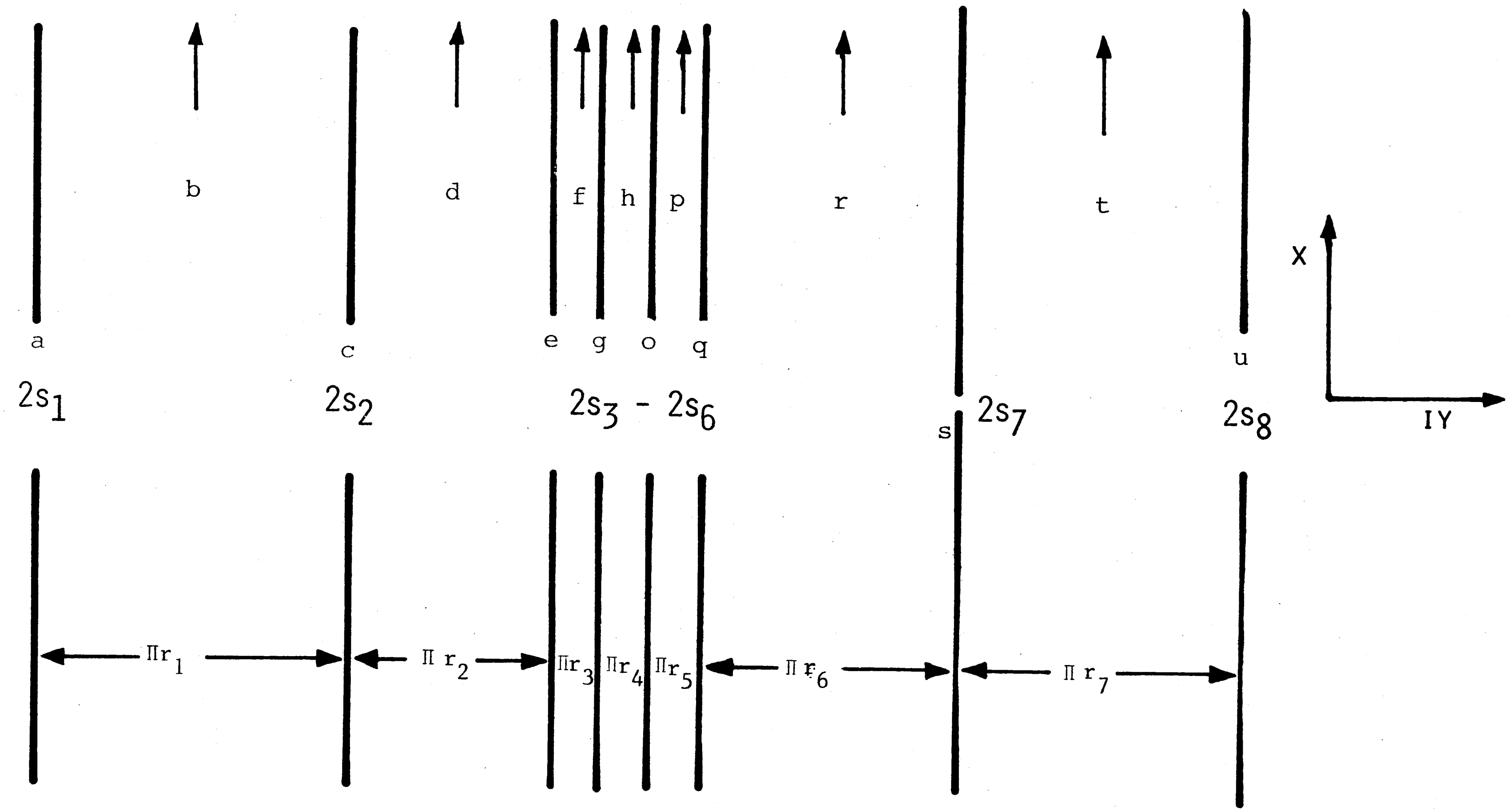

Figure 42. Cross Section of Eight Element Lens System

TABLE V

EQUATIONS TO DETERMINE THE PARAMETERS GOVERNING THE CONFORMAL MAPPING

$$r_1 = \frac{(a^2-b^2)(b^2-c^2)(b^2-e^2)(b^2-g^2)(b^2-o^2)(b^2-q^2)(b^2-s^2)(b^2-u^2)}{2b(b^2-d^2)(b^2-f^2)(b^2-h^2)(b^2-p^2)(b^2-r^2)(b^2-t^2)b^2}$$

$$r_2 = \frac{(a^2-d^2)(c^2-d^2)(d^2-e^2)(d^2-g^2)(d^2-o^2)(d^2-q^2)(d^2-s^2)(d^2-u^2)}{2d(b^2-d^2)(d^2-f^2)(d^2-h^2)(d^2-p^2)(d^2-r^2)(d^2-t^2)d^2}$$

$$r_3 = \frac{(a^2-f^2)(c^2-f^2)(e^2-f^2)(f^2-g^2)(f^2-o^2)(f^2-q^2)(f^2-s^2)(f^2-u^2)}{2f(b^2-f^2)(d^2-f^2)(f^2-h^2)(f^2-p^2)(f^2-r^2)(f^2-t^2)f^2}$$

$$r_4 = \frac{(a^2-h^2)(c^2-h^2)(e^2-h^2)(g^2-h^2)(h^2-o^2)(h^2-q^2)(h^2-s^2)(h^2-u^2)}{2h(b^2-h^2)(d^2-h^2)(f^2-h^2)(h^2-p^2)(h^2-r^2)(h^2-t^2)h^2}$$

$$r_5 = \frac{(a^2-p^2)(c^2-p^2)(e^2-p^2)(g^2-p^2)(o^2-p^2)(p^2-q^2)(p^2-s^2)(p^2-u^2)}{2p(b^2-p^2)(d^2-p^2)(f^2-p^2)(h^2-p^2)(p^2-r^2)(p^2-t^2)p^2}$$

$$r_6 = \frac{(a^2-r^2)(c^2-r^2)(e^2-r^2)(g^2-r^2)(o^2-r^2)(q^2-r^2)(r^2-s^2)(r^2-u^2)}{2r(b^2-r^2)(d^2-r^2)(f^2-r^2)(h^2-r^2)(p^2-r^2)(r^2-t^2)r^2}$$

$$r_7 = \frac{(a^2-t^2)(c^2-t^2)(e^2-t^2)(g^2-t^2)(o^2-t^2)(q^2-t^2)(s^2-t^2)(t^2-u^2)}{2t(b^2-t^2)(d^2-t^2)(f^2-t^2)(h^2-t^2)(p^2-t^2)(r^2-t^2)t^2}$$

$$s_1 = a + r_1 \ln\frac{a+b}{a-b} + r_2 \ln\frac{a+d}{a-d} + r_3 \ln\frac{a+f}{a-f} + r_4 \ln\frac{a+h}{a-h} + r_5 \ln\frac{a+p}{a-p} + r_6 \ln\frac{a+r}{a-r} + r_7 \ln\frac{a+t}{a-t} + \frac{ac^2e^2g^2o^2q^2s^2u^2}{b^2d^2f^2h^2p^2r^2t^2}$$

TABLE V (Continued)

$$s_2 = c + r_1 \ln \frac{b+e}{b-e} + r_2 \ln \frac{c+d}{c-d} + r_3 \ln \frac{c+f}{c-f} + r_4 \ln \frac{c+h}{c-h} + r_5 \ln \frac{c+p}{c-p} + r_6 \ln \frac{c+r}{c-r} + r_7 \ln \frac{c+t}{c-t} + \frac{a^2 c e^2 g^2 o^2 q^2 s^2 u^2}{b^2 d^2 f^2 h^2 p^2 r^2 t^2}$$

$$s_3 = e + r_1 \ln \frac{b+e}{b-e} + r_2 \ln \frac{d+e}{d-e} + r_3 \ln \frac{e+f}{e-f} + r_4 \ln \frac{e+h}{e-h} + r_5 \ln \frac{e+p}{e-p} + r_6 \ln \frac{e+r}{e-r} + r_7 \ln \frac{e+t}{e-t} + \frac{a^2 c^2 e g^2 o^2 q^2 s^2 u^2}{b^2 d^2 f^2 h^2 p^2 r^2 t^2}$$

$$s_4 = g + r_1 \ln \frac{b+g}{b-g} + r_2 \ln \frac{d+g}{d-g} + r_3 \ln \frac{f+g}{f-g} + r_4 \ln \frac{g+h}{g-h} + r_5 \ln \frac{g+p}{g-r} + r_6 \ln \frac{g+r}{g-r} + r_7 \ln \frac{g+t}{g-t} + \frac{a^2 c^2 e^2 g o^2 q^2 s^2 u^2}{b^2 d^2 f^2 h^2 p^2 r^2 t^2}$$

$$s_5 = o + r_1 \ln \frac{b+o}{b-o} + r_2 \ln \frac{d+o}{d-o} + r_3 \ln \frac{f+o}{f-o} + r_4 \ln \frac{h+o}{h-o} + r_5 \ln \frac{o+p}{o-p} + r_6 \ln \frac{o+r}{o-r} + r_7 \ln \frac{o+t}{o-t} + \frac{a^2 c^2 e^2 g^2 o q^2 s^2 u^2}{b^2 d^2 f^2 h^2 p^2 r^2 t^2}$$

$$s_6 = q + r_1 \ln \frac{b+q}{b-q} + r_2 \ln \frac{d+q}{d-q} + r_3 \ln \frac{f+q}{f-q} + r_4 \ln \frac{h+q}{h-q} + r_5 \ln \frac{p+q}{p-q} + r_6 \ln \frac{q+r}{q-r} + r_7 \ln \frac{q+t}{q-t} + \frac{a^2 c^2 e^2 g^2 o^2 q s^2 u^2}{b^2 d^2 f^2 h^2 p^2 r^2 t^2}$$

$$s_7 = s + r_1 \ln \frac{b+s}{b-s} + r_2 \ln \frac{d+s}{d-s} + r_3 \ln \frac{f+s}{f-s} + r_4 \ln \frac{h+s}{h-s} + r_5 \ln \frac{p+s}{p-s} + r_6 \ln \frac{r+s}{r-s} + r_7 \ln \frac{s+t}{s-t} + \frac{a^2 c^2 e^2 g^2 o^2 q^2 s u^2}{b^2 d^2 f^2 h^2 p^2 r^2 t^2}$$

$$s_8 = u + r_1 \ln \frac{b+u}{b-u} + r_2 \ln \frac{d+u}{d-u} + r_3 \ln \frac{f+u}{f-u} + r_4 \ln \frac{h+u}{h-u} + r_5 \ln \frac{p+u}{p-u} + r_6 \ln \frac{r+u}{r-u} + r_7 \ln \frac{t+u}{t-u} + \frac{a^2 c^2 e^2 g^2 o^2 q^2 s^2 u^2}{b^2 d^2 f^2 h^2 p^2 r^2 t^2}$$

Part I - The Transformation Constants

Boerboom (47) has introduced a general method for obtaining the transformation constants for linear electrostatic lens systems where all slit dimensions are smaller than the distances between successive apertured planes ($\frac{1}{4}\pi r_{\#} > 2s_{\#}$, Figure 42). Although this was not the case for the lenses in the present study, the approximation will serve as a basis for procedures to obtain the transformation constants. Subject to the constraint $\frac{1}{4}\pi r_{\#} > 2s_{\#}$, $a^2 \gg b^2 \gg c^2 \gg$ etc.; therefore, $a \gg c \gg e \gg g \gg o \gg q \gg s \gg u$ and likewise $b \gg d \gg g \gg h \gg p \gg r \gg t$. Using the series expansion

$$\ln \frac{a+b}{a-b} = 2\,\frac{b}{a}\left\{1 + \frac{1}{3}\frac{b^2}{a^2} + \frac{1}{5}\frac{b^4}{a^4} + \cdots\right\} \quad (b<a) \qquad \text{(A-2)}$$

and neglecting terms of order higher than one, the following equations clearly follow from Table V.

$$a + 2r_1\left(\frac{b}{a}\right) = s_1 \qquad \text{(A-3)} \qquad\qquad r_1 = \frac{a^2}{2b} \qquad \text{(A-11)}$$

$$2r_1\left(\frac{c}{b}\right) + 2r_2\left(\frac{d}{c}\right) = s_2 \qquad \text{(A-4)} \qquad\qquad r_2 = \frac{r_1 c^2}{bd} \qquad \text{(A-12)}$$

$$2r_2\left(\frac{e}{d}\right) + 2r_3\left(\frac{f}{e}\right) = s_3 \qquad \text{(A-5)} \qquad\qquad r_3 = \frac{r_2 e^2}{df} \qquad \text{(A-13)}$$

$$2r_3\left(\frac{g}{f}\right) + 2r_4\left(\frac{h}{g}\right) = s_4 \qquad \text{(A-6)} \qquad\qquad r_4 = \frac{r_3 g^2}{fh} \qquad \text{(A-14)}$$

$$2r_4\left(\frac{o}{h}\right) + 2r_5\left(\frac{p}{o}\right) = s_5 \qquad \text{(A-7)} \qquad\qquad r_5 = \frac{r_4 o^2}{hp} \qquad \text{(A-15)}$$

$$2r_5\left(\frac{q}{p}\right) + 2r_6\left(\frac{r}{q}\right) = s_6 \qquad \text{(A-8)} \qquad\qquad r_6 = \frac{r_5 q^2}{pr} \qquad \text{(A-16)}$$

$$2r_6\left(\frac{s}{r}\right) + 2r_7\left(\frac{t}{s}\right) = s_7 \qquad \text{(A-9)} \qquad\qquad r_7 = \frac{r_6 s^2}{rt} \qquad \text{(A-17)}$$

$$2r_7\left(\frac{u}{t}\right) + \frac{a^2c^2e^2g^2o^2q^2s^2u^2}{b^2d^2f^2h^2p^2r^2t^2} \qquad \text{(A-10)}$$

The approximate equations (A-3)-(A-17) were solved to obtain expressions for the transformation constants, Table VI. Equations (A-5) - (A-17) were made exact by adding the terms ignored when Equation (A-2) was used to approximate the solutions. For example, Equation (A-3) was re-written

$$a + 2r_1\left(\frac{b}{a}\right) = s_1 - \left(r_1 \ln\frac{a+b}{a-b} - 2r_1\left(\frac{b}{a}\right)\right) - r_2 \ln\frac{a+d}{a-d} - r_3 \ln\frac{a+f}{a-f} - r_4 \ln\frac{a+h}{a-h} -$$

$$r_5 \ln\frac{a+p}{a-p} - r_6 \ln\frac{a+r}{a-r} - r_7 \ln\frac{a+t}{a-t} - \frac{ac^2e^2g^2o^2q^2s^2u^2}{b^2d^2f^2h^2p^2r^2t^2} \qquad \text{(A-3a)}$$

To avoid repetition, the *exact* presentation of Equations (A-3a) - (A-17a) are listed in Appendix B, Program 2, Subroutine CONMP8, Statements #0112 - #0126. The values generated for S11,S22,...,S88,R11,..., R77 were used to replace $s_1,s_2,\ldots,s_8,r_1,\ldots,r_7$ respectively in Equations (A-3) - (A-17). The new equations were solved for the transformation constants a,b,c,...,u in terms of S11,S22,...,S88,R11,...,R77 and $s_1,s_2,\ldots,s_8,r_1,\ldots,r_7$. The equations are given in Appendix B, program 2, Subroutine CONMP8, statements #0143 - #0157. The variable names in the computer program A1,B1,...,RB1,SB1,...,U1 correspond to the transformation constants a,b,...,r,s,...,u.

The new values of the constants were substituted into the *exact* equations (Appendix B, Program 2, Subroutine CONMP8, Statements 0112 - 0126) to generate new values for S11,...,S88,R11,...,R77 which were in turn used to calculate better values for the transformation constants

TABLE VI

SOLUTIONS TO APPROXIMATE EQUATIONS (A-3)-(A-17)

$$a = \frac{s_1}{2}$$

$$b = \frac{s_1^2}{2^3 r_1}$$

$$c = \frac{s_2 s_1^2}{2^5 r_1^2}$$

$$d = \frac{s_2^2 s_1^2}{2^7 r_2 r_1^2}$$

$$e = \frac{s_3 s_2^2 s_1^2}{2^9 r_2^2 r_1^2}$$

$$f = \frac{s_3^2 s_2^2 s_1^2}{2^{11} r_3 r_2^2 r_1^2}$$

$$g = \frac{s_4 s_3^2 s_2^2 s_1^2}{2^{13} r_3^2 r_2^2 r_1^2}$$

$$h = \frac{s_4^2 s_3^2 s_2^2 s_1^2}{2^{15} r_4 r_3^2 r_2^2 r_1^2}$$

$$o = \frac{s_5 s_4^2 s_3^2 s_2^2 s_1^2}{2^{17} r_4^2 r_3^2 r_2^2 r_2^2}$$

$$p = \frac{s_5^2 s_4^2 s_3^2 s_2^2 s_1^2}{2^{19} r_5 r_4^2 r_3^2 r_2^2 r_1^2}$$

$$q = \frac{s_6 s_5^2 s_4^2 s_3^2 s_2^2 s_1^2}{2^{21} r_5^2 r_4^2 r_3^2 r_2^2 r_1^2}$$

$$r = \frac{s_6^2 s_5^2 s_4^2 s_3^2 s_2^2 s_1^2}{2^{23} r_6 r_5^2 r_4^2 r_3^2 r_2^2 r_1^2}$$

$$s = \frac{s_7 s_6^2 s_5^2 s_4^2 s_3^2 s_2^2 s_1^2}{2^{25} r_6^2 r_5^2 r_4^2 r_3^2 r_2^2 r_1^2}$$

$$t = \frac{s_7^2 s_6^2 s_5^2 s_4^2 s_3^2 s_2^2 s_1^2}{2^{27} r_7 r_6^2 r_5^2 r_4^2 r_3^2 r_2^2 r_1^2}$$

$$u = \frac{s_8 s_7^2 s_6^2 s_5^2 s_4^2 s_3^2 s_2^2 s_1^2}{2^{29} r_7^2 r_6^2 r_5^2 r_4^2 r_3^2 r_2^2 r_1^2}$$

(Program 2, Subroutine CONMP8, Statements 0143 - 0157). The iteration process was terminated when two successive values of e differed by less than 10^{-9}. In general convergence is within a few iterations; however, for certain lens geometries successive values of the transformation constants oscillated with increasing divergence about their respective true values. Wallington (46) found that by employing an additional sequence to the iteration scheme the oscillation could be damped. The modified procedure was to carry out the first two iterations in the normal manner, and for the third iteration to use as the latest values the mean of the values generated in the previous two iterations. The fourth iteration was carried out normally using the values from the third iteration, but the fifth used the mean of the third and fourth iterations. By use of this weighting procedure, convergence was obtained within 30 iterations for all lens geometries studied.

Up to this point lenses have been considered in which slit dimensions were smaller than the distances between successive apertured planes. In lens systems where the slit dimensions are large compared to distances between successive apertures, Wallington (46) and Boerboom (53) have developed special mathematical procedures for approximating and refining the transformation constants. Although these procedures are general, for large lens systems (over 3 or 4 electrode pairs) the mathematics becomes extensive. It was therefore decided to develop a simplier procedure which would be generally applicable. The procedure was to first obtain the transformation constants for a lens which had the proper slit widths and reasonably large spacing between adjacent slits (i.e. $\frac{1}{4}\pi r_{\#} > 2s_{\#}$). For this system Equations (A-3) - (A-17) were applicable; so approximate, then *exact* solutions were possible. The lens system was then changed slightly by decreasing the distances between apertured planes. Approximate solutions were not obtained for this second lens but rather the more accurate solutions from the previous lens were used as approximate solutions. The transformation constants were refined by iterations with the more exact equations (Program 2, Subroutine CONMP8, Statements 112 - 126) until constant values were obtained. A third lens was then considered in which the distances between adjacent planes was further decreased. The approximate transformation constants for the third lens were the *exact* values from the second lens. This procedure was repeated until the desired lens geometry was obtained.

Part II - Determination of Potentials in the Lens System

The central axis of the lens system coincides with the imaginary axis in both the z-plane and the w-plane. The equation which couples points on one imaginary axis to those on the other was obtained from Equation (A-1)(47).

$$y = v + 2r_1 \tan^{-1}\frac{v}{b} + 2r_2 \tan^{-1}\frac{v}{d} + 2r_3 \tan^{-1}\frac{v}{f} + 2r_4 \tan^{-1}\frac{v}{h} + 2r_5 \tan^{-1}\frac{v}{p} + 2r_6 \tan^{-1}\frac{v}{r} + 2r_7 \tan^{-1}\frac{v}{t} - \frac{a^2c^2e^2g^2o^2q^2s^2u^2}{b^2d^2f^2h^2p^2r^2t^2} / v \qquad \text{(A-18)}$$

where $r_1,\ldots,r_7$ and $a,b,\ldots,u$ correspond to the distances between apertured planes and the conformal mapping constants respectively, Figure 42. Equation (A-18) was solved iteratively for $\underline{v}$ at specified $\underline{y}$ positions along the imaginary axis in the z-plane. The total potential acting at the y-coordinate is the sum of the contributions of each individual electrode and in the case of symmetric potentials, each electrode pair.

$$V_{total} = \sum_{i=1}^{8} V'_i \qquad \text{(A-19)}$$

where,

$$V'_1 = \frac{2V_1}{\pi} \tan^{-1} \frac{v}{b}$$

$$V'_2 = \frac{2V_2}{\pi} \left(\tan^{-1} \frac{v}{d} - \tan^{-1} \frac{v}{b}\right)$$

$$V'_3 = \frac{2V_3}{\pi} \left(\tan^{-1} \frac{v}{f} - \tan^{-1} \frac{v}{d}\right)$$

$$V'_4 = \frac{2V_4}{\pi} \left(\tan^{-1} \frac{v}{h} - \tan^{-1} \frac{v}{f}\right)$$

$$V'_5 = \frac{2V_5}{\pi} \left(\tan^{-1} \frac{v}{p} - \tan^{-1} \frac{v}{h}\right)$$

$$V'_6 = \frac{2V_6}{\pi} \left(\tan^{-1} \frac{v}{r} - \tan^{-1} \frac{v}{p}\right)$$

$$V'_7 = \frac{2V_7}{\pi} \left(\tan^{-1} \frac{v}{t} - \tan^{-1} \frac{v}{r}\right)$$

$$V'_8 = \frac{2V_8}{\pi} \left(\frac{\pi}{2} - \tan^{-1} \frac{v}{t}\right)$$

and $V_1, V_2, \ldots, V_8$ are the potentials on each electrode pair.

The potentials at off-axis points were calculated with Equation (IV-5). The necessary first, second, third, and fourth derivatives of the potential required by Equations (IV-5) - (IV-7) are calculated in subroutines 'FSTPOT', 'SNDPOT', 'TRDPOT', and 'FRHPOT' respectively (Program 3, Appendix B).

PLEASE NOTE:

Appendix B has extremely small print. Filmed in the best possible way.

UNIVERSITY MICROFILMS.

APPENDIX B

COMPUTER PROGRAMS

```
C
C
C                    * * *   PROGRAM #1   * * *
C
C
C
C     ION TRAJECTORY CALCULATIONS THROUGH A 31.8 DEGREE ELECTROSTATIC SECTOR
C           BASED ON A CEC 21-110B MASS SPECTROMETER
C
C           THE CALCULATION STARTS WITH THE ION AT THE FINAL (ADJUSTABLE)
C     SLIT OF THE ION SOURCE.  A MASS, ANGULAR DIVERGENCE ALPHA (IN THE
C     X-Y PLANE), AND ACCELERATING POTENTIAL ARE ASSIGNED TO THE ION.  THE
C     ION TRAVERSES THE FIRST FIELD-FREE REGION AND IF IT HAS THE CORRECT
C     COORDINATES ENTERS THE ELECTROSTATIC ANALYZER.  BY KNOWING THE POSITION
C     AND THE FORCES ACTING ON THE ION NEW VELOCITIES ARE CALCULATED
C     EVERY DT (DELTA TIME).
C     TERMINATION OF THE PROGRAM OCCURS WHENEVER THE ION FAILS TO ENTER
C     THE ELECTROSTATIC SECTOR, HITS EITHER SECTOR PLATE, OR COMPLETES THE
C     TRIP THROUGH THE SECTOR.  THE OUTPUT CONSISTS OF ALL INPUT DATA,
C     A MESSAGE INDICATING WHY PROGRAM WAS TERMINATED, WHETHER THE ION
C     REACHES THE SECOND FIELD-FREE REGION, AND FINALLY THE POSITION
C     AND THE VELOCITY OF THE ION AT ITS LAST POINT.
C
C
C
C     CALCULATED PROGRAM VARIABLE NAMES
C           V = TOTAL VELOCITY OF THE ION IN THE FIRST FIELD-FREE REGION (CM/SEC)
C           VX = X-COMPONENT OF VELOCITY OF THE ION IN THE FIRST FIELD-
C                FREE REGION (CM/SEC)
C           VY = Y-COMPONENT OF VELOCITY OF ION IN THE FIRST FIELD-
C                FREE REGION (CM/SEC)
C           T = TIME TO TRAVERSE THE FIRST FIELD-FREE REGION (SEC)
C           Y = Y-POSITION OF THE PARTICLE AT THE ENTRANCE OF THE ELECTRIC
C                SECTOR -- REFERENCED TO THE CENTER LINE OF THE FIRST
C                FIELD-FREE REGION, THEN TO THE VERTEX OF THE ELECTROSTATIC
C                SECTOR (CM)
C           R = RADIAL DISPLACEMENT OF ION IN THE ELECTRIC SECTOR (CM)
C           VTHETA = VELOCITY OF ION IN ELECTRIC SECTOR IN THE THETA
C                    DIRECTION (RADIANS/SEC)
C           THETA = ANGULAR POSITION OF THE PARTICLE AT ANY TIME  (RADIANS)
C           VR = VELOCITY OF THE ION IN ELECTRIC SECTOR IN THE RADIAL
C                DIRECTION (CM/SEC)
C           AA = ELECTROSTATIC FORCE ACTING ON THE ION IN THE ELECTRIC
C                SECTOR (ERGS)
C           BB = CENTRIPETAL FORCE OF THE ION IN THE ELECTRIC SECTOR (ERGS)
C           FNET = NET FORCE ACTING ON THE ION IN THE ELECTRIC SECTOR (ERGS)
C           ER = ELECTRIC FIELD STRENGTH AT A GIVEN R (VOLTS/CM)
C           VX2 = X-COMPONENT OF VELOCITY OF THE ION AFTER LEAVING THE
C                 ELECTRIC SECTOR (CM/SEC)
C           VY2 = Y-COMPONENT OF VELOCITY OF THE ION AFTER LEAVING THE
C                 ELECTRIC SECTOR (CM/SEC)
C           XKEX2 = KINETIC ENERGY OF THE ION IN X-DIRECTION AFTER LEAVING
C                   THE ELECTRIC SECTOR (VOLTS)
C           XKEY2 = KINETIC ENERGY OF ION IN Y-DIRECTION AFTER LEAVING
C                   THE ELECTRIC SECTOR (VOLTS)
C
C
C     VARIABLES FOR A GIVEN RUN
C           DT = TIME INTERVAL FOR INCREMENT (SEC)
C           AMU = MASS OF ION (AMU)
C           YISS = Y-COORDINATE OF ION IN ION SOURCE SLIT
C                  ZERO TAKEN AS CENTER (CM)
C           XKE = KINETIC ENERGY OF ION - ACTUALLY ACCELERATING
C                 VOLTAGE (VOLTS)
C           ESP = ELECTRIC SECTOR POTENTIAL, POSITIVE PLATE WITH RESPECT
C                 TO INSTRUMENT GROUND (VOLTS)
C           ALPHA = ANGULAR DIVERGENCE OF ION FROM THE NORMAL X-Y PLANE
C                   (POSITIVE OR NEGATIVE RADIANS)
C
C
C     INSTRUMENT AND PHYSICAL CONSTANTS
C           AE = RADIUS OF CURVATURE OF ELECTRIC SECTOR (CM)
C           XTHETA = ELECTRIC SECTOR CURVATURE = (PI/(4*SQRT(2)) RADIANS)
C           R1 = RADIUS TO INNER ELECTRIC SECTOR PLATE (CM)
C           R2 = RADIUS TO OUTER ELECTRIC SECTOR PLATE (CM)
C           SEI = ENTRANCE SLIT WIDTH TO ELECTROSTATIC SECTOR (CM)
C           SEO = EXIT SLIT FROM ELECTROSTATIC SECTOR (CM)
C           XLE = LENGTH OF FIRST FIELD-FREE REGION (CM)
C           E = ELECTRON CHARGE = 1.6021917 E-19 COUL.
C           ONE AMU = 1.66043 E-24 GRAMS
C
C           ------------------------------------------------------------------
      IMPLICIT REAL*8 (A-H,O-Z)
      SQRT(X)=DSQRT(X)
      SIN(X)=DSIN(X)
      COS(X)=DCOS(X)
      ALOG(X)=DLOG(X)
      ARSIN(X)=DARSIN(X)
      ESP=372
      DO 69 LL=1,3
      ALPHA=-.00044
      DO 110 J=1,3
      XKE=7525.0
      DO 112 JJ=1,3
      XKE=XKE+.5
C
C        VARIABLES FOR THIS RUN
      DT=1.0D-10
      AMU=39.948D 00
      YISS=0.0D 00
C
C        INSTRUMENT AND PHYSICAL CONSTANTS
      AE=64D 00
      XTHETA=.555360367
      SEI=.04064
      SEO=.15240
      XLE=AE/SQRT(2.0D 00)
      R1=62.40615
      R2=65.59385
      E=1.6021917D-19
C
C        CONVERSIONS AND OTHER USEFUL QUANTITIES
      XMASS=AMU*(1.66043D-24)
      THETA=0.0
      AAA=AE-SEO/2.
      BBB=AE+SEO/2.
C
```

```
C         INITIALIZATION OF VARIABLES TO ZERO
      VX2=0.0
      VY2=0.0
      XKEX2=0.0
      XKEY2=0.0
      X=0.0
      Y=0.0
      R=0.0
      I=0
C
C         VELOCITY OF ION
      V=SQRT((2.D 00*E*XKE*1.0D 07)/XMASS)
C
C         COMPONENT OF VELOCITY IN X AND Y DIRECTIONS
      VX=V*COS(ALPHA)
      VY=V*SIN(ALPHA)
C
C         TIME TO REACH THE ELECTRIC SECTOR
      T=XLE/VX
C
C         POSITION OF ION AT ELECTRIC SECTOR
      Y=YISS+VY*T
      X=XLE
C
C         CHECK TO SEE IF ION WILL ENTER ELECTRIC SECTOR
      IF(Y)1,2,3
    3 IF(Y-SEI/2)2,2,4
    1 IF(Y+SEI/2)4,2,2
    4 WRITE(6,5)
    5 FORMAT(1H ,'ION FAILED TO MAKE ENTRANCE TO ELECTRIC SECTOR')
      GO TO 121
C
C         CHANGE ORIGIN TO VERTEX OF ELECTRIC SECTOR
    2 X=0.0
      Y=AE+Y
C
C         ELECTRIC FIELD IN ELECTROSTATIC SECTOR
      ESP1=-ESP
      XK1=(ESP1-ESP)/ALOG(R2/R1)
C
C         CHANGE TO CYLINDERICAL COORDINATES
      R=Y
      VTHETA=VX/R
      VR=VY
   10 ER=XK1/R
      I=I+1
C
C         FORCES ACTING IN RADIAL DIRECTION
      AA=E*ER*1.0D 07
      BB=XMASS*R*VTHETA*VTHETA
      FNET=AA+BB
C
C         NEW RADIAL ION VELOCITY
      VR=(FNET*DT)/XMASS+VR
C
C         POSITION OF ION AFTER TIME INTERVAL DT
      VTHETA=VX/R
      R=R+VR*DT
      THETA=THETA+VTHETA*DT
C
C         CHECK TO SEE IF ION HAS HIT ELECTRIC SECTOR WALL
      IF(R-AE)11,12,13
   11 IF(R-R1)14,14,12
   13 IF(R2-R)14,14,12
C
C         CHECK TO SEE IF ION IS AT EXIT SLIT OF ELECTRIC SECTOR
   12 IF(XTHETA-THETA)20,20,21
   21 GO TO 10
   14 WRITE (6,25)
   25 FORMAT(1H ,'ION HIT PLATE IN ELECTROSTATIC SECTOR')
      GO TO 121
C
C         CHECK TO SEE IF ION WILL EXIT ELECTRIC SECTOR INTO SECOND FIELD
C         FREE REGION
   20 IF(R-AE)31,32,33
   31 IF(R-AAA)34,34,32
   33 IF(BBB-R)34,34,32
   32 WRITE(6,40)
   40 FORMAT(1H ,'ION HAS PASSED THROUGH EXIT SLIT OF ELECTRIC SECTOR')
C
C         X- AND Y-COMPONENTS OF VELOCITY OF ION IN SECOND FIELD-FREE
C         REGION
      VX2=R*VTHETA
      XKEX2=(XMASS*VX2*VX2)/(2.0D 00*E*1.0D 07)
      VY2=VR
      XKEY2=(XMASS*VY2*VY2)/(2.D 00*E*1.0D 07)
      WRITE(6,102)XKE,YISS,ESP,ALPHA,AMU,DT,SEI,SEO,X,Y,R,THETA,VX2,
     2XKEX2,VY2,XKEY2,I
  102 FORMAT(1H ,//,' INITIAL CONDITIONS',/,' XKE= ',F7.2,/,' YISS= ',
     2E12.4,/' ESP= ',F6.1,/,' ALPHA= ',F8.5,/,' AMU= ',F8.4,/,' DT= ',
     3E15.7,/,' SEI= ',F7.5,/,' SEO= ',F7.5,////,' FINAL VALUES',/,
     4' X= ',F10.6,/,' Y= ',F10.6,/,' R= ',F10.6,/,' THETA= ',F8.6,/,
     5' VX2= ',E14.6,5X,'XKEX2= ',F8.2,/,' VY2= ',E14.6,5X,'XKEY2= ',
     6F8.2,/,' I= ',I8)
      GO TO 112
   34 WRITE(6,41)
   41 FORMAT(1H ,'ION HAS COMPLETED PASS THROUGH ELECTRIC SECTOR BUT FAI
     2LED TO PASS EXIT SLIT')
C
C         X- AND Y-COMPONENTS OF VELOCITY OF ION IN SECOND FIELD-FREE
C         REGION
  100 VX2=R*VTHETA
      XKEX2=(XMASS*VX2*VX2)/(2.0D 00*E*1.0D 07)
      VY2=VR
      XKEY2=(XMASS*VY2*VY2)/(2.D 00*E*1.0D 07)
      WRITE(6,102)XKE,YISS,ESP,ALPHA,AMU,DT,SEI,SEO,X,Y,R,THETA,VX2,
     2XKEX2,VY2,XKEY2,I
      GO TO 112
  121 WRITE(6,101)XKE,YISS,ESP,ALPHA,AMU,DT,SEI,SEO,X,Y,R,THETA,I
  101 FORMAT(1H ,//,' INITIAL CONDITIONS',/,' XKE= ',F7.2,/,' YISS= ',
     2E12.4,/' ESP= ',F6.1,/,' ALPHA= ',F8.5,/,' AMU= ',F8.4,/,' DT= ',
     3E15.7,/,' SEI= ',F7.5,/,' SEO= ',F7.5,////,' FINAL VALUES',/,
     4' X= ',F10.6,/,' Y= ',F10.6,/,' R= ',F10.6,/,' THETA= ',F8.6,/,
     5' I= ',I8)
  112 CONTINUE
  110 ALPHA=ALPHA+.00011
```

```
   69 ESP=ESP+3
      STOP
      END
```

```
C
C
C                       * * *   PROGRAM #2   * * *
C
C
C     CONFORMAL MAPPING USING THE SCHWARZ-CHRISTOFFEL TRANSFORMATION
C
C          THE PROGRAM DETERMINES TRANSFORMATION CONSTANTS FOR A LINEAR
C     EIGHT APERTURED ELECTROSTATIC LENS.  THE MAIN PROGRAM SUPPLIES THE
C     LENS GEOMETRY TO SUBROUTINE 'CONMP8'.  THE SUBROUTINE CALCULATES
C     THE CONFORMAL MAPPING TRANSFORMATION CONSTANTS USING APPROXIMATE AS
C     WELL AS THE 'EXACT' EQUATIONS.  AFTER THE CONSTANTS FOR THE FIRST
C     GEOMETRY ARE CALCULATED AND PRINTED, THE MAIN PROGRAM SUPPLIES A
C     SECOND GEOMETRY TO THE SUBROUTINE.  'CONMP8' DOES NOT CALCULATE
C     APPROXIMATE CONSTANTS FOR THIS SECOND AND SUBSEQUENT GEOMETRIES
C     BUT USES THE 'EXACT' SOLUTION  FROM THE PREVIOUS GEOMETRY AS A
C     FIRST APPROXIMATION.
C          WHEN TOO LARGE OF A CHANGE IN GEOMETRY IS ENCOUNTERED, THE
C     PROGRAM WILL BOMB -- USUALLY WITH A NEGATIVE LOG ARGUMENT.  AT THIS
C     POINT "XMOVE" SHOULD BE DECREASED AND THE PROGRAM RE-INITIATED
C     STARTING AT THE LAST SET OF TRANSFORMATION CONSTANTS.
C
C
      IMPLICIT REAL*8 (A-H,O-Z)
      COMMON PI,A,B,C,D,E,F,G,H,O,P,Q,R,S,T,U,XS1,XS2,XS3,XS4,XS5,XS6,
     2XS7,XS8,R1,R2,R3,R4,R5,R6,R7,XMESS,IFLAG
C
C          INITIAL LENS GEOMETRY
      XS1=.1
      XS2=.1
      XS3=.1
      XS4=.1
      XS5=.1
      XS6=.1
      XS7=.1
      XS8=.1
      XD1=.5
      XD2=.557
      XD3=.234
      XD4=.234
      XD5=.234
      XD6=.557
      XD7=.5
      Z=.000000001
      PI=3.141592653589793
      XMOVE=.055
      NUM=11
      IFLAG=0
      DO 1 I=1,NUM
      CALL CONMP8 (XD1,XD2,XD3,XD4,XD5,XD6,XD7,Z)
      IFLAG=1
C
C          CHANGES IN LENS GEOMETRY
      XD2=XD2-XMOVE
      XD3=XD3-2*XMOVE/3
      XD4=XD4-2*XMOVE/3
      XD5=XD5-2*XMOVE/3
    1 XD6=XD6-XMOVE
```

```
      STOP
      END
```

```
      SUBROUTINE CONMP8 (XD1,XD2,XD3,XD4,XD5,XD6,XD7,Z)
      IMPLICIT REAL*8 (A-H,O-Z)
      COMMON PI,A,B,C,D,E,F,G,H,O,P,Q,R,S,T,U,XS1,XS2,XS3,XS4,XS5,XS6,
     2XS7,XS8,R1,R2,R3,R4,R5,R6,R7,XMESS,IFLAG
      ABS(X)=DABS(X)
      ALOG(X)=DLOG(X)
      WRITE(6,5)XS1,XS2,XS3,XS4,XS5,XS6,XS7,XS8,XD1,XD2,XD3,XD4,XD5,XD6,
     2XD7
    5 FORMAT(1HO,' USING THE FOLLOWING INPUT PARAMETERS --',//,5X,'S1 ='
     2,F7.4,/,5X,'S2 =',F7.4,/,5X,'S3 =',F7.4,/,5X,'S4 =',F7.4,/,5X,'S5
     3=',F7.4,/,5X,'S6 =',F7.4,/,5X,'S7 =',F7.4,/,5X,'S8 =',F7.4,/,5X,'D
     41 =',F7.4,/,5X,'D2 =',F7.4,/,5X,'D3 =',F7.4,/,5X,'D4 =',F7.4,/,5X,
     5'D5 =',F7.4,/,5X,'D6 =',F7.4,/,5X,'D7 =',F7.4)
C
C         IF "IFLAG=1" THE SUBROUTINE DOES NOT CALCULATE APPROXIMATE
C         TRANSFORMATION CONSTANTS, THEY MUST ALREADY EXIST IN MEMORY --
C         EITHER FROM THE PREVIOUS GEOMETRY OR READ IN VIA THE MAIN
C         PROGRAM
      AA=0
      N=0
      IF(IFLAG.EQ.1) GO TO 55
      S1=XS1
      S2=XS2
      S3=XS3
      S4=XS4
      S5=XS5
      S6=XS6
      S7=XS7
      S8=XS8
      R1=XD1/PI
      R2=XD2/PI
      R3=XD3/PI
      R4=XD4/PI
      R5=XD5/PI
      R6=XD6/PI
      R7=XD7/PI
    1 A=S1/2
      V1=S1/(4*R1)
      B=V1*A
      V2=S2/(4*R1)
      C=V2*B
      V3=S2/(4*R2)
      D=V3*C
      V4=S3/(4*R2)
      E=V4*D
      V5=S3/(4*R3)
      F=V5*E
      V6=S4/(4*R3)
      G=V6*F
      V7=S4/(4*R4)
      H=V7*G
      V8=S5/(4*R4)
      O=V8*H
      V9=S5/(4*R5)
      P=V9*O
      V10=S6/(4*R5)
      Q=V10*P
      V11=S6/(4*R6)
```

```
      R=V11*Q
      V12=S7/(4*R6)
      S=V12*R
      V13=S7/(4*R7)
      T=V13*S
      V14=S8/(4*R7)
      U=V14*T
C        CHECK FOR CONVERGENCE OF "A" VALUE
      DIFF=ABS(AA-A)
      IF(DIFF.GT.Z) GO TO 2
      WRITE(6,6)N,A,B,C,D,E,F,G,H,O,P,Q,R,S,T,U
    6 FORMAT(1HO,//,' AFTER',I3,' ITERATIONS OF THE APPROXIMATE EQUATION
     2S ',//,5X,'A =',E14.6,/,5X,'B =',E14.6,/,5X,'C =',E14.6,/,5X,'D ='
     3,E14.6,/,5X,'E =',E14.6,/,5X,'F =',E14.6,/,5X,'G =',E14.6,/,5X,'H
     4=',E14.6,/,5X,'O =',E14.6,/,5X,'P =',E14.6,/,5X,'Q =',E14.6,/,5X,'
     5R =',E14.6,/,5X,'S =',E14.6,/,5X,'T =',E14.6,/,5X,'U =',E14.6)
      S1=A+2*R1*B/A
      S2=2*R1*C/B+2*R2*D/C
      S3=2*R2*E/D+2*R3*F/E
      S4=2*R3*G/F+2*R4*H/G
      S5=2*R4*O/H+2*R5*P/O
      S6=2*R5*Q/P+2*R6*R/Q
      S7=2*R6*S/P+2*R7*T/S
      S8=2*R7*U/T+(A*A/(B*B))*(C*C/(D*D))*(E*E/(F*F))*(G*G/(H*H))*(O*O/(
     2P*P))*(Q*Q/(R*R))*(S*S/(T*T))*U
      R1=A*A/(2*B)
      R2=R1*C*C/(B*D)
      R3=R2*E*E/(D*F)
      R4=R3*G*G/(F*H)
      R5=R4*O*O/(H*P)
      R6=R5*Q*Q/(P*R)
      R7=R6*S*S/(R*T)
      GO TO 10
    2 AA=A
      N=N+1
      S1=A+2*R1*B/A
      S2=2*R1*C/B+2*R2*D/C
      S3=2*R2*E/D+2*R3*F/E
      S4=2*R3*G/F+2*R4*H/G
      S5=2*R4*O/H+2*R5*P/O
      S6=2*R5*Q/P+2*R6*R/Q
      S7=2*R6*S/R+2*R7*T/S
      S8=2*R7*U/T+(A*A/(B*B))*(C*C/(D*D))*(E*E/(F*F))*(G*G/(H*H))*(O*O/(
     2P*P))*(Q*Q/(R*R))*(S*S/(T*T))*U
      R1=A*A/(2*B)
      R2=R1*C*C/(B*D)
      R3=R2*E*E/(D*F)
      R4=R3*G*G/(F*H)
      R5=R4*O*O/(H*P)
      R6=R5*Q*Q/(P*R)
      R7=R6*S*S/(R*T)
      GO TO 1
C        HIGHER APPROXIMATIONS OF SOLUTIONS
   55 R1=XD1/PI
      R2=XD2/PI
      R3=XD3/PI
      R4=XD4/PI
      R5=XD5/PI
      R6=XD6/PI
      R7=XD7/PI
      S1=XS1
      S2=XS2
      S3=XS3
      S4=XS4
      S5=XS5
      S6=XS6
      S7=XS7
      S8=XS8
   10 AA=E
      N=0
      JFLAG=0
      KFLAG=-1
C
C        'EXACT' EQUATIONS
   11 S11=S1-(R1*ALOG((A+B)/(A-B))-2*R1*B/A)
     2     -R2*ALOG((A+D)/(A-D))-R3*ALOG((A+F)/(A-F))-R4*ALOG((A+H)/(A-H)
     3)-R5*ALOG((A+P)/(A-P))-R6*ALOG((A+R)/(A-R))-R7*ALOG((A+T)/(A-T))-(
     4A*C*C/(B*B))*(E*E/(D*D))*(G*G/(F*F))*(O*O/(H*H))*(Q*Q/(P*P))*(S*S/
     5(R*R))*(U*U/(T*T))
C
      S22=S2-C-(R1*ALOG((B+C)/(B-C))-2*R1*C/B)
     2       -(R2*ALOG((C+D)/(C-D))-2*R2*D/C)
     3    -R3*ALOG((C+F)/(C-F))-R4*ALOG((C+H)/(C-H))-R5*ALOG((C+P)/(C-P)
     4)-R6*ALOG((C+R)/(C-R))-R7*ALOG((C+T)/(C-T))-(A*A*C/(B*B))*(E*E/(D*
     5D))*(G*G/(F*F))*(O*O/(H*H))*(Q*Q/(P*P))*(S*S/(R*R))*(U*U/(T*T))
C
      S33=S3-E-R1*ALOG((B+E)/(B-E))-(R2*ALOG((D+E)/(D-E))-2*R2*E/D)
     2                                -(R3*ALOG((E+F)/(E-F))-2*R3*F/E)
     3                               -R4*ALOG((E+H)/(E-H))-R5*ALOG((E+P)/(E-P)
     4)-R6*ALOG((E+R)/(E-R))-R7*ALOG((E+T)/(E-T))-(A*A/(B*B))*(C*C/(D*D)
     5)*(E*G*G/(F*F))*(O*O/(H*H))*(Q*Q/(P*P))*(S*S/(R*R))*(U*U/(T*T))
C
      S44=S4-G-R1*ALOG((B+G)/(B-G))-R2*ALOG((D+G)/(D-G))-(R3*ALOG((F+G)/
     2(F-G))-2*R3*G/F)                                  -(R4*ALOG((G+H)/
     3(G-H))-2*R4*H/G)                                 -R5*ALOG((G+P)/(G-P)
     4)-R6*ALOG((G+R)/(G-R))-R7*ALOG((G+T)/(G-T))-(A*A/(B*B))*(C*C/(D*D)
     5)*(E*E/(F*F))*(G*O*O/(H*H))*(Q*Q/(P*P))*(S*S/(R*R))*(U*U/(T*T))
C
      S55=S5-O-R1*ALOG((B+O)/(B-O))-R2*ALOG((D+O)/(D-O))-R3*ALOG((F+O)/(
     2F-O))-(R4*ALOG((H+O)/(H-O))-2*R4*O/H)
     3   -(R5*ALOG((O+P)/(O-P))-2*R5*P/O)
     4 -R6*ALOG((O+R)/(O-R))-R7*ALOG((O+T)/(O-T))-(A*A/(B*B))*(C*C/(D*D)
     5)*(E*E/(F*F))*(G*G/(H*H))*(O*Q*Q/(P*P))*(S*S/(R*R))*(U*U/(T*T))
C
      S66=S6-Q-R1*ALOG((B+Q)/(B-Q))-R2*ALOG((D+Q)/(D-Q))-R3*ALOG((F+Q)/(
     2F-Q))-P4*ALOG((H+Q)/(H-Q))-(R5*ALOG((P+Q)/(P-Q))-2*R5*Q/P)
     3                             -(R6*ALOG((Q+R)/(Q-R))-2*R6*R/Q)
     4                          -R7*ALOG((Q+T)/(Q-T))-(A*A/(B*B))*(C*C/(D*D)
     5)*(E*E/(F*F))*(G*G/(H*H))*(O*O/(P*P))*(Q*S*S/(R*R))*(U*U/(T*T))
C
      S77=S7-S-R1*ALOG((B+S)/(B-S))-R2*ALOG((D+S)/(D-S))-R3*ALOG((F+S)/(
     2F-S))-R4*ALOG((H+S)/(H-S))-R5*ALOG((P+S)/(P-S))-(R6*ALOG((R+S)/(R-
     3S))-2*R6*S/R)                                    -(R7*ALOG((S+T)/(S-T)
     4)-2*R7*T/S)                                   -(A*A/(B*B))*(C*C/(D*D)
     5)*(E*E/(F*F))*(G*G/(H*H))*(O*O/(P*P))*(Q*Q*S/(R*R))*(U*U/(T*T))
C
```

```
      S88=S8-U-R1*ALOG((B+U)/(B-U))-R2*ALOG((D+U)/(D-U))-R3*ALOG((F+U)/(
     2F-U))-R4*ALOG((U+H)/(H-U))-R5*ALOG((P+U)/(P-U))-R6*ALOG((R+U)/(R-U
     3))-(R7*ALOG((T+U)/(T-U))-2*R7*U/T)
C
      R11=R1*((B*B-D*D)/(B*B-C*C))*((B*B-F*F)/(B*B-E*E))*((B*B-H*H)/(B*B
     2-G*G))*((B*B-P*P)/(B*B-O*O))*((B*B-R*R)/(B*B-Q*Q))*((B*B-T*T)/(B*B
     3-S*S))*(B*B/(B*B-U*U))+B/2
C
      R22=R2*(C*C/(C*C-D*D))*((B*B-D*D)/(B*B))*((D*D-F*F)/(D*D-E*E))*((D
     2*D-H*H)/(D*D-G*G))*((D*D-P*P)/(D*D-O*O))*((D*D-R*R)/(D*D-Q*Q))*((D
     3*D-T*T)/(D*D-S*S))*(D*D/(D*D-U*U))+(D*C*C)/(2*B*B)
C
      R33=R3*(C*C/(C*C-F*F))*((B*B-F*F)/(B*B))*(E*E/(E*E-F*F))*((D*D-F*F
     2)/(D*D))*((F*F-H*H)/(F*F-G*G))*((F*F-P*P)/(F*F-O*O))*((F*F-R*R)/(F
     3*F-Q*Q))*((F*F-T*T)/(F*F-S*S))*(F*F/(F*F-U*U))+(F*C*C/(2*B*B))*(E*
     4E/(D*D))
C
      R44=R4*(C*C/(C*C-H*H))*((B*B-H*H)/(B*B))*(E*E/(E*E-H*H))*((D*D-H*H
     2)/(D*D))*(G*G/(G*G-H*H))*((F*F-H*H)/(F*F))*((H*H-P*P)/(H*H-O*O))*
     3((H*H-R*R)/(H*H-Q*Q))*((H*H-T*T)/(H*H-S*S))*(H*H/(H*H-U*U))+(H*C*C
     3/(2*B*B))*(E*E/(D*D))*(G*G/(F*F))
C
      R55=R5*(C*C/(C*C-P*P))*((B*B-P*P)/(B*B))*(E*E/(E*E-P*P))*((D*D-P*P
     2)/(D*D))*(G*G/(G*G-P*P))*((F*F-P*P)/(F*F))*(O*O/(O*O-P*P))*((H*H-P
     3*P)/(H*H))*((P*P-R*R)/(P*P-Q*Q))*((P*P-T*T)/(P*P-S*S))*(P*P/(P*P-U
     4*U))+(P*C*C/(2*B*B))*(E*E/(D*D))*(G*G/(F*F))*(O*O/(H*H))
C
      R66=R6*(C*C/(C*C-R*R))*((B*B-R*R)/(B*B))*(E*E/(E*E-R*R))*((D*D-R*R
     2)/(D*D))*(G*G/(G*G-R*R))*((F*F-R*R)/(F*F))*(O*O/(O*O-R*R))*((H*H-R
     3*R)/(H*H))*(Q*Q/(Q*Q-R*R))*((P*P-R*R)/(P*P))*((R*R-T*T)/(R*R-S*S))
     4*(R*R/(R*R-U*U))+(R*C*C/(2*B*B))*(E*E/(D*D))*(G*G/(F*F))*(O*O/(H*H
     5))*(Q*Q/(P*P))
C
      R77=R7*(C*C/(C*C-T*T))*((B*B-T*T)/(B*B))*(E*E/(E*E-T*T))*((D*D-T*T
     2)/(D*D))*(G*G/(G*G-T*T))*((F*F-T*T)/(F*F))*(O*O/(O*O-T*T))*((H*H-T
     3*T)/(H*H))*(Q*Q/(Q*Q-T*T))*((P*P-T*T)/(P*P))*(S*S/(S*S-T*T))*((R*R
     4-T*T)/(R*R))*(T*T/(T*T-U*U))+(T*C*C/(2*B*B))*(E*E/(D*D))*(G*G/(F*F
     5))*(O*O/(H*H))*(Q*Q/(P*P))*(S*S/(R*R))
C
      VV1=S11/(2*(R1+R11))
      VV2=S22*R22/(2*(R1*R22+R2*R11))
      VV3=S22*R11/(2*(R1*R22+R2*R11))
      VV4=S33*R33/(2*(R2*R33+R3*R22))
      VV5=S33*R22/(2*(R2*R33+R3*R22))
      VV6=S44*R44/(2*(R3*R44+R4*R33))
      VV7=S44*R33/(2*(R3*R44+R4*R33))
      VV8=S55*R55/(2*(R4*R55+R5*R44))
      VV9=S55*R44/(2*(R4*R55+R5*R44))
      VV10=S66*R66/(2*(R5*R66+R6*R55))
      VV11=S66*R55/(2*(R5*R66+R6*R55))
      VV12=S77*R77/(2*(R6*R77+R7*R66))
      VV13=S77*R66/(2*(R6*R77+R7*R66))
      VV14=S88/(2*(R7+R77))
      IF(N.GT.1000) GO TO 100
      IF(JFLAG.EQ.1)GO TO 56
      A1=S11*R11/(R1+R11)
      B1=A1*VV1
      C1=B1*VV2
      D1=C1*VV3
      E1=D1*VV4
      F1=E1*VV5
      G1=F1*VV6
      H1=G1*VV7
      O1=H1*VV8
      P1=O1*VV9
      Q1=P1*VV10
      RB1=Q1*VV11
      SB1=RB1*VV12
      T1=SB1*VV13
      U1=T1*VV14
      JFLAG=1
      DIF=ABS(AA-E1)
      IF(DIF.GT.Z) GO TO 20
      A=A1
      B=B1
      C=C1
      D=D1
      E=E1
      F=F1
      G=G1
      H=H1
      O=O1
      P=P1
      Q=Q1
      R=RB1
      S=SB1
      T=T1
      U=U1
   31 WRITE(6,60)N,A,B,C,D,E,F,G,H,O,P,Q,R,S,T,U
   60 FORMAT(1H0,//,' AFTER',I5,' ITERATIONS OF "EXACT" EQUATIONS, THE C
     2ONFORMAL MAP CONSTANTS ARE --',//,5X,'A =',E14.6,/,5X,'B =',E14.6,
     3/,5X,'C =',E14.6,/,5X,'D =',E14.6,/,5X,'E =',E14.6,/,5X,'F =',E14.
     46,/,5X,'G =',E14.6,/,5X,'H =',E14.6,/,5X,'O =',E14.6,/,5X,'P =',E1
     54.6,/,5X,'Q =',E14.6,/,5X,'R =',E14.6,/,5X,'S =',E14.6,/,5X,'T =',
     6E14.6,/,5X,'U =',E14.6)
      WRITE(6,61)A,B,C,D,E,F,G,H,O,P,Q,R,S,T,U
   61 FORMAT(1H0,5(/,3(E22.14,5X)))
C         CALCULATED VALUES OF PHYSICAL ASPECTS OF LENS SYSTEM
   69 FORMAT(1H0,//,' PRESENT CALCULATED VALUES FOR S1, S2, S3, S4, S5,
     2S6, S7, S8',/,' D1, D2, D3, D4, D5, D6, D7 RESPECTIVELY --',15(/,
     35X,E14.6))
      GO TO 100
   20 N=N+1
      A=A1
      B=B1
      C=C1
      D=D1
      E=E1
      F=F1
      G=G1
      H=H1
      O=O1
      P=P1
      Q=Q1
      R=RB1
      S=SB1
```

```
      T=T1
      U=U1
      AA=E
      GO TO 11
   56 A2=S11*R11/(R1+R11)
      B2=A2*VV1
      C2=B2*VV2
      D2=C2*VV3
      E2=D2*VV4
      F2=E2*VV5
      G2=F2*VV6
      H2=G2*VV7
      O2=H2*VV8
      P2=O2*VV9
      Q2=P2*VV10
      RB2=Q2*VV11
      SB2=RB2*VV12
      T2=SB2*VV13
      U2=T2*VV14
      DIF=ABS(AA-E2)
      IF(DIF.GT.Z) GO TO 30
      A=A2
      B=B2
      C=C2
      D=D2
      E=E2
      F=F2
      G=G2
      H=H2
      O=O2
      P=P2
      Q=Q2
      R=RB2
      S=SB2
      T=T2
      U=U2
      GO TO 31
   30 A1=(A1+A2)/2
      B1=(B1+B2)/2
      C1=(C1+C2)/2
      D1=(D1+D2)/2
      E1=(E1+E2)/2
      F1=(F1+F2)/2
      G1=(G1+G2)/2
      H1=(H1+H2)/2
      O1=(O1+O2)/2
      P1=(P1+P2)/2
      Q1=(Q1+Q2)/2
      RB1=(RB1+RB2)/2
      SB1=(SB1+SB2)/2
      T1=(T1+T2)/2
      U1=(U1+U2)/2
      AA=E1
      N=N+1
      A=A1
      B=B1
      C=C1
      D=D1
      E=E1
      F=F1
      G=G1
      H=H1
      O=O1
      P=P1
      Q=Q1
      R=RB1
      S=SB1
      T=T1
      U=U1
      IF(N.EQ.100) KFLAG=0
      IF(KFLAG.EQ.0) GO TO 32
      IF(KFLAG.EQ.1) GO TO 33
      GO TO 11
   32 A3=A1
      B3=B1
      C3=C1
      D3=D1
      E3=E1
      F3=F1
      G3=G1
      H3=H1
      O3=O1
      P3=P1
      Q3=Q1
      RB3=RB1
      SB3=SB1
      T3=T1
      U3=U1
      KFLAG=1
      GO TO 11
   33 KFLAG=0
      A1=(A1+   A3)/2
      B1=(B1+   B3)/2
      C1=(C1+   C3)/2
      D1=(D1+   D3)/2
      E1=(E1+   E3)/2
      F1=(F1+   F3)/2
      G1=(G1+   G3)/2
      H1=(H1+   H3)/2
      O1=(O1+   O3)/2
      P1=(P1+   P3)/2
      Q1=(Q1+   Q3)/2
      RB1=(RB1+    RB3)/2
      SB1=(SB1+    SB3)/2
      T1=(T1+   T3)/2
      U1=(U1+   U3)/2
      A=A1
      B=B1
      C=C1
      D=D1
      E=E1
      F=F1
      G=G1
      H=H1
      O=O1
      P=P1
```

```
      Q=Q1
      R=RB1
      S=SB1
      T=T1
      U=U1
      GO TO 11
  100 RETURN
      END
```

```
C
C
C                      * * *   PROGRAM #3   * * *
C
C
C     NUMERICAL CALCULATIONS OF THE POTENTIAL DISTRIBUTION AND ION  TRAJECTORIES
C     IN A SYMMETRIC LINEAR SIXTEEN ELEMENT ELECTROSTATIC LENS.
C
C
C          THE CONSTANTS OF THE TRANSFORMATION HAVING ALREADY BEEN DETERMINED
C     ARE KEY-PUNCHED INTO THIS PROGRAM AND CHECKED BY CALCULATING THE PHYSICAL
C     CONSTANTS OF THE LENS IN THE Z-PLANE.  AFTER INITIALIZATION OF THE LENS
C     VOLTAGES, ION POSITION, AND ENERGY, ROOTS ARE FOUND FOR THE 'INVERSE
C     FUNCTION'.  THE FIRST THROUGH THE FOURTH DERIVATIVES OF THE POTENTIAL
C     WITH RESPECT TO POSITION ARE ALSO FOUND SO THE FORCES ACTING ON OFF-AXIS
C     IONS CAN BE CALCULATED.  BY KNOWING THE POSITION AND THE FORCES ACTING ON
C     THE ION, NEW VELOCITIES AND POSITIONS ARE CALCULATED EVERY DT (DELTA TIME).
C
C
C
C     MAIN PROGRAM VARIABLE NAMES
C          A,B,C,....,U (EXCLUDING I-N) = CONFORMAL TRANSFORMATION CONSTANTS
C          XMESS = THE LARGE CONSTANT IN THE 'INVERSE FUNCTION'
C          XMASS = MASS OF THE ION.  (GRAMS)
C          RR1,RR2,....,RR7 = CALCULATED VALUES FOR THE PHYSICAL DISTANCES
C                             BETWEEN ELECTRODE PAIRS IN THE Z-PLANE (CM)
C          SS1,SS2,....,SS8 = CALCULATED VALUES FOR THE PHYSICAL SLIT WIDTHS
C                             FROM THE CENTER LINE OF THE LENS SYSTEM (CM)
C          Q2,Q3,....,Q7 = POTENTIAL ON A GIVEN ELECTRODE PAIR.  (VOLTS)
C          TOL = TOLERANCE TO WHICH SUCCESSIVE VALUES OF THE 'INVERSE FUNCTION'
C                MUST MEET BEFORE A "ROOT" IS DECLARED.  USED IN SUBROUTINE
C                'FIND'
C          XLNGTH = TOTAL LENGTH OF LENS.  (CM)
C          DT = TIME INTERVAL FOR SUCCESSIVE CALCULATIONS OF FORCES.  (SEC)
C          XKE = KINETIC ENERGY OF ION.  (ELECTRON-VOLTS)
C          V = TOTAL VELOCITY OF THE ION.  (CM/SEC)
C          VX = COMPONENT OF THE ION VELOCITY IN THE X-DIRECTION.  (CM/SEC)
C          VY = COMPONENT OF THE ION VELOCITY IN THE Y-DIRECTION.  (CM/SEC)
C          X = X-COORDINATE OF THE ION IN THE LENS.  (CM)
C          Y = Y-COORDINATE OF THE ION IN THE LENS.  (CM)
C          FORCEX = FORCE ACTING ON THE ION IN THE X-DIRECTION.  (DYNES)
C          FORCEY = FORCE ACTING ON THE ION IN THE Y-DIRECTION.  (DYNES)
C
C          -----------------------------------------------------------------
C
      IMPLICIT REAL*8 (A-H,O-Z)
      COMMON PI,A,B,C,D,E,F,G,H,O,P,Q,R,S,T,U,XS1,XS2,XS3,XS4,XS5,XS6,
     2XS7,XS8,R1,R2,R3,R4,R5,R6,R7,XMESS,Q2,Q3,Q4,Q5,Q6,Q7,DVDR2,DVDR3,
     3DVDR4,DVDR5,DVDR6,DVDR7,SVR22,SVR23,SVR24,SVR25,SVR26,SVR27,TVR32,
     4TVR33,TVR34,TVR35,TVR36,TVR37,DVDY2,DVDY3,DVDY4,DVDY5,DVDY6,DVDY7,
     5SVY22,SVY23,SVY24,SVY25,SVY26,SVY27,TVY32,TVY33,TVY34,TVY35,TVY36,
     6TVY37,DYDR,SYR2,TYR3,SYRY,DRDY,SRY2,TRY3,FVR42,FVR43,FVR44,FVR45,
     7FVR46,FVR47,FVY42,FVY43,FVY44,FVY45,FVY46,FVY47,FYR4,FRY4,TOTALV,
     8TOTAL1,TOTAL2,TOTAL3,TOTAL4,ZB,ZD,ZF,ZH,ZP,ZR,ZT
      ALOG(X)=DLOG(X)
      SQRT(X)=DSQRT(X)
      ABS(X)=DABS(X)
      SIN(X)=DSIN(X)
```

```
0007        COS(X)=DCOS(X)
      C
      C        PHYSICAL CONSTANTS OF LENS SYSTEM IN THE Z-PLANE
0008        XS1=.1
0009        XS2=.1
0010        XS3=.102
0011        XS4=.102
0012        XS5=.102
0013        XS6=.102
0014        XS7=.002
0015        XS8=.1
0016        XD1=2.0306
0017        XD2=.5
0018        XD3=.0873
0019        XD4=.0873
0020        XD5=.0873
0021        XD6=.5
0022        XD7=.5
0023        PI=3.141592653589793
      C
      C        FROM THE CONFORMAL MAP PROGRAM THE FOLLOWING CONSTANTS WERE OBTAINED
0024        A=.500247747285230-01
0025        B=.193008626358800-02
0026        C=.750283723969140-04
0027        D=.113548487324950-04
0028        E=.189247324922000-05
0029        F=.101214725095590-05
0030        G=.564944277279560-06
0031        H=.318563285470290-06
0032        O=.179636240229680-06
0033        P=.100279107881800-06
0034        Q=.536573067272460-07
0035        R=.914603868576420-08
0036        S=.280764740961650-10
0037        T=.860935221589060-13
0038        U=.133064656696310-13
0039        XMESS=(A*A/(B*B))*(C*C/(D*D))*(E*E/(F*F))*(G*G/(H*H))*(O*O/(P*P))*
           2(Q*Q/(R*R))*(S*S/(T*T))*(U*U)
      C
      C        USING CONFORMAL TRANSFORMATION MAPPING CONSTANTS THE PHYSICAL
      C        CONSTANTS OF THE LENS SYSTEM IN THE Z-PLANE ARE CALCULATED
0040        RR1=((A*A-B*B)/(2*B))*((B*B-C*C)/(B*B-D*D))*((B*B-E*E)/(B*B-F*F))*
           2((B*B-G*G)/(B*B-H*H))*((B*B-O*O)/(B*B-P*P))*((B*B-Q*Q)/(B*B-R*R))*
           3((B*B-S*S)/(B*B-T*T))*((B*B-U*U)/(B*B))
0041        RR2=((A*A-D*D)/(2*D))*((C*C-D*D)/(B*B-D*D))*((D*D-E*E)/(D*D-F*F))*
           2((D*D-G*G)/(D*D-H*H))*((D*D-O*O)/(D*D-P*P))*((D*D-Q*Q)/(D*D-R*R))*
           3((D*D-S*S)/(D*D-T*T))*((D*D-U*U)/(D*D))
0042        RR3=((A*A-F*F)/(2*F))*((C*C-F*F)/(B*B-F*F))*((E*E-F*F)/(D*D-F*F))*
           2((F*F-G*G)/(F*F-H*H))*((F*F-O*O)/(F*F-P*P))*((F*F-Q*Q)/(F*F-R*R))*
           3((F*F-S*S)/(F*F-T*T))*((F*F-U*U)/(F*F))
0043        RR4=((A*A-H*H)/(2*H))*((C*C-H*H)/(B*B-H*H))*((E*E-H*H)/(D*D-H*H))*
           2((G*G-H*H)/(F*F-H*H))*((H*H-O*O)/(H*H-P*P))*((H*H-Q*Q)/(H*H-R*R))*
           3((H*H-S*S)/(H*H-T*T))*((H*H-U*U)/(H*H))
0044        RR5=((A*A-P*P)/(2*P))*((C*C-P*P)/(B*B-P*P))*((E*E-P*P)/(D*D-P*P))*
           2((G*G-P*P)/(F*F-P*P))*((O*O-P*P)/(H*H-P*P))*((P*P-Q*Q)/(P*P-R*R))*
           3((P*P-S*S)/(P*P-T*T))*((P*P-U*U)/(P*P))
0045        RR6=((A*A-R*R)/(2*R))*((C*C-R*R)/(B*B-R*R))*((E*E-R*R)/(D*D-R*R))*
           2((G*G-R*R)/(F*F-R*R))*((O*O-R*R)/(H*H-R*R))*((Q*Q-R*R)/(P*P-R*R))*
           3((R*R-S*S)/(R*R-T*T))*((R*R-U*U)/(R*R))
0046        RR7=((A*A-T*T)/(2*T))*((C*C-T*T)/(B*B-T*T))*((E*E-T*T)/(D*D-T*T))*
           2((G*G-T*T)/(F*F-T*T))*((O*O-T*T)/(H*H-T*T))*((Q*Q-T*T)/(P*P-T*T))*
           3((S*S-T*T)/(R*R-T*T))*((T*T-U*U)/(T*T))
0047        R1=RR1
0048        R2=RR2
0049        R3=RR3
0050        R4=RR4
0051        R5=RR5
0052        R6=RR6
0053        R7=RR7
0054        SS1=A+R1*ALOG((A+B)/(A-B))+R2*ALOG((A+D)/(A-D))+R3*ALOG((A+F)/(A-F
           2))+R4*ALOG((A+H)/(A-H))+R5*ALOG((A+P)/(A-P))+R6*ALOG((A+R)/(A-R))+
           3R7*ALOG((A+T)/(A-T))+(A*C*C/(B*B))*(E*E/(D*D))*(G*G/(F*F))*(O*O/(H
           4*H))*(Q*Q/(P*P))*(S*S/(R*R))*(U*U/(T*T))
0055        SS2=C+R1*ALOG((B+C)/(B-C))+R2*ALOG((C+D)/(C-D))+R3*ALOG((C+F)/(C-F
           2))+R4*ALOG((C+H)/(C-H))+R5*ALOG((C+P)/(C-P))+R6*ALOG((C+R)/(C-R))+
           3R7*ALOG((C+T)/(C-T))+(A*A/(B*B))*(C*E*E/(D*D))*(G*G/(F*F))*(O*O/(H
           4*H))*(Q*Q/(P*P))*(S*S/(R*R))*(U*U/(T*T))
0056        SS3=E+R1*ALOG((B+E)/(B-E))+R2*ALOG((D+E)/(D-E))+R3*ALOG((E+F)/(E-F
           2))+R4*ALOG((E+H)/(E-H))+R5*ALOG((E+P)/(E-P))+R6*ALOG((E+R)/(E-R))+
           3R7*ALOG((E+T)/(E-T))+(A*A/(B*B))*(C*C/(D*D))*(E*G*G/(F*F))*(O*O/(H
           4*H))*(Q*Q/(P*P))*(S*S/(R*R))*(U*U/(T*T))
0057        SS4=G+R1*ALOG((B+G)/(B-G))+R2*ALOG((D+G)/(D-G))+R3*ALOG((F+G)/(F-G
           2))+R4*ALOG((G+H)/(G-H))+R5*ALOG((G+P)/(G-P))+R6*ALOG((G+R)/(G-R))
           3+R7*ALOG((G+T)/(G-T))+(A*A/(B*B))*(C*C/(D*D))*(E*E/(F*F))*(G*O*O/(
           4H*H))*(Q*Q/(P*P))*(S*S/(R*R))*(U*U/(T*T))
0058        SS5=O+R1*ALOG((B+O)/(B-O))+R2*ALOG((D+O)/(D-O))+R3*ALOG((F+O)/(F-O
           2))+R4*ALOG((H+O)/(H-O))+R5*ALOG((O+P)/(O-P))+R6*ALOG((O+R)/(O-R))+
           3R7*ALOG((O+T)/(O-T))+(A*A/(B*B))*(C*C/(D*D))*(E*E/(F*F))*(G*G/(H*H
           4))*(O*Q*Q/(P*P))*(S*S/(R*R))*(U*U/(T*T))
0059        SS6=Q+R1*ALOG((B+Q)/(B-Q))+R2*ALOG((D+Q)/(D-Q))+R3*ALOG((F+Q)/(F-Q
           2))+R4*ALOG((H+Q)/(H-Q))+R5*ALOG((P+Q)/(P-Q))+R6*ALOG((Q+R)/(Q-R))+
           3R7*ALOG((Q+T)/(Q-T))+(A*A/(B*B))*(C*C/(D*D))*(E*E/(F*F))*(G*G/(H*H
           4))*(O*O/(P*P))*(Q*S*S/(R*R))*(U*U/(T*T))
0060        SS7=S+R1*ALOG((B+S)/(B-S))+R2*ALOG((D+S)/(D-S))+R3*ALOG((F+S)/(F-S
           2))+R4*ALOG((H+S)/(H-S))+R5*ALOG((P+S)/(P-S))+R6*ALOG((R+S)/(R-S))+
           3R7*ALOG((S+T)/(S-T))+(A*A/(B*B))*(C*C/(D*D))*(E*E/(F*F))*(G*G/(H*H
           4))*(O*O/(P*P))*(Q*Q/(R*R))*(S*U*U/(T*T))
0061        SS8=U+R1*ALOG((B+U)/(B-U))+R2*ALOG((D+U)/(D-U))+R3*ALOG((F+U)/(F-U
           2))+R4*ALOG((H+U)/(H-U))+R5*ALOG((P+U)/(P-U))+R6*ALOG((R+U)/(R-U))+
           3R7*ALOG((T+U)/(T-U))+(A*A/(B*B))*(C*C/(D*D))*(E*E/(F*F))*(G*G/(H*H
           4))*(O*O/(P*P))*(Q*Q/(R*R))*(S*S*U/(T*T))
0062        RR1=RR1*PI
0063        RR2=RR2*PI
0064        RR3=RR3*PI
0065        RR4=RR4*PI
0066        RR5=RR5*PI
0067        RR6=RR6*PI
0068        RR7=RR7*PI
0069        WRITE(6,69)SS1,SS2,SS3,SS4,SS5,SS6,SS7,SS8,RR1,RR2,RR3,RR4,RR5,
           2RR6,RR7
0070     69 FORMAT (1H1,//,' TRAJECTORY CALCULATION ON A LENS SYSTEM WITH S1,
           2S2, S3, S4, S5, S6, S7, S8',/,' D1, D2, D3, D4, D5, D6, D7 RESPECT
           3IVELY --',15(/,5X,F7.4))
0071        R1=RR1/PI
0072        R2=RR2/PI
0073        R3=RR3/PI
```

```
      R4=RR4/PI
      R5=RR5/PI
      R6=RR6/PI
      R7=RR7/PI
      Q2=0.0 D 00
      Q3=7.440D 03
      Q4=Q3
      Q5=Q3
      Q6=Q3
      Q7=Q2
      TOL=1.E-14
      XLNGTH=XD1+XD2+XD3+XD4+XD5+XD6+XD7
      GUARD=XLNGTH-XD7
      ALPHA=0.0
      AMU=39.948
      CHARGE=1.60219170-19
      DT=.75D-09
      NUM=5
      NUM2=5
      XKE=7.280D 03
      XMASS=AMU*(1.66043E-24)
      START=XLNGTH
C
C        THE NUMBER OF ADDITIONAL ION KINETIC ENERGIES STARTING AT 'XKE'
      DO 40 I=1,NUM
      XX=.01
C
C        THE NUMBER OF PARAXIAL TRAJECTORIES IN ADDITION TO THE INITIAL 'XX'
      DO 10 II=1,NUM2
      V=SQRT((2*CHARGE*XKE*1.0D 07)/XMASS)
      V=-V
      N=0
      Y=START
      X=XX
      VX=V*SIN(ALPHA)
      VY=V*COS(ALPHA)
      WRITE(6,17)X,VX,VY,XKE
   17 FORMAT(1H0,//,' INITIAL VALUES OF X, VX, VY, & XKE',/,F8.4,
     23(2X,E14.6))
C
C        START OF STEP-BY-STEP RAY TRACE LOOP
   13 CALL FIND(Y,TOL,ROOT,BOMB)
      IF(BOMB.EQ.1) GO TO 50
      CALL FSTPOT(ROOT)
      CALL SNDPOT(ROOT)
      CALL TRDPOT(ROOT)
      CALL FRHPOT(ROOT)
      FORCEX=-X*TOTAL2+X*X*X*TOTAL4/6
      FORCEY=TOTAL1-X*X*TOTAL3/2
      N=N+1
   21 VX=-CHARGE*FORCEX*DT*1.0D 07/XMASS+VX
      VY=-CHARGE*FORCEY*DT*1.0D 07/XMASS+VY
      X=X+VX*DT
      Y=Y+VY*DT
      IF(VY)11,10,10
   11 IF(Y-XD7)15,15,13
   15 WRITE(6,36)N
   36 FORMAT(1H0,' POSITION OF PARTICLE AT GUARD ELECTRODE AFTER',I8,2X,
     2'ITERATIONS')
      WRITE(6,99)X,VX,Y,VY
   99 FORMAT(5X,'X-POSITION =',F8.4,10X,'X-VELOCITY =',E14.6,/,5X,'Y-POS
     2ITION =',F8.4,10X,'Y-VELOCITY ='E14.6)
   10 XX=XX-.002
   40 XKE=XKE+1.0D 01
   50 STOP
      END
```

```
      SUBROUTINE FUNC(X,Y,VAL)
C
C
C     SUBROUTINE 'FUNC' IS USED TO EVALUATE THE 'INVERSE FUNCTION'  AND RETURN
C     A NUMERICAL VALUE ("VAL") OF THIS FUNCTION FOR ANY X AND Y.
C
C          Y = Y-COORDINATE OF THE ION IN THE LENS, Z-PLANE.  (CM)
C          X = VARIABLE NAME -- NOT THE COORDINATE IN THE Z-PLANE
C
C          -----------------------------------------------------------------
C
      IMPLICIT REAL*8 (A-H,O-Z)
      COMMON PI,A,B,C,D,E,F,G,H,O,P,Q,R,S,T,U,XS1,XS2,XS3,XS4,XS5,XS6,
     2XS7,XS8,R1,R2,R3,R4,R5,R6,R7,XMESS,Q2,Q3,Q4,Q5,Q6,Q7,DVDR2,DVDR3,
     3DVDR4,DVDR5,DVDR6,DVDR7,SVR22,SVR23,SVR24,SVR25,SVR26,SVR27,TVR32,
     4TVR33,TVR34,TVR35,TVR36,TVR37,DVDY2,DVDY3,DVDY4,DVDY5,DVDY6,DVDY7,
     5SVY22,SVY23,SVY24,SVY25,SVY26,SVY27,TVY32,TVY33,TVY34,TVY35,TVY36,
     6TVY37,DYDR,SYR2,TYR3,SYRY,DRDY,SRY2,TRY3,FVR42,FVR43,FVR44,FVR45,
     7FVR46,FVR47,FVY42,FVY43,FVY44,FVY45,FVY46,FVY47,FYR4,FRY4,TOTALV,
     8TOTAL1,TOTAL2,TOTAL3,TOTAL4,ZB,ZD,ZF,ZH,ZP,ZR,ZT
      ATAN(X)=DATAN(X)
      VAL=X+2*R1*ATAN(X/B)+2*R2*ATAN(X/D)+2*R3*ATAN(X/F)+2*R4*ATAN(X/H)+
     22*R5*ATAN(X/P)+2*R6*ATAN(X/R)+2*R7*ATAN(X/T)-XMESS/X-Y
      RETURN
      END
```

```
      SUBROUTINE FIND (Y,TOL,ROOT,BOMB)
C
C
C          SUBROUTINE 'FIND' IS RESPONSIBLE FOR FINDING ROOTS FOR THE
C     'INVERSE FUNCTION'.  STARTING AT AN ARBITRARY POINT OF "X" AND PROCEED-
C     ING IN ORDER OF MAGNITUDE STEPS SUBROUTINE FUNC IS CALLED TO RETURN
C     VALUES FOR THE 'INVERSE FUNCTION'.  THE RANGE OF SEARCH IS DICTATED
C     BY THE SIZE OF 'DO 1 I=1,##'.  THE SEARCH RUNS THEREFORE FROM X TO
C     X*(10**(##)).  A ROOT IS ZEROED IN ON WHENEVER SUCCESSIVE VALUES OF
C     'FUNC' CHANGE SIGN.  IF NO POSITIVE ROOT IS FOUND THE PROGRAM RETURNS
C     A FLAG "BOMB" INDICATING TO THE MAIN PROGRAM THAT THE RANGE OF SEARCH
C     WAS NOT LARGE ENOUGH.
C
C     -------------------------------------------------------------------
C
      IMPLICIT REAL*8 (A-H,O-Z)
      COMMON PI,A,B,C,D,E,F,G,H,O,P,Q,R,S,T,U,XS1,XS2,XS3,XS4,XS5,XS6,
     2XS7,XS8,R1,R2,R3,R4,R5,R6,R7,XMESS,Q2,Q3,Q4,Q5,Q6,Q7,DVDR2,DVDR3,
     3DVDR4,DVDR5,DVDR6,DVDR7,SVR22,SVR23,SVR24,SVR25,SVR26,SVR27,TVR32,
     4TVR33,TVR34,TVR35,TVR36,TVR37,DVDY2,DVDY3,DVDY4,DVDY5,DVDY6,DVDY7,
     5SVY22,SVY23,SVY24,SVY25,SVY26,SVY27,TVY32,TVY33,TVY34,TVY35,TVY36,
     6TVY37,DYDR,SYR2,TYR3,SYRY,DRDY,SRY2,TRY3,FVR42,FVR43,FVR44,FVR45,
     7FVR46,FVR47,FVY42,FVY43,FVY44,FVY45,FVY46,FVY47,FYR4,FRY4,TOTALV,
     8TOTAL1,TOTAL2,TOTAL3,TOTAL4,ZB,ZD,ZF,ZH,ZP,ZR,ZT
      SIGN(X,Y)=DSIGN(X,Y)
      ABS(X)=DABS(X)
C
C          STARTING POINT IN SEARCH OF ROOT
      X=1.E-20
      X1=X
      IFLAG=0
      BOMB=0.
    2 CALL FUNC(X,Y,TRY1)
      DO 1 I=1,40
      X=X*10
      X2=X
      CALL FUNC(X,Y,TRY2)
      CHANGE=SIGN(TRY1,TRY2)
      IF(CHANGE.NE.TRY1) GO TO 10
      X1=X2
    1 TRY1=TRY2
      IF(IFLAG.NE.0) GO TO 3
C
C          THESE STATEMENTS EXECUTED ONLY IF NO POSITIVE ROOT IS FOUND
      X=-1.E-20
      IFLAG=1
      GO TO 2
    3 X1=-1.E-9
      X=-1.E-9
      CALL FUNC(X,Y,TRY1)
      X2=1.5E-9
      X=1.5E-9
      CALL FUNC(X,Y,TRY2)
      CHANGE=SIGN(TRY1,TRY2)
      IF(CHANGE.NE.TRY1) GO TO 10
      BOMB=1.
      WRITE(6,8)Y
    8 FORMAT(1H0,'ROOT CANNOT BE BRACKETED USING THE LIMITS IN SUBROUTIN
```

```
      2E FIND FOR Y= ',E14.6)
0034   RETURN
C
C         ROOT IS BRACKETED -- BISECTION BEGINS
0035 10 IF(ABS((X1-X2)/X1).LE.TOL) GO TC 25
0036   X=(X1+X2)/2.
0037   CALL FUNC(X,Y,TRY)
0038   CHANGE=SIGN(TRY,TRY1)
0039   IF (CHANGE.NE.TRY) GO TO 15
0040   X1=X
0041   TRY1=TRY
0042   GO TO 10
0043 15 X2=X
0044   TRY2=TRY
0045   GO TO 10
0046 25 ROOT=X1
0047   RETURN
0048   END
```

```
0001      SUBROUTINE FSTPOT (ROOT)
     C
     C
     C         SUBROUTINE FSTPOT CALCULATES THE FIRST DERIVATIVE OF THE POTENTIAL
     C    WITH RESPECT TO THE Y-COORDINATE (Z-PLANE).
     C
     C    ------------------------------------------------------------------------
     C
0002      IMPLICIT REAL*8 (A-H,O-Z)
0003      COMMON PI,A,B,C,D,E,F,G,H,O,P,Q,R,S,T,U,XS1,XS2,XS3,XS4,XS5,XS6,
         2XS7,XS8,R1,R2,R3,R4,R5,R6,R7,XMESS,Q2,Q3,Q4,Q5,Q6,Q7,DVDR2,DVDR3,
         3DVDR4,DVDR5,DVDR6,DVDR7,SVR22,SVR23,SVR24,SVR25,SVR26,SVR27,TVR32,
         4TVR33,TVR34,TVR35,TVR36,TVR37,DVDY2,DVDY3,DVDY4,DVDY5,DVDY6,DVDY7,
         5SVY22,SVY23,SVY24,SVY25,SVY26,SVY27,TVY32,TVY33,TVY34,TVY35,TVY36,
         6TVY37,DYDR,SYR2,TYR3,SYRY,DRDY,SRY2,TRY3,FVR42,FVR43,FVR44,FVR45,
         7FVR46,FVR47,FVY42,FVY43,FVY44,FVY45,FVY46,FVY47,FYR4,FRY4,TOTALV,
         8TOTAL1,TOTAL2,TOTAL3,TOTAL4,ZB,ZD,ZF,ZH,ZP,ZR,ZT
0004      ZB=B*B+ROOT*ROOT
0005      ZD=D*D+RCOT*ROOT
0006      ZF=F*F+ROOT*ROOT
0007      ZH=H*H+ROOT*ROOT
0008      ZP=P*P+ROOT*ROOT
0009      ZR=R*R+ROOT*ROOT
0010      ZT=T*T+ROOT*ROOT
     C
     C         FIRST DERIVATIVE OF THE POTENTIAL WITH RESPECT TO THE ROOT,R,
     C         FOR THE ELECTRODE PAIRS #2-#7.
0011      DVDR2   =Q2*(2/PI)*((T/ZT)-(R/ZR))
0012      DVDR3   =Q3*(2/PI)*((R/ZR)-(P/ZP))
0013      DVDR4   =Q4*(2/PI)*((P/ZP)-(H/ZH))
0014      DVDR5   =Q5*(2/PI)*((H/ZH)-(F/ZF))
0015      DVDR6   =Q6*(2/PI)*((F/ZF)-(D/ZD))
0016      DVDR7   =Q7*(2/PI)*((D/ZD)-(B/ZB))
     C
     C         FIRST DERIVATIVE OF THE Y-COORDINATE WITH RESPECT TO THE ROOT,R.
0017      DYDR    =1+2*R1*B/ZB+2*R2*D/ZD+2*R3*F/ZF+2*R4*H/ZH+2*R5*P/ZP+2*R6*R
         2/ZR+2*R7*T/ZT+XMESS/(ROOT*ROOT)
     C
     C         FIRST DERIVATIVE OF THE POTENTIAL WITH RESPECT TO THE Y-COORDINATE
     C         FOR ELECTRODE PAIRS #2-#7.
0018      DVDY2   =DVDR2   /DYDR
0019      DVDY3   =DVDR3   /DYDR
0020      DVDY4   =DVDR4   /DYDR
0021      DVDY5   =DVDR5   /DYDR
0022      DVDY6   =DVDR6   /DYDR
0023      DVDY7   =DVDR7   /DYDR
     C
     C         FIRST DERIVATIVE OF THE ROOT,R, WITH RESPECT TO THE Y-COORDINATE.
0024      DRDY    =1/DYDR
     C
     C         TOTAL CONTRIBUTION OF THE ELECTRODE PAIRS #2-#7 TO THE FIRST
     C         DERIVATIVE OF THE POTENTIAL WITH RESPECT TO THE Y-COORDINATE.
0025      TOTAL1=DVDY2+DVDY3+DVDY4+DVDY5+DVDY6+DVDY7
0026      RETURN
0027      END
```

```
0001          SUBROUTINE SNDPOT (ROOT)
         C
         C
         C        SUBROUTINE 'SNDPOT' CALCULATES THE SECOND DERIVATIVE OF THE POTENTIAL
         C     WITH RESPECT TO THE Y-COORDINATE (Z-PLANE).
         C
         C     ----------------------------------------------------------------------
         C
0002          IMPLICIT REAL*8 (A-H,O-Z)
0003          COMMON PI,A,B,C,D,E,F,G,H,O,P,Q,R,S,T,U,XS1,XS2,XS3,XS4,XS5,XS6,
             2XS7,XS8,R1,R2,R3,R4,R5,R6,R7,XMESS,Q2,Q3,Q4,Q5,Q6,Q7,DVDR2,DVDR3,
             3DVDR4,DVDR5,DVDR6,DVDR7,SVR22,SVR23,SVR24,SVR25,SVR26,SVR27,TVR32,
             4TVR33,TVR34,TVR35,TVR36,TVR37,DVDY2,DVDY3,DVDY4,DVDY5,DVDY6,DVDY7,
             5SVY22,SVY23,SVY24,SVY25,SVY26,SVY27,TVY32,TVY33,TVY34,TVY35,TVY36,
             6TVY37,DYDR,SYR2,TYR3,SYRY,DRDY,SRY2,TRY3,FVR42,FVR43,FVR44,FVR45,
             7FVR46,FVR47,FVY42,FVY43,FVY44,FVY45,FVY46,FVY47,FYR4,FRY4,TOTALV,
             8TOTAL1,TOTAL2,TOTAL3,TOTAL4,ZB,ZD,ZF,ZH,ZP,ZR,ZT
         C
         C        SECOND DERIVATIVE OF THE POTENTIAL WITH RESPECT TO THE ROOT,R,
         C        SQUARED FOR ELECTRODE PAIRS #2-#7.
0004          SVR22   =Q2*(-((4/PI)*T*ROOT)/(ZT*ZT)+((4/PI)*R*ROOT)/(ZR*ZR))
0005          SVR23   =Q3*(-((4/PI)*R*ROOT)/(ZR*ZR)+((4/PI)*P*ROOT)/(ZP*ZP))
0006          SVR24   =Q4*(-((4/PI)*P*ROOT)/(ZP*ZP)+((4/PI)*H*ROOT)/(ZH*ZH))
0007          SVR25   =Q5*(-((4/PI)*H*ROOT)/(ZH*ZH)+((4/PI)*F*ROOT)/(ZF*ZF))
0008          SVR26   =Q6*(-((4/PI)*F*ROOT)/(ZF*ZF)+((4/PI)*D*ROOT)/(ZD*ZD))
0009          SVR27   =Q7*(-((4/PI)*D*ROOT)/(ZD*ZD)+((4/PI)*B*ROOT)/(ZB*ZB))
         C
         C        SECOND DERIVATIVE OF THE Y-CCORDINATE WITH RESPECT TO THE
         C        ROOT,R, SQUARED.
0010          SYR2   =-(4*R1*B*ROOT)/(ZB*ZB)-(4*R2*D*ROOT)/(ZD*ZD)-(4*R3*F*ROOT)
             2/(ZF*ZF)-(4*R4*H*ROOT)/(ZH*ZH)-(4*R5*P*ROOT)/(ZP*ZP)-(4*R6*R*ROOT)
             3/(ZR*ZR)-(4*R7*T*ROOT)/(ZT*ZT)-2*XMESS/(ROOT**3)
         C
         C        SECOND DERIVATIVE OF THE Y-CCORDINATE WITH RESPECT TO THE ROOT,R,
         C        AND Y.
0011          SYRY   =SYR2   *DRDY
         C
         C        SECOND DERIVATIVE OF THE ROOT,R, WITH RESPECT TO THE Y-COORDINATE
         C        SQUARED.
0012          SRY2=-SYRY/(DYDR*DYDR)
         C
         C        SECOND DERIVATIVE OF THE POTENTIAL WITH RESPECT TO THE Y-COORBINATE
         C        SQUARED FOR ELECTRODE PAIRS #2-#7.
0013          SVY22=DVDR2*SRY2+SVR22*DRDY*DRDY
0014          SVY23=DVDR3*SRY2+SVR23*DRDY*DRDY
0015          SVY24=DVDR4*SRY2+SVR24*DRDY*DRDY
0016          SVY25=DVDR5*SRY2+SVR25*DRDY*DRDY
0017          SVY26=DVDR6*SRY2+SVR26*DRDY*DRDY
0018          SVY27=DVDR7*SRY2+SVR27*DRDY*DRDY
         C
         C        TOTAL CONTRIBUTION OF ELECTRCDE PAIRS #2-#7 TO THE SECOND DERIVATIVE
         C        OF THE POTENTIAL WITH RESPECT TO THE Y-COORDINATE SQUARED.
0019          TOTAL2=SVY22+SVY23+SVY24+SVY25+SVY26+SVY27
0020          RETURN
0021          END
```

```
0001          SUBROUTINE TRDPOT (ROOT)
         C
         C
         C        SUBROUTINE 'TRDPOT' CALCULATES THE THIRD QERIVATIVE OF THE POTENTIAL
         C     WITH RESPECT TO THE Y-COORDINATE (Z-PLANE).
         C
         C     ----------------------------------------------------------------------
         C
0002          IMPLICIT REAL*8 (A-H,O-Z)
0003          COMMON PI,A,B,C,D,E,F,G,H,O,P,Q,R,S,T,U,XS1,XS2,XS3,XS4,XS5,XS6,
             2XS7,XS8,R1,R2,R3,R4,R5,R6,R7,XMESS,Q2,Q3,Q4,Q5,Q6,Q7,DVDR2,DVDR3,
             3DVDR4,DVDR5,DVDR6,DVDR7,SVR22,SVR23,SVR24,SVR25,SVR26,SVR27,TVR32,
             4TVR33,TVR34,TVR35,TVR36,TVR37,DVDY2,DVDY3,DVDY4,DVDY5,DVDY6,DVDY7,
             5SVY22,SVY23,SVY24,SVY25,SVY26,SVY27,TVY32,TVY33,TVY34,TVY35,TVY36,
             6TVY37,DYDR,SYR2,TYR3,SYRY,DRDY,SRY2,TRY3,FVR42,FVR43,FVR44,FVR45,
             7FVR46,FVR47,FVY42,FVY43,FVY44,FVY45,FVY46,FVY47,FYR4,FRY4,TOTALV,
             8TOTAL1,TOTAL2,TOTAL3,TOTAL4,ZB,ZD,ZF,ZH,ZP,ZR,ZT
         C
         C        THIRD DERIVATIVE OF THE POTENTIAL WITH RESPECT TO THE ROOT,R, CUBED
         C        FOR ELECTRODE PAIRS #2-#7.
0004          TVR32   =Q2*(-(4/PI)*T/(ZT*ZT)+((16/PI)*T*ROOT*ROOT)/(ZT*ZT*ZT)+((
             24/PI)*R)/(ZR*ZR)-((16/PI)*R*ROOT*ROOT)/(ZR*ZR*ZR))
0005          TVR33   =Q3*(-(4/PI)*R/(ZR*ZR)+((16/PI)*R*ROOT*ROOT)/(ZR*ZR*ZR)+((
             24/PI)*P)/(ZP*ZP)-((16/PI)*P*ROOT*ROOT)/(ZP*ZP*ZP))
0006          TVR34   =Q4*(-(4/PI)*P/(ZP*ZP)+((16/PI)*P*ROOT*ROOT)/(ZP*ZP*ZP)+((
             24/PI)*H)/(ZH*ZH)-((16/PI)*H*ROOT*ROOT)/(ZH*ZH*ZH))
0007          TVR35   =Q5*(-(4/PI)*H/(ZH*ZH)+((16/PI)*H*ROOT*ROOT)/(ZH*ZH*ZH)+((
             24/PI)*F)/(ZF*ZF)-((16/PI)*F*ROOT*ROOT)/(ZF*ZF*ZF))
0008          TVR36   =Q6*(-(4/PI)*F/(ZF*ZF)+((16/PI)*F*ROOT*ROOT)/(ZF*ZF*ZF)+((
             24/PI)*D)/(ZD*ZD)-((16/PI)*D*ROOT*ROOT)/(ZD*ZD*ZD))
0009          TVR37   =Q7*(-(4/PI)*D/(ZD*ZD)+((16/PI)*D*ROOT*ROOT)/(ZD*ZD*ZD)+((
             24/PI)*B)/(ZB*ZB)-((16/PI)*B*ROOT*ROOT)/(ZB*ZB*ZB))
         C
         C        THIRD DERIVATIVE OF THE Y-COORDINATE WITH RESPECT TO THE ROOT,R, CUBED.
0010          TYR3   =-(4*R1*B)/(ZB*ZB)+(16*R1*B*ROOT*ROOT)/(ZB**3)-(4*R2*D)/(ZD
             2*ZD)+(16*R2*D*ROOT*ROOT)/(ZD**3)-(4*R3*F)/(ZF*ZF)+(16*R3*F*ROOT*
             3ROOT)/(ZF**3)-(4*R4*H)/(ZH*ZH)+(16*R4*H*ROOT*ROOT)/(ZH**3)-(4*R5*
             4P)/(ZP*ZP)+(16*R5*P*ROOT*ROOT)/(ZP**3)-(4*R6*R)/(ZR*ZR)+((16*R6*R*
             5ROOT)/(ZR*ZR))*ROOT/ZR-(4*R7*T)/(ZT*ZT)+((16*R7*T*ROOT)/(ZT*ZT))*
             6ROOT/ZT+((6*XMESS)/(ROOT*ROOT))*1/(ROOT*ROOT)
         C
         C        THIRD DERIVATIVE OF THE ROOT,R, WITH RESPECT TO THE Y-COORDINATE CUBED.
0011          TRY3   =-TYR3   /(DYDR   **4)+3*SYR2   *SYR2   /(DYDR   **5)
         C
         C        THIRD DERIVATIVE OF THE POTENTIAL WITH RESPECT TO THE Y-COORDINATE
         C        CUBED FOR ELECTRODE PAIRS #2-#7.
0012          TVY32=DVDR2*TRY3+3*SRY2*SVR22*DRDY+TVR32*(DRDY**3)
0013          TVY33=DVDR3*TRY3+3*SRY2*SVR23*DRDY+TVR33*(DRDY**3)
0014          TVY34=DVDR4*TRY3+3*SRY2*SVR24*DRDY+TVR34*(DRDY**3)
0015          TVY35=DVDR5*TRY3+3*SRY2*SVR25*DRDY+TVR35*(DRDY**3)
0016          TVY36=DVDR6*TRY3+3*SRY2*SVR26*DRDY+TVR36*(DRDY**3)
0017          TVY37=DVDR7*TRY3+3*SRY2*SVR27*DRDY+TVR37*(DRDY**3)
         C
         C        TOTAL CONTRIBUTION OF ELECTRODE PAIRS #2-#7 TO THE THIRD DERIVATIVE
         C        OF THE POTENTIAL WITH RESPECT TO THE Y-COORDINATE CUBED.
0018          TOTAL3=TVY32+TVY33+TVY34+TVY35+TVY36+TVY37
0019          RETURN
0020          END
```

```
0001          SUBROUTINE FRHPOT (ROOT)
          C
          C
          C       SUBROUTINE 'FRHPOT' CALCULATES THE FOURTH DERIVATIVE OF THE POTENTIAL
          C    WITH RESPECT TO THE Y-COORDINATE (Z-PLANE).
          C
          C    ---------------------------------------------------------------------
          C
0002          IMPLICIT REAL*8 (A-H,O-Z)
0003          COMMON PI,A,B,C,D,E,F,G,H,O,P,Q,R,S,T,U,XS1,XS2,XS3,XS4,XS5,XS6,
             2XS7,XS8,R1,R2,R3,R4,R5,R6,R7,XMESS,Q2,Q3,Q4,Q5,Q6,Q7,DVDR2,DVDR3,
             3DVDR4,DVDR5,DVDR6,DVDR7,SVR22,SVR23,SVR24,SVR25,SVR26,SVR27,TVR32,
             4TVR33,TVR34,TVR35,TVR36,TVR37,DVDY2,DVDY3,DVDY4,DVDY5,DVDY6,DVDY7,
             5SVY22,SVY23,SVY24,SVY25,SVY26,SVY27,TVY32,TVY33,TVY34,TVY35,TVY36,
             6TVY37,DYDR,SYR2,TYR3,SYRY,DRDY,SRY2,TRY3,FVR42,FVR43,FVR44,FVR45,
             7FVR46,FVR47,FVY42,FVY43,FVY44,FVY45,FVY46,FVY47,FYR4,FRY4,TOTALV,
             8TOTAL1,TOTAL2,TOTAL3,TOTAL4,ZB,ZD,ZF,ZH,ZP,ZR,ZT
          C
          C       FOURTH DERIVATIVE OF THE POTENTIAL WITH RESPECT TO THE ROOT,R, TO THE
          C       FOURTH POWER FOR ELECTRODE PAIRS #2-#7.
0004          FVR42    =Q2*(48/PI)*ROOT*((T/(ZT**3))*(1-2*ROOT*ROOT/ZT)-(R/(ZR**3
             2))*(1-2*ROOT*ROOT/ZR))
0005          FVR43    =Q3*(48/PI)*ROOT*((R/(ZR**3))*(1-2*ROOT*ROOT/ZR)-(P/(ZP**3
             2))*(1-2*ROOT*ROOT/ZP))
0006          FVR44    =Q4*(48/PI)*ROOT*((P/(ZP**3))*(1-2*ROOT*ROOT/ZP)-(H/(ZH**3
             2))*(1-2*ROOT*ROOT/ZH))
0007          FVR45    =Q5*(48/PI)*ROOT*((H/(ZH**3))*(1-2*ROOT*ROOT/ZH)-(F/(ZF**3
             2))*(1-2*ROOT*ROOT/ZF))
0008          FVR46    =Q6*(48/PI)*ROOT*((F/(ZF**3))*(1-2*ROOT*ROOT/ZF)-(D/(ZD**3
             2))*(1-2*ROOT*ROOT/ZD))
0009          FVR47    =Q7*(48/PI)*ROOT*((D/(ZD**3))*(1-2*ROOT*ROOT/ZD)-(B/(ZB**3
             2))*(1-2*ROOT*ROOT/ZB))
          C
          C       FOURTH DERIVATIVE OF THE Y-COORDINATE WITH RESPECT TO THE ROOT,R, TO
          C       THE FOURTH POWER.
0010          FYR4    =-48*ROOT*((R1*B/(ZB**3))*(-1+2*ROOT*ROOT/ZB)+(R2*D/(ZD**3)
             2)*(-1+2*ROOT*ROOT/ZD)+(R3*F/(ZF**3))*(-1+2*ROOT*ROOT/ZF)+(R4*H/(ZH
             3**3))*(-1+2*ROOT*ROOT/ZH)+(R5*P/(ZP**3))*(-1+2*ROOT*ROOT/ZP)+(R6*R
             4/(ZR**3))*(-1+2*ROOT*ROOT/ZR)+ ((R7*T/(ZT*ZT))*(1/ZT))*(-1+2*ROOT*
             5ROOT/ZT))-((24*XMESS/(ROOT**3))*(1/(ROOT**2)))
          C
          C       FOURTH DERIVATIVE OF THE ROOT,R, WITH RESPECT TO THE Y-COORDINATE
          C       TO THE FOURTH POWER.
0011          FRY4=-(FYR4/(DYDR**2))*(1/(DYDR**3))+(10*TYR3*SYR2/(DYDR**3))*(1/(
             2DYDR**3))-15*((SYR2/DYDR)**3)*(1/(DYDR**4))
          C
          C       FOURTH DERIVATIVE OF THE POTENTIAL WITH RESPECT TO THE Y-COORDINATE
          C       TO THE FOURTH POWER FOR ELECTRODE PAIRS #2-#7.
0012          FVY42=DVDR2*FRY4+4*TRY3*SVR22*DRDY+3*SRY2*SRY2*SVR22+6*SRY2*DRDY*
             2DRDY*TVR32+FVR42*(DRDY**4)
0013          FVY43=DVDR3*FRY4+4*TRY3*SVR23*DRDY+3*SRY2*SRY2*SVR23+6*SRY2*DRDY*
             2DRDY*TVR33+FVR43*(DRDY**4)
0014          FVY44=DVDR4*FRY4+4*TRY3*SVR24*DRDY+3*SRY2*SRY2*SVR24+6*SRY2*DRDY*
             2DRDY*TVR34+FVR44*(DRDY**4)
0015          FVY45=DVDR5*FRY4+4*TRY3*SVR25*DRDY+3*SRY2*SRY2*SVR25+6*SRY2*DRDY*
             2DRDY*TVR35+FVR45*(DRDY**4)
0016          FVY46=DVDR6*FRY4+4*TRY3*SVR26*DRDY+3*SRY2*SRY2*SVR26+6*SRY2*DRDY*
             2DRDY*TVR36+FVR46*(DRDY**4)
0017          FVY47=DVDR7*FRY4+4*TRY3*SVR27*DRDY+3*SRY2*SRY2*SVR27+6*SRY2*DRDY*
             2DRDY*TVR37+FVR47*(DRDY**4)
          C
          C       TOTAL CONTRIBUTION OF ELECTRODE PAIRS #2-#7 TO THE FOURTH DERIVATIVE
          C       OF THE POTENTIAL WITH RESPECT TO THE Y-COORDINATE TO THE FOURTH
          C       POWER.
0018          TOTAL4=FVY42+FVY43+FVY44+FVY45+FVY46+FVY47
0019          RETURN
0020          END
```

VITA 2

Robert Joseph Ryba

Candidate for the Degree of

Doctor of Philosophy

Thesis: MODIFICATION OF A MATTAUCH-HERZOG GEOMETRY MASS SPECTROMETER FOR IMPROVED RESOLUTION ION KINETIC ENERGY SPECTROMETRY

Major Field: Chemistry

Biographical:

Personal Data: Born in Detroit, Michigan, on November 19, 1945, the son of Mr. and Mrs. Joseph Ryba.

Education: Graduated from Edwin Denby High School, Detroit, Michigan in June, 1963; received the Bachelor of Science in Chemistry degree from Wayne State University, Detroit, Michigan, August, 1967; completed requirements for the Doctor of Philosophy degree at Oklahoma State University, May, 1976.

Professional Experience: Graduate Teaching Assistant, Oklahoma State University, 1971-1975; Research Award, Oklahoma State University, summers 1972 and 1974; Continental Oil Company Fellow, Summer, 1973, June 1 - December 31, 1974; Phillips Oil Company Fellow, Summer 1975.

Membership in Honorary and Professional Societies: Phi Lambda Upsilon, Honorary Chemical Society; American Chemical Society.